



Missouri State
UNIVERSITY

BearWorks
Institutional Repository

MSU Graduate Theses


Spring 2017

Using Survey Data and HEC-RAS Modeling to Assess a Riffle-Remediation Structure on the Big River, Bonne Terre, Missouri

Nichole Renee Weedman

Missouri State University, Nichole11@live.missouristate.edu

Follow this and additional works at: <http://bearworks.missouristate.edu/theses>

 Part of the [Sedimentology Commons](#), and the [Water Resource Management Commons](#)

Recommended Citation

Weedman, Nichole Renee, "Using Survey Data and HEC-RAS Modeling to Assess a Riffle-Remediation Structure on the Big River, Bonne Terre, Missouri" (2017). *MSU Graduate Theses*. 3093.

<http://bearworks.missouristate.edu/theses/3093>

This article or document was made available through BearWorks, the institutional repository of Missouri State University. The work contained in it may be protected by copyright and require permission of the copyright holder for reuse or redistribution.

For more information, please contact BearWorks@library.missouristate.edu.

**USING SURVEY DATA AND HEC-RAS MODELING TO ASSESS A RIFFLE-
REMEDICATION STRUCTURE ON THE BIG RIVER, BONNE TERRE,
MISSOURI**

A Masters Thesis

Presented to

The Graduate College of

Missouri State University

In Partial Fulfillment

Of the Requirements for the Degree

Master of Science, Geospatial Sciences in Geography, Geology, and Planning

By

Nichole R. Weedman

May 2017

Copyright 2017 by Nichole Renee Weedman

**USING SURVEY DATA AND HEC-RAS MODELING TO ASSESS A RIFFLE-
REMEDICATION STRUCTURE ON THE BIG RIVER, BONNE TERRE,
MISSOURI**

Geography, Geology and Planning

Missouri State University, May 2017

Master of Science

Nichole R. Weedman

ABSTRACT

Sediment transport and deposition in river channels can vary for many reasons including flooding, dredging, channel velocity, and grain size. On the Big River, the Army Corps of Engineers constructed a riffle ramp structure to trap and remediate lead-contaminated sediments. The performance of the structure is unknown. The goal of this study is to evaluate the storage capabilities of the riffle structure. To do this, survey data was collected to analyze sediment storage and entered into the HEC-RAS 5.0 to model the hydraulics of the channel before and after the riffle installation. Samples were collected to assess the level of lead contamination. The results indicate the riffle structure has caused the deposition of approximately 61,898 ft³ of sediment.

KEYWORDS: sedimentation, riffle, model, lead, survey, HEC-RAS, flood, erosion, remediation

This abstract is approved as to form and content

Dr. Matthew C. Pierson
Chairperson, Advisory Committee
Missouri State University

**USING SURVEY DATA AND HEC-RAS MODELING TO ASSESS A RIFFLE-
REMEDICATION STRUCTURE ON THE BIG RIVER, BONNE TERRE,
MISSOURI**

By

Nichole R. Weedman

A Masters Thesis
Submitted to the Graduate College
Of Missouri State University
In Partial Fulfillment of the Requirements
For the Degree of Master of Science, Geospatial Sciences in Geography, Geology, and
Planning

May 2017

Approved:

Matthew C. Pierson, PhD

Robert Pavlowsky, PhD

Toby Dogwiler, PhD

Julie Masterson, PhD: Dean, Graduate College

ACKNOWLEDGEMENTS

I want to thank so many people for their help and involvement with this project. I want to begin by thanking my committee members. Dr. Matthew Pierson, thank you for being so willing to take me on as your first graduate student. You have been the most amazing advisor, and I can't thank you enough for all of your guidance, encouragement, and support these past 2 years. I honestly do not know how I would have gotten through this without you, and I just want to say I appreciate it more than you know. Dr. Robert Pavlowsky and Dr. Toby Dogwiler, thank you for everything you both have done for me. From your guidance to the support, I just want to say thank you both for all you have helped me accomplish.

Next I want to say thank you to the OEWRI crew. I want to begin by thanking Marc Owen. Marc, thank you for always being around when I had questions, putting up with me, and always giving me a laugh. You've been such a huge help in all things Big River, and honestly I can't say thank you enough. Next I want to thank Josh Voss. Josh, you've been my Big River partner in crime, and I just want you to know I appreciate all your help. Finally I want to thank the OEWRI graduate assistance. Matt Thies, Joey Nash, Megan Hente, Kayla Geier, Holly Duff, Ellie Bradley, and Nick Bradley thank you for all of your assistance in field. From clearing brush to surveying, this project would not have gotten done without all of your help, so thank you all.

Finally I want to say thank you to the most important people in my life, my family and friends. Mom and Dad, thank you for being so supportive and always offering up the encouragement that I needed. It is definitely your love and support that has gotten me to this point and helped shape the woman I am today. I also want to thank a few people who have supported and encouraged me along this journey. James, thank you for your love, support, and encouragement. You are a big part of my journey and I appreciate all that you have done for me. Megan, I just wanted to say thanks for being such a great friend and roommate. I could not have asked for a better friend to share the graduate school experience with.

Last but not least a quick thank you to Vaughn Count for allowing us access to your property and Jason Gunter for your coordination and support in the completion of this study. This study has been funded by the USEPA-Region 7 grant number 97751001 entitled "Big River Riffle-Basin Structure Monitoring Project" awarded to Dr. Robert Pavlowsky and Dr. Matthew Pierson.

TABLE OF CONTENTS

Chapter 1- Introduction	1
Purpose and Objectives	1
Study Area	4
Chapter 2- Literature Review	10
Rifle Structures	10
Sediment Transport	11
Sediment Deposition	13
HEC-RAS Modeling	14
Chapter 3 - Methods.....	17
Surveying	17
Geochemical Analysis	20
PeakFQ Analysis.....	22
GIS	23
HEC-RAS Modeling	26
Chapter 4 - Results and Discussion	32
Survey Results	32
Survey Discussion.....	37
Geochemical Results.....	40
Geochemical Discussion.....	43
HEC-RAS Results.....	45
HEC-RAS Discussion.....	75
Chapter 5 - Summary and Conclusions	78
Significant Results	78
Future Work.....	79
References.....	81
Appendices	85
Appendix A. Collection of Survey Data	85
Appendix B. Geochemical Data	96
Appendix C. Pre-construction model velocity simulations	98
Appendix D. Post-construction model velocity simulations.....	105
Appendix E. Pre-construction model water depth simulations.....	112
Appendix F. Post-construction model water depth simulations	119

LIST OF TABLES

Table 1. Channel sediment storage	39
Table 2. Discharge of flood recurrence intervals (Big River below Desloge).....	52
Table 3. Velocity comparison in areas of high deposition (Transects 10-16)	69

LIST OF FIGURES

Figure 1. Riffle structure engineering plans (plan).....	2
Figure 2. Riffle structure engineering plans (profile).....	3
Figure 3. Location of study area	5
Figure 4. Aerial image of study area	6
Figure 5. Hydrograph of Big River below Desloge (August 2015 – November 2016).....	7
Figure 6. Big River Mine Tailings site	8
Figure 7. Profile and plan depictions of riffle pool sequence	11
Figure 8. Methods of sediment transport	12
Figure 9. HEC-RAS modeling relationship between channel and floodplain	16
Figure 10. Example of the posts and numbered signs used for surveying.....	18
Figure 11. Location of Transects 1-22	19
Figure 12. Location of sediment samples	21
Figure 13. Pre-construction DEM with hillshade	24
Figure 14. Post-construction DEM with hillshade.....	25
Figure 15. 2D flow area with break lines	27
Figure 16. Mesh shape at riffle structure	28
Figure 17. Mesh sizes used to determine final mesh size	29
Figure 18. Land use layer used for HEC-RAS modeling	30
Figure 19. Example of survey classified as no change	33
Figure 20. Example of survey classified as only erosion.....	34
Figure 21. Example of survey classified as only deposition.....	35

Figure 22. Example of survey classified as erosion and deposition	35
Figure 23. Comparison of the cross-sectional data for Transect 10	36
Figure 24. Comparison of the cross-sectional data for Transect 13	37
Figure 25. Area of sediment deposition between Transects 10-16.....	38
Figure 26. September 2015 minimum and maximum Pb and Zn locations.....	41
Figure 27. November 2016 minimum and maximum Pb and Zn locations.....	42
Figure 28. Concentrations of Pb (ppm) from sediment samples	44
Figure 29. Concentrations of Zn (ppm) from sediment samples	44
Figure 30. Water surface elevation & cell size relationship near Transect 21	46
Figure 31. Water surface elevation & cell size relationship near Transect 18	46
Figure 32. Water surface elevation & cell size relationship between Transect 15 & 16...47	
Figure 33. Water surface elevation vs cell size relationship near Transect 11	47
Figure 34. Velocity & cell size relationship near Transect 21.....	48
Figure 35. Velocity & cell size relationship near Transect 18.....	48
Figure 36. Velocity & cell size relationship near between Transect 15 & 16	49
Figure 37. Velocity & cell size relationship near Transect 11	49
Figure 38. Water surface elevation & Manning's n relationship at Transect 22	50
Figure 39. Water surface elevation & Manning's n relationship at Transect 17	50
Figure 40. Water surface elevation & Manning's n relationship at Transect 13	51
Figure 41. Water surface elevation & Manning's n relationship at Transect 4	51
Figure 42. PeakFQ results.....	53
Figure 43. Pre- and post-construction comparison of the 1.5-year flood	54
Figure 44. Pre- and post-construction comparison of the 2-year flood	55

Figure 45. Pre- and post-construction comparison of the 5-year flood	57
Figure 46. Pre- and post-construction comparison of the 10-year flood	58
Figure 47. Pre- and post-construction comparison of the 25-year flood	59
Figure 48. Pre- and post-construction comparison of the 50-year flood	60
Figure 49. Pre- and post-construction comparison of the 100-year flood	61
Figure 50. Model simulation of sediment transport capacity	62
Figure 51. Velocity location for pre- & post-construction comparison at 600 cfs	62
Figure 52. Simulation indicating riffle is a velocity control.....	64
Figure 53. Velocity location for pre- & post-construction comparison at 2000 cfs	65
Figure 54. Simulation indicating basin flooding.....	66
Figure 55. Simulation of 2-year flood within the basin	67
Figure 56. Voss (2017) survey results of basin	67
Figure 57. Effect of land use layer on flood simulations.....	68
Figure 58. Simulation focusing on velocities upstream and downstream of Transects 10-16	70
Figure 59. Simulation of high velocity on outlet road	72
Figure 60. Simulation of high velocity near developing headcut	73
Figure 61. Simulation of water depth during 5-year flood near large woody debris deposits	74
Figure 62. Simulation of ~100cfs depicting sedimentation at low flows	77

CHAPTER 1 - INTRODUCTION

Understanding the hydraulics and flow patterns of a channel is critical to the prediction and evaluation of structures designed to alter the flow and confine sediments. Factors that affect sediment transport and deposition are flooding, dredging, sediment type, water velocity, armoring, vegetation, and others. Hydraulic models are powerful tools that allow for predictions of flow behavior and for observation of details that may not be easily observable in the field. In this way, using a hydraulic model to predict behavior can make remediation more efficient and cost effective.

The United States Army Corps of Engineers (USACE) and the United States Environmental Protection Agency (USEPA) have installed a riffle structure on the Big River near Bonne Terre, Missouri, designed to cause deposition of lead-contaminated sediment (Figure 1 and 2). The purpose of the structure is to concentrate contamination for later remediation. Using such a riffle structure for remediation is a relatively untested approach in this area of Missouri. Therefore, it is vital to monitor the deposition rate, location, and contamination of sediment near this site. Additionally, modeling the hydraulics of the structure will provide insight to river processes and allow prediction of behaviors, helping remediation operations.

Purpose and Objectives

The purpose of this study is to evaluate the effectiveness of the constructed riffle at remediating contaminated sediment in the Big River. The objectives of this study are to: (1) evaluate if the constructed riffle is successful at capturing sediment; (2) create a

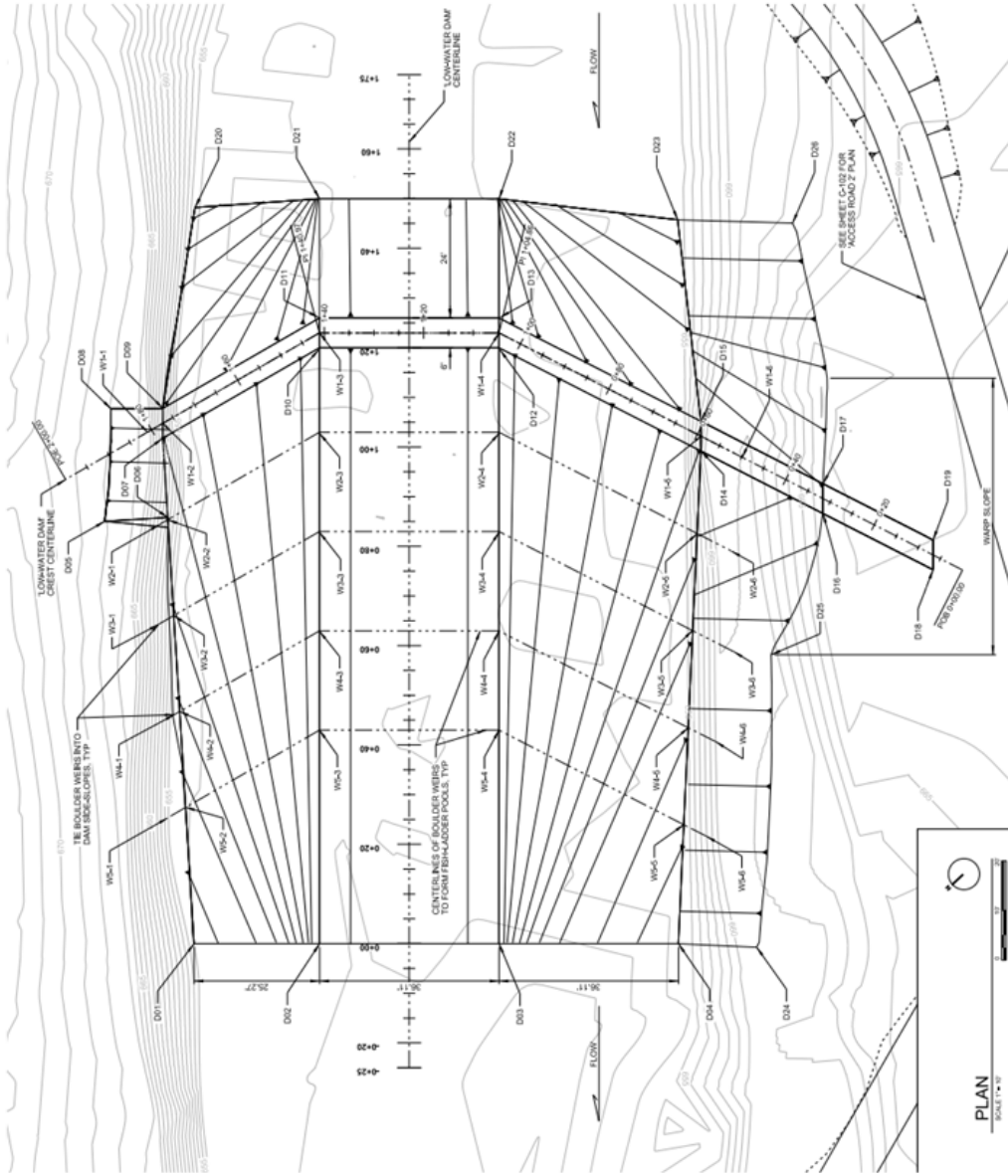


Figure 1 – Riffle structure engineering plans (plan view) (OEWR database).

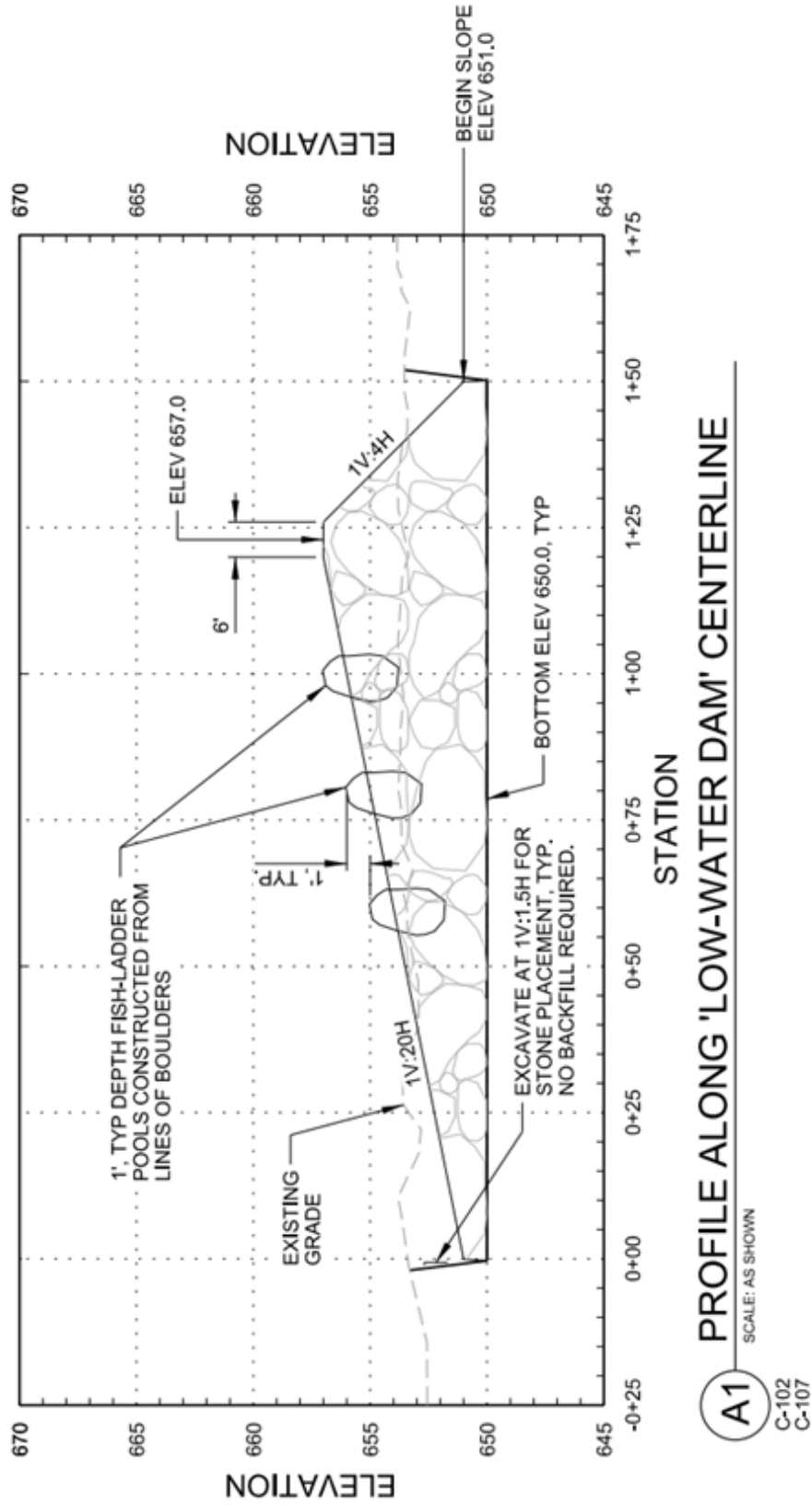


Figure 2 – Riffle structure engineering plans (profile view) (OEWR database).

hydraulic model that can be used as a field analog and prediction method; and (3) evaluate the level of lead (Pb) and zinc (Zn) contamination in the trapped sediment.

These objectives will provide insight into the success of this remediation structure. If remediation is a success at the Big River then this remediation method could be duplicated in similar situations. Creating an effective model to use as a field analog and prediction method will allow the USEPA to more efficiently predict what is happening at the site and provide information on the location and storage of contaminated sediment and knowledge of how to improve performance. The third objective, to evaluate the level of lead contamination in the sediment, is needed to determine if the structure is trapping primarily contaminated or uncontaminated sediments.

To accomplish these objectives survey data is collected to analyze sediment storage. The survey data is entered into the USACE's Hydraulic Engineering Center River Analysis System (HEC-RAS) 5.0.3 to model the hydraulics and flow patterns of the channel. X-ray fluorescence is used to evaluate the level of lead contamination in the sediment.

Accomplishing these objectives will determine if the constructed riffle is successful, and will present a model that will help predict how sediment is transported within the reach. This study will aid the understanding of remediation structures as well as using HEC-RAS 5.0.3 as a hydraulic model.

Study Area

Located in St. Francois County, in eastern Missouri, the Big River flows northerly on the eastern boundary of the Ozarks into the Meramec River (Figure 3) (Brown, 1981).

The headwaters of the Big River are located in the St. Francois Mountains, allowing the river to drain approximately 970 square miles (sq. mi.) (Owen et al., 2012). Within the study area, the Big River also has a tributary flowing into it, Flat River Creek. Flat River Creek is located upstream of both the constructed and natural riffles (Figure 4). The drainage area of the study area is approximately 260 sq. mi.

St. Francois County has hot summers that average between 75 and 88 degrees Fahrenheit, and winters that are moderate with average temperatures ranging from 24 to 35 degrees Fahrenheit (Brown, 1981). Rainfall occurs throughout the year, with 60 percent occurring between April and September (Brown, 1981). During the time of monitoring (August 2015-November 2016) the Big River site had multiple flood events (Figure 5). One flood discharge reached the approximate magnitude of the 5-year flood.

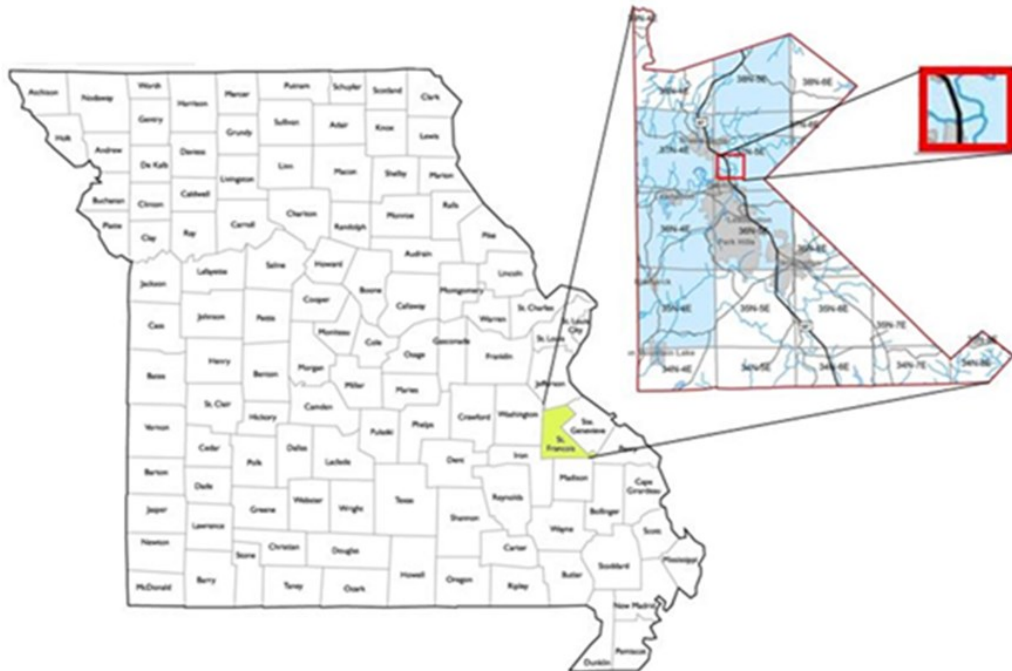


Figure 3 – Location of study area from the Missouri to St. Francois County (in yellow) to study area on the Big River (modified from MDNR, 2016A and World Atlas, 2016).



Figure 4 – Aerial image of the study area showing the Big River – Flat River Creek confluence (Modified from OEWR database).

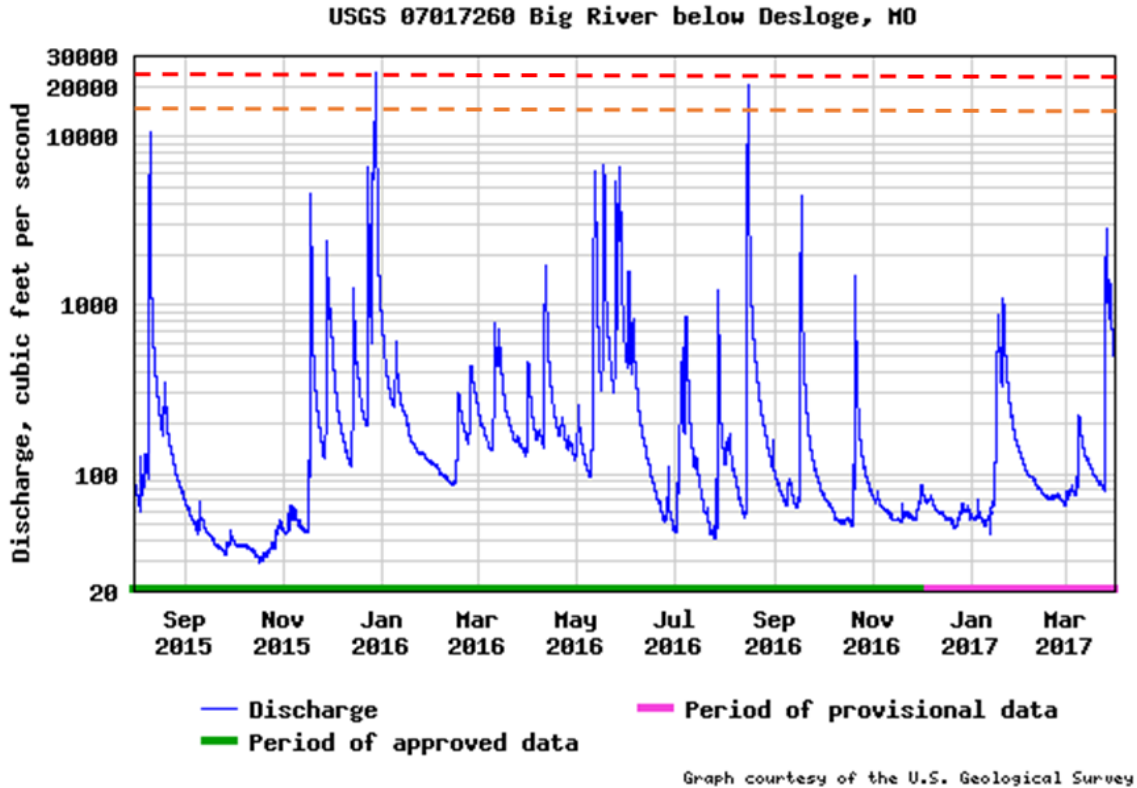


Figure 5 - Hydrograph of the Big River below Desloge from August 2015 to November 2016 with the 2-year (~15,000cfs) and the 5-year (~25,000cfs) plotted with an orange dotted line and a red dotted line, respectively (modified from the USGS, 2017).

Igneous rocks are beneath the headwaters of the Big River while sedimentary rocks lie beneath the rest of the drainage area (Owen et al., 2012). The sedimentary rocks that underlay the drainage area are predominately dolomite, limestone, sandstone, and shale.

St. Francois County has a significant lead mining history. Cambrian dolomite was the primary unit mined for lead and zinc. Mining peaked around the Big River in 1942 (FWS, 2008; USEPA, 1993). One area that was mined significantly was the Big River Mine Tailings (BMRT) site (Figure 6). The BMRT site covers approximately 110 square miles of land that is located approximately 70 miles south of St. Louis in the Old Lead

belt, and comprises 6 mining sites: National, Leadwood, Desloge, Federal, Elvins/Rivermines, and Bonne Terre (USEPA, 2016; ITRC, 2010; Moby et al., 2009; and FWS, 2008). At the Desloge site alone, it has been estimated the BRMT site contains 3,500,000-6,500,000 tons of tailings and chat, which is leftover sand to gravel-sized material that is produced by the separation of ore from rock bodies (Moby et al., 2009; FWS, 2008; and USEPA, 2011).

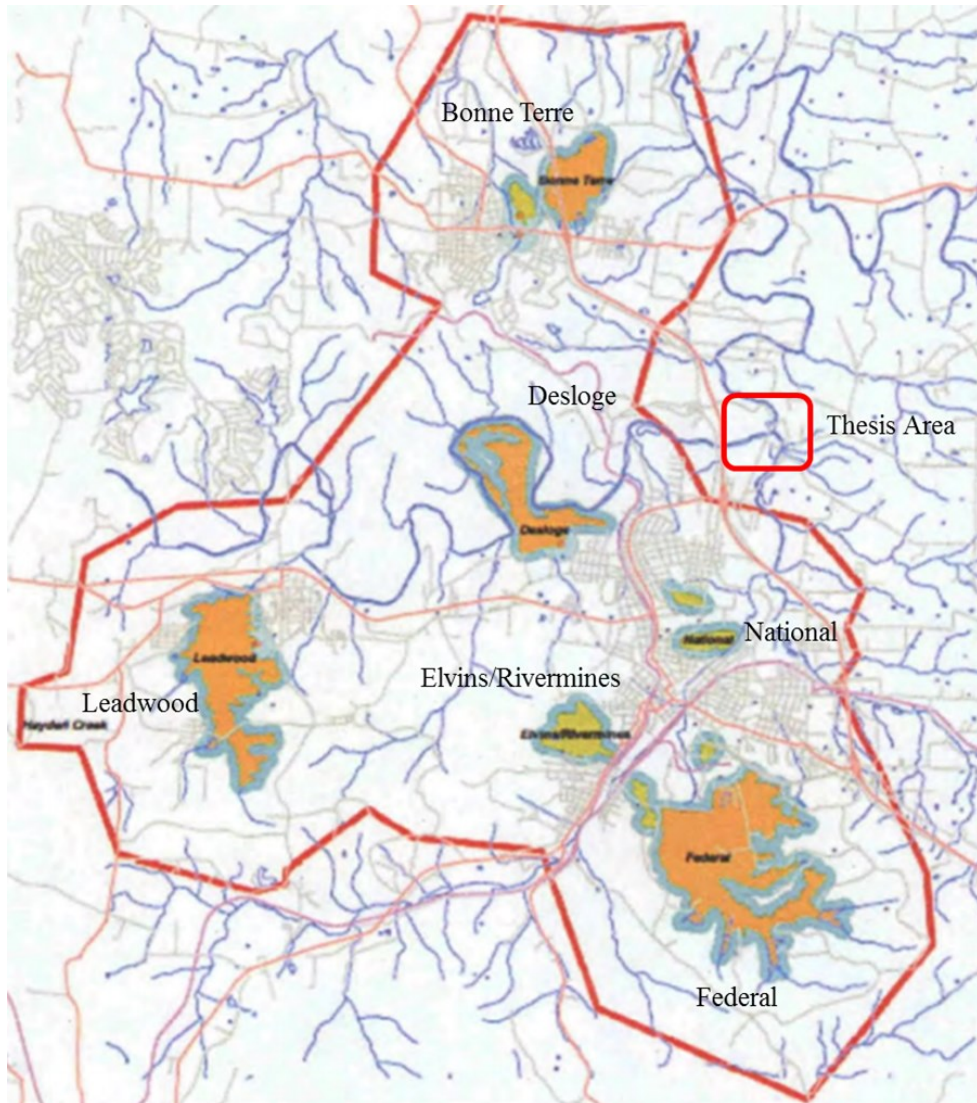


Figure 6 – The BRMT site and the 6 tailings piles that fall within it (USEPA, 2011).

Chat primarily composes the large piles of material throughout St. Francois County, while tailings compose the finer material impounded behind dam and berms (Moby et al., 2009; FWS, 2008). Since the waste material was placed, it has been contaminating the surrounding area due to transportation and erosion. The angular crushed limestone in chat piles has a steep angle of repose allowing miners to build the piles relatively high. When a tall chat pile has a slope failure it releases more material than a shorter pile would have. The largest release occurred in 1977. During this event large amounts of precipitation caused 50,000 cubic yards (yr³) of tailings to slump into the adjacent Big River (EPA, 2016; ITRC, 2010; Moby et al., 2009; FWS, 2008). In 1947, Davis Creek was dammed for supplementary tailings storage, the dam failed a short time later resulting in the release of thousands of tons of tailings into Davis and Flat River Creeks, as well as the Big River (Moby et al., 2009; FWS, 2008). The downstream effect of these contaminants can still be seen for the majority of the 93 miles the Big River travels (Moby, et al., 2009; FWS, 2008).

The contamination of sediments is well above the EPA standard of 400 parts per million (ppm) in bare soil play areas and 1,200 ppm for non-play areas (USEPA, 2001; ATSDR, 2010). The contamination at the BMRT ranges from 349 to 17,000 ppm (MDNR, 2016B; Moby et al., 2009; FWS, 2008). In 1992, the USEPA added the BRMT site to their National Priorities List by designating it as an EPA Superfund Site, and the Desloge site was named as the highest priority of the six sites (MDNR, 2016B; ITRC, 2010; Moby et al., 2009; FWS, 2008). The EPA began implementing remedial action and engineering remedial technologies in 1995, and continues remediation to present day (EPA, 2016; ITRC, 2010; Moby et al, 2009).

CHAPTER 2 – LITERATURE REVIEW

The purpose of this chapter is to review published works that are relevant to this study. This chapter begins with a background on natural and constructed riffles and looks at a study on how constructed riffles have been used for restoration. This chapter also looks at both sediment transport and deposition to give the reader a basic understanding of how the contaminated sediment within the channel may be moving. The chapter ends with a background on HEC-RAS modeling.

Riffle Structures

Natural riffles are geomorphic areas within a channel where the depth of the channel decreases, bed slope increases, bed material becomes coarse, and water moves quickly creating a disturbance on the surface at low flows (Lisle, 1982; Radspinner, 2009; Legasse et al., 2014). Natural riffles are commonly found in a riffle-pool sequence (Figure 7), and occur approximately every 5 to 7 channel widths along a stream, but can vary based on the bed and bank material (Leopold et al., 1964; Keller, 1978; Keller and Melhorn, 1978; Roy and Abrahams, 1980; Radspinner, 2009).

Constructed riffles have been used in the restoration and rehabilitation of aquatic habitats, however, using constructed riffles for remediation of contaminated sediment is a relatively new method. Due to increased water resource demands, river restoration and rehabilitation have become an important issue in society resulting in the creation and implementation of new restoration and rehabilitation designs (Fischenich 1994; Ferguson et al. 1998; Kondolf 1998; Walker et al., 2004). Walker et al. (2004) conducted a study

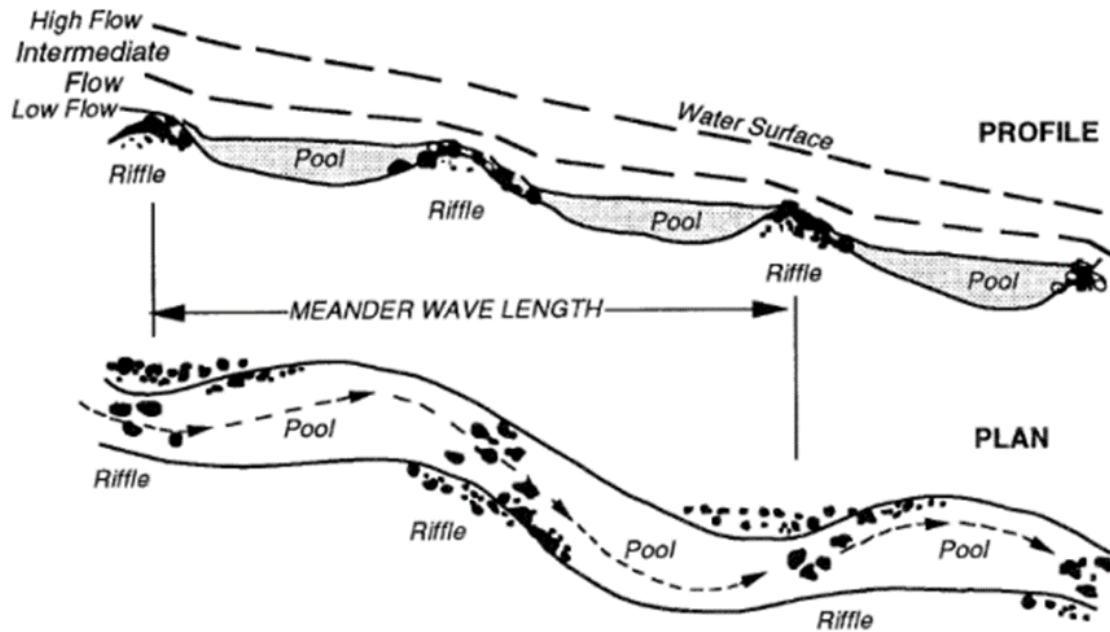


Figure 7 - Profile and plan depictions of a riffle-pool sequence (Newbury and Gaboury, 1993; Radspinner, 2009).

comparing energy profiles at constructed riffles. To do this, steel rods were placed throughout the constructed riffles as staff gages to record water surface profiles, as well as to be used in the determination of a Manning's n value. In their study, energy loss over the length of the constructed riffles varied between 50 and 100% of all energy loss in the channel (Walker et al., 2004; Radspinner, 2009). This energy loss is notable because constructed riffles have a significant effect on the overall sediment transport within a channel (Radspinner, 2009).

Sediment Transport

For sediment transport to occur in a stream or channel, a supply of sediment and energy to move it has to exist. Van Rijn (1984) defines bed load transport as rolling,

sliding, saltation (leaping), and suspension of particles (Figure 8). Sediment transport within a channel is largely dependent on sediment-water interactions. One property dictating sediment transport within a channel is the size of particles being transported (Hassanzadeh, 2012). Large material, such as cobble to boulder size, require more energy to move. Particle size is typically broken down into categories: clay, silt, sand, gravel, cobble, and boulder.

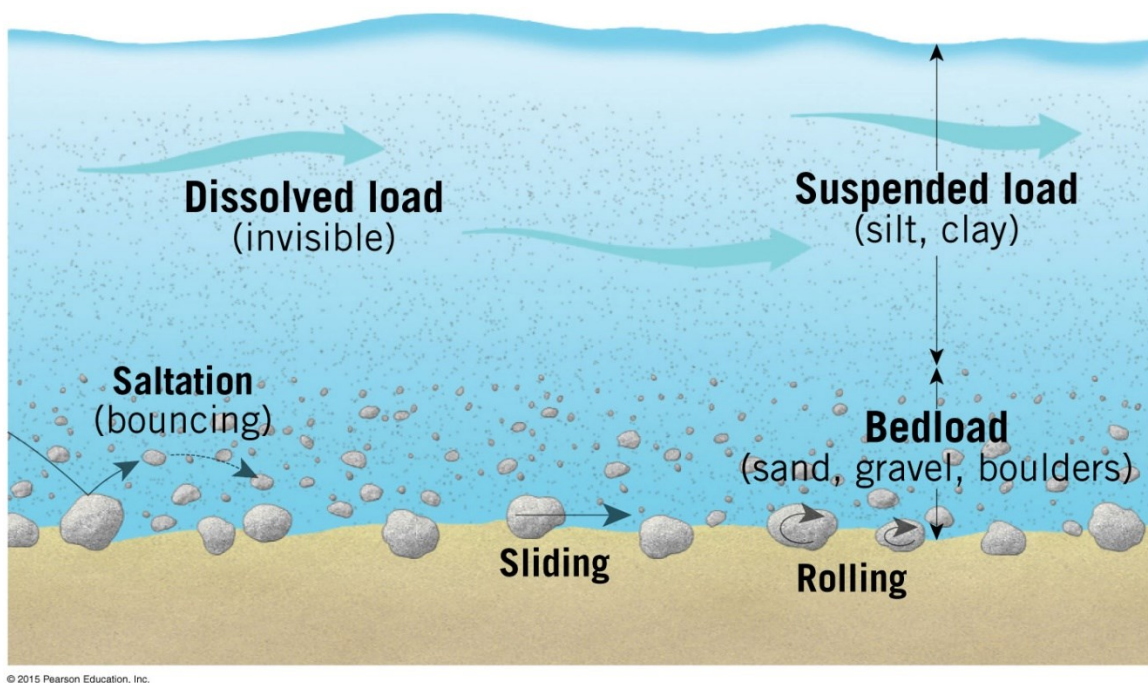


Figure 8 – Methods of sediment transport within a channel (Lutgens and Tarbuck, 2015).

The force needed to put a grain in motion is known as critical shear stress (Hassanzadeh, 2012). When a grain is on the surface of a bed it can be subject to multiple components that might cause it to move. One component is flow velocity. If the force created by flow velocity is higher than the critical shear stress on the particle, then the particle has a high probability of being transported (Hassanzadeh, 2012). However, the

critical bed shear stress can be affected when the channel bed is mixed. When the size of the bed materials are mixed, the larger particles can hide the smaller particles resulting in bed armoring (Hassanzadeh, 2012). Armoring of a bed consists of coarser sediment grains covering the surface of finer sediment on the streambed (Wilcock and DeTemple, 2005). The armoring of channel beds can result in the inhibition of sediment transport within a channel.

Sediment Deposition

Sediment deposition within a channel occurs for a variety of reasons such as increased sediment supply or decreasing water velocity within the channel (Lisle, 1982). According to Gibson and Boyd (2016), sediment deposition and accumulation is a common problem that occurs at dams and reservoirs. On the Niobrara River in Nebraska dam operators regularly deal with the effects of sediment deposition and accumulation. Along with past accumulation, after every sediment flush, the sediment replaces itself in the reservoir. At Spencer Dam, roughly 350,000 cubic meters (m³) of sediment entered the reservoir in the form of a prograding delta in the five months after a flush in 2014 (Gibson and Boyd, 2016).

On the Big River, near Desloge, Missouri, Owen et al. (2012), measured sediment accumulation behind a low-water crossing before and after sediment was excavated behind the crossing. Unlike the prograding delta that occurred on the Niobara River in Nebraska, on the Big River the sediment in the crossing had accumulated as a middle bar. That sediment was dredged, and surveys were taken fifteen days, twenty-four days, and six months after excavation following flooding events. With the analysis of survey data,

it was found that around 388 m³ of sediment was dredged from the site, but with the occurrence of one ten-year flood 80% of the sediment removed was replaced (Owen et al., 2012).

When a structure that decreases the velocity in a fluvial system is introduced, deposition is expected to occur. This type of deposition occurs in both large and small-scale fluvial systems as is illustrated above. Velocity plays a great role in both sediment transport and deposition, and one method that can be used to better understand the hydraulics of a channel is through modeling.

HEC-RAS Modeling

The USACE has a branch called the Hydraulic Engineering Center (HEC). HEC has created many models that allow users to model channels. In the early 1990's HEC developed a model that could be used on a Microsoft platform known as the River Analysis System (RAS) (Maeder, 2015). This model was known as HEC-RAS 1.0, and the USACE-HEC released updated software packages every few years including versions 1.1, 1.2, 2.0, 2.1, 2.2, 2.21, 3.0, 3.1, 3.11, 4.0, 4.1, 5.0, and the latest version 5.0.3 (Maeder, 2015; Goodell and Brunner, 2004). The older versions of HEC-RAS (1-4) allow users to model steady and unsteady flow computations, as well as sediment transport computations (Goodell and Brunner, 2004).

Steady flow computations allow users to calculate the water surface profiles where flow may vary over a reach, but flow stays the same over time (Goodell and Brunner, 2004; Bedient et al., 2008). With steady flow a user can model situations where flow is subcritical, critical, and supercritical (Goodell and Brunner, 2004). To model

these situations the energy conservation equation is the basic equation the model uses, and the variance in energy is attributed to friction loss using the Manning's Equation (Fan et al., 2012; Goodell and Brunner, 2004).

Unsteady flow computations allow users to determine water surface profiles when conditions change over time (Bedient et al., 2008). Unsteady flow analysis was developed to allow users to effectively model subcritical flows, but the newer versions allow users to model subcritical and supercritical flows as well (Goodell and Brunner, 2004). Because physical laws are what control the flow of water in a stream, the unsteady flow analysis uses the continuity equations as well as the momentum equation (Brunner, 2016B). These equations are used to conserve the mass of the water in the stream (continuity), as well as to conserve the momentum of the water within the channel (momentum) (Brunner, 2016B). The unsteady flow simulation allows users to successfully model hydraulic obstacles within a channel.

HEC-RAS 5.0, the newest 2D model uses the Navier-Stokes equation to represent water movement in three dimensions. However, when modeling the channel and flood events the equations are simplified averaging the incompressible flow, uniform density and hydrostatic pressure resulting in an approximated turbulent motion (Brunner, 2016B). HEC-RAS 5.0 allows users to perform all of the same evaluations, but they can be done in two dimensions and at quasi-steady or unsteady flows. The model also allows users to model interactions between the channel and floodplain that may be too intricate for the older 1D HEC-RAS models (Figure 9) (Knight and Shiono, 1996; Ervine and MacLeod, 1999; Sellin et al.; Pappenberger, et al., 2004). Unfortunately, modeling sediment transport within a channel using the 2D model can be difficult due to the hydraulics of

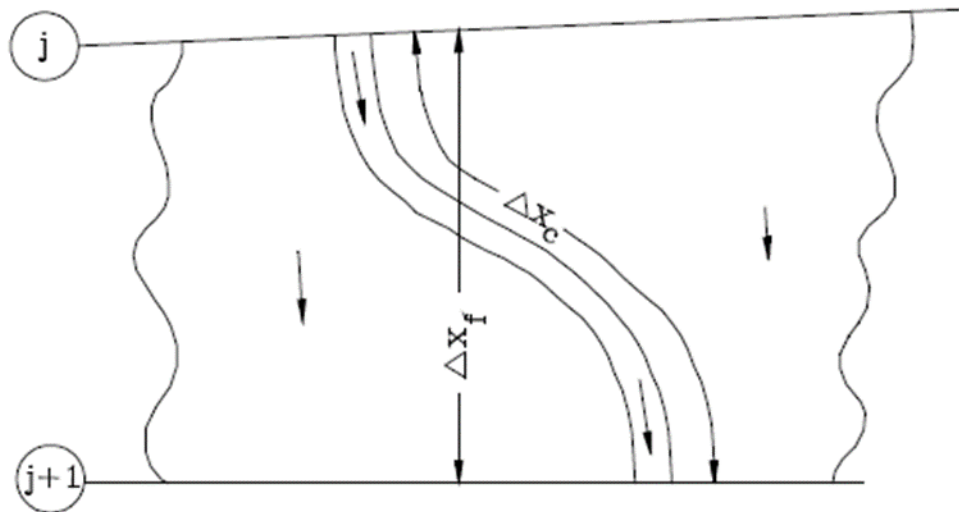


Figure 9 – Relationship between channel and floodplain flows within a 2-D model (Brunner, 2016A).

sediment transport. Sediment transport is a complex process where parameters are not always easy to determine in 2D flow areas, and may be better suited for 1D modeling (Brunner, 2016A). Sediment transport and moveable boundary computations allow users to simulate sediment movement throughout a channel the way a channel would sort and move sediment and armor the bed (Goodell and Brunner, 2004).

To effectively model the movement of sediment within a channel, the hydraulics of the model have to be calibrated correctly. 2D versions of HEC-RAS allow users to evaluate and predict rates of sedimentation and scour, which could be used to predict the rate and location of dredging at quasi-unsteady flows (Goodell and Brunner, 2004). The erosion or deposition of the channel bottom is only an average value, and does not reflect local changes.

CHAPTER 3 – METHODS

Chapter three will discuss the methods used to complete this study. First discussed will be survey methods used to create cross-sectional representations of the channel. After reviewing survey methodology, geochemical analysis will be discussed. The geochemical section will explain the collection of sediment samples, as well as laboratory analysis. The methodology behind the use of the USGS software, PeakFQ, and GIS will follow the geochemical analysis. The chapter will end with a review of the methods used to create a simulation of the hydraulics of the study area in the HEC-RAS model.

Surveying

To understand the effectiveness of the remediation structure, cross-sectional surveys of the channel were conducted. Survey posts and benchmarks were placed to maintain consistency of the channel surveys (Figure 10). Thirty-nine posts were placed, two (one on each bank) for the first 17 cross-sections, and one (only on the left bank) for the remaining cross-sections. Three cross-sections were placed downstream of the constructed riffle, two were placed on the constructed riffle (one at the bottom and one at the top of the riffle), and seventeen were placed upstream of the constructed riffle. The spacing between the cross-sections varied from 50-440 feet (ft) over the length of the channel due to where sedimentation was hypothesized to occur and limited visibility for surveying (Figure 11). Transects 1 and 3 ranged from 98 ft to 165 ft apart and cross-sections four and five were located adjacent to the riffle. The spacing between Transects



Figure 10 - An example of the posts and numbered signs used to set up survey transects.

6 through 10 varied between 50 ft and 65 ft. Transects 10 through 16 ranged between 50 ft and 82 ft apart. The remaining cross-sections ranged from 165 ft to 440 ft apart. To collect survey data a total station was primarily used, as well as an auto-level and a Real Time Kinematic (RTK) Global Positioning System (GPS) receiver. The RTK was used to survey the longitudinal profile of the channel. To observe changes within the channel, surveys were taken in August 2015, September 2015, December 2015, January 2016, June 2016, and November 2016.

The survey data collected was entered into Excel, and manipulated to observe and analyze changes in storage for each cross-section. Cross-sectional survey results were overlain with corresponding cross-sections to observe deposition and erosion over time.

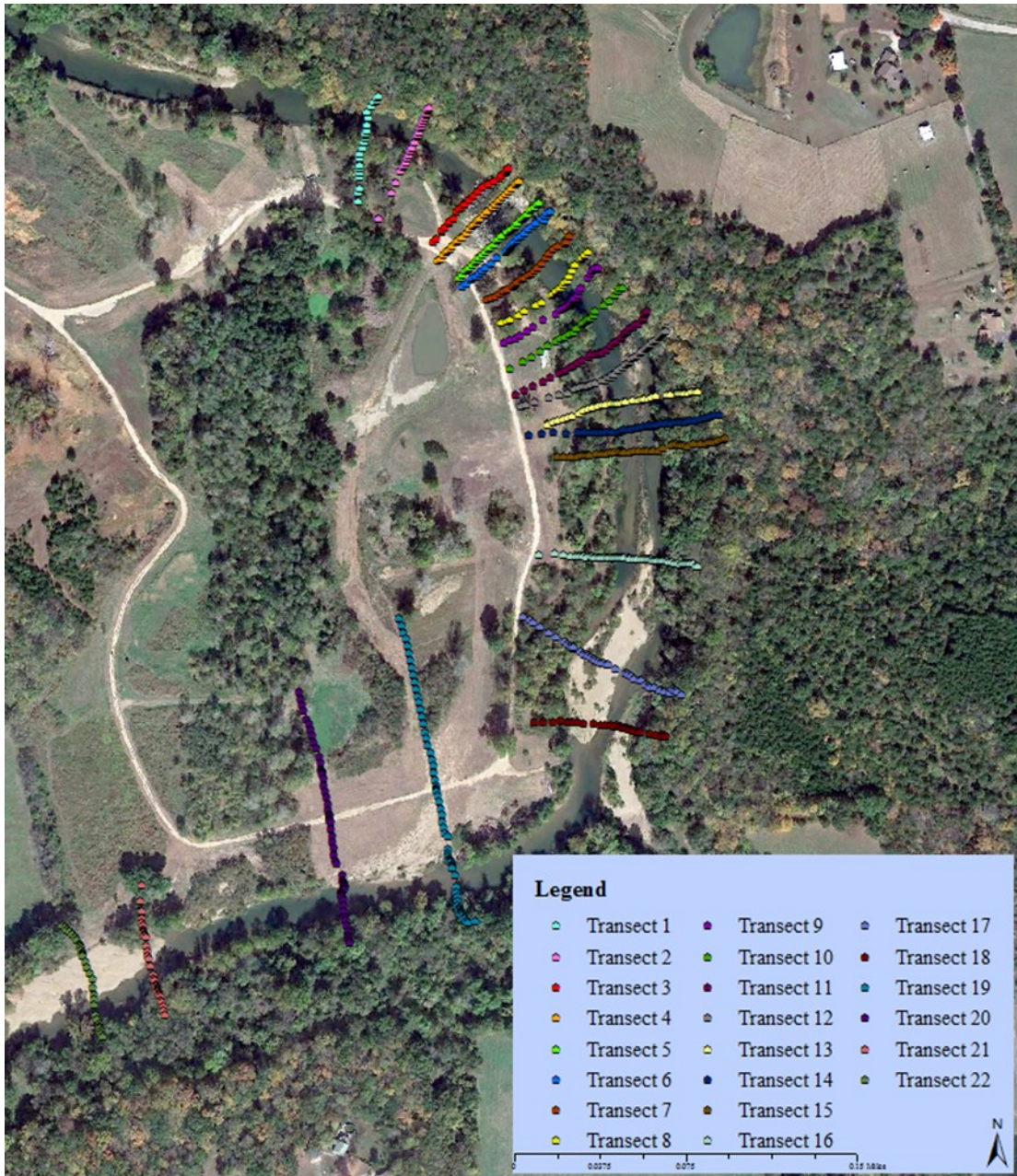


Figure 11 - Location of the Transects 1-22 used to collect cross-sectional survey data.

Geochemical Analysis

Due to the history of contamination within the study area, sediment samples were collected to assess levels of lead (Pb) and zinc (Zn). Thirty-eight total sediment samples were collected in September 2015 and November 2016. The 20 samples collected in September 2015 were collected from either bar or channel, and a GPS camera was used to record the location of each sample. The 18 samples collected in November 2016 were collected from within the channel, and a Trimble GPS unit was used to record the location of each sample. These samples were collected using a shovel and bagged in plastic freezer bags that were labeled with the date and sample identification. Figure 12 shows the location of the sediment sample sites.

To prepare the samples for x-ray fluorescence (XRF) analysis, samples were left in freezer bags and dried in a drying oven set at 60 degrees Celsius (°C). After drying, samples were sieved down to less than 250 micrometers (μm) and bagged in lead-free bags with sample ID and date.

Analysis for Pb and Zn was completed with an X-MET3000TXS+ Handheld X-Ray Fluorescence (XRF) Analyzer. To control and assure the quality of results from analysis standards, blanks, and duplicates were ran with samples. The standard used for this study was the USGS Jasperoid, GXR-1 standard, with a known Pb concentration of 856ppm. The method detection limit for Pb and Zn for the handheld XRF are 15 ppm and 8 ppm, respectively

Standards and blanks are used to ensure performance of the instrument was accurate and to ensure that no outside contamination was introduced to samples, respectively (OEWR, 2007). For the 20 samples collected in September 2015 a standard

and blank were analyzed at the beginning of the run, after the 10th sample, and at the end of the run. For the 18 samples collected in November 2016 a standard and blank were analyzed at the beginning of the run, after the 9th sample, and at the end of the run.

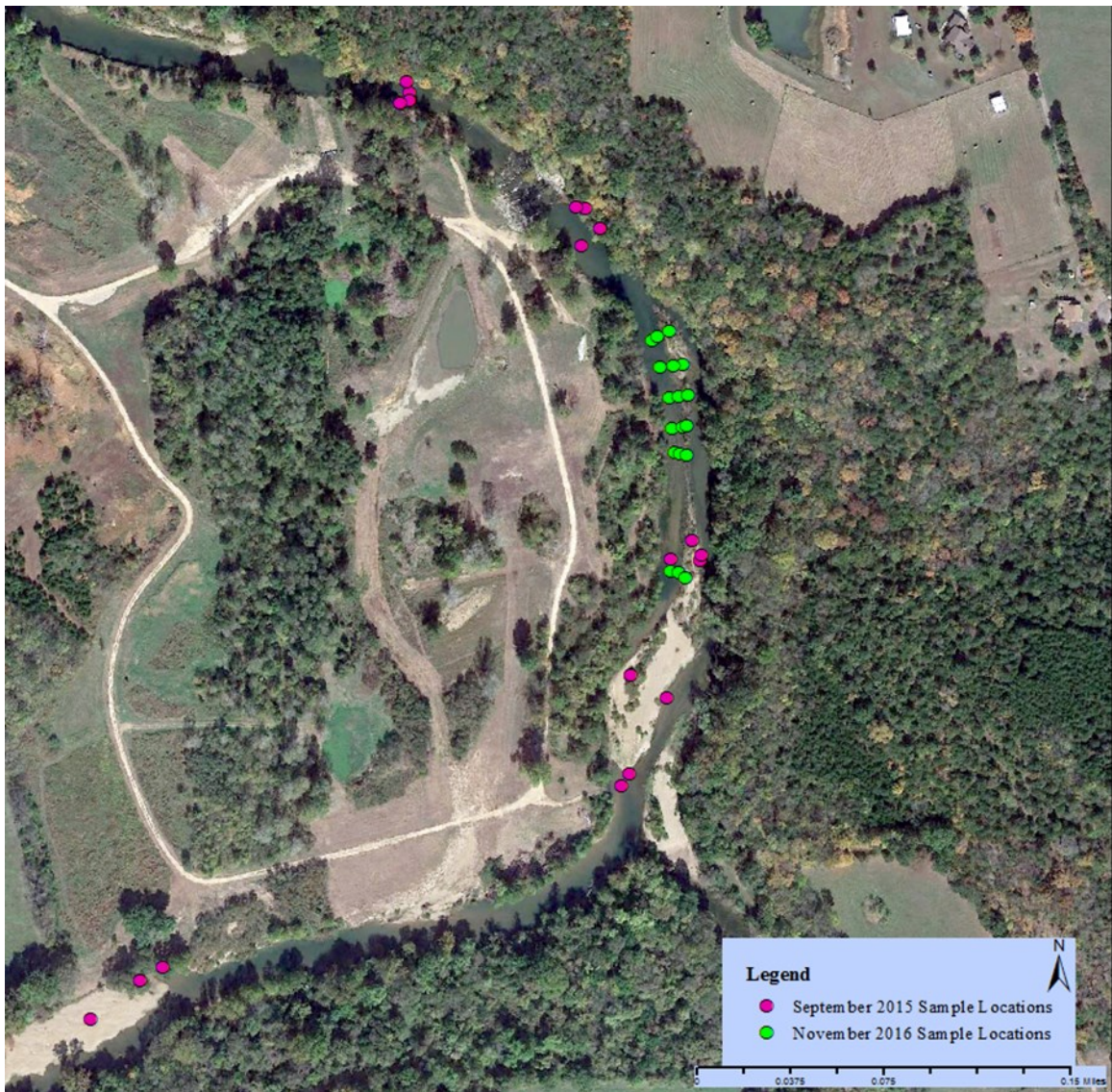


Figure 12 - Location of the sediment samples collected in September 2015 (pink) and November 2016 (green).

Laboratory duplicates are used to ensure the precision of the instrument and to evaluate for errors (OEWR, 2007). A laboratory duplicate for the 20 samples collected in September 2015 was analyzed for the 10th sample. A laboratory duplicate for the 18 samples collected in November 2016 was analyzed for the 9th sample.

PeakFQ Analysis

A USGS stream gage located just upstream of the study site and will be referred to as the USGS gage below Desloge. The gage below Desloge did not contain a long enough record to accurately estimate large recurrence interval events or to estimate the recurrence interval for events that were recorded during the study.

Several flood events occurred during the monitoring period. The USGS software PeakFQ was used to assess the recurrence interval of these flood events and determine the flow rate of larger return period events. The peak annual flood data was downloaded from the USGS gages on the Big River at Irondale, Richwoods, and Byrnesville. These gages were chosen because they held ~50 years of data or more and are either up or downstream of the study site. The data from these three gages was analyzed with PeakFq to determine flow rates of specific recurrence interval events.

The recurrence intervals and associated discharges produced by PeakFQ were used to compare the discharge, measured in cubic feet per second (cfs), for Irondale, Byrnesville, and Richwoods against the size of the drainage area in square miles (sq. mi.). Using the drainage area of the USGS gage below Desloge and the data from PeakFq, the discharge was interpolated for each recurrence interval on the Big River below Desloge. The discharges produced from this interpolation were later used for HEC-RAS modeling.

GIS

Maps of the study area containing field data were created using Light Detection and Ranging (LiDAR) Digital Elevation Model (DEM) data. The LiDAR DEM for St. Francois County, the location of the study area, was collected between December 2010 and April 2010, before construction occurred at the study area. The LiDAR DEM was downloaded from the Missouri Spatial Data Information Service (MSDIS).

In ArcMap 10.4.1 the resolution of the DEM was converted from meters to feet, and the coordinate system was changed to Missouri State Plane East. For faster processing, the DEM was extracted to contain only the relevant study area. An aerial image was added from base maps provided by Environmental Systems Research Institute (ESRI). This DEM represents the study area before construction of the basin and riffle occurred.

To represent the landscape after construction the original DEM needed to be altered to create an accurate representation of the current site. The original DEM from the MSDIS was again converted to feet, the coordinate system was changed to Missouri State Plane East, and the DEM was extracted to contain the study area. To accurately portray the basin a DEM from related GPS surveys was obtained from the Ozarks Environmental and Water Resource Institute (OEWRI) database and was mosaicked with the MSDIS LiDAR DEM.

The before and after construction DEMs were created to be used in HEC-RAS modeling. To ensure the compatibility of the DEMs with HEC-RAS the DEMs were exported as Tagged Image File Format (TIFF) images. Both the before and after construction DEMs with hillshade can be seen in Figure 13 and 14, respectively.



Figure 13 – Pre-construction DEM with hillshade.

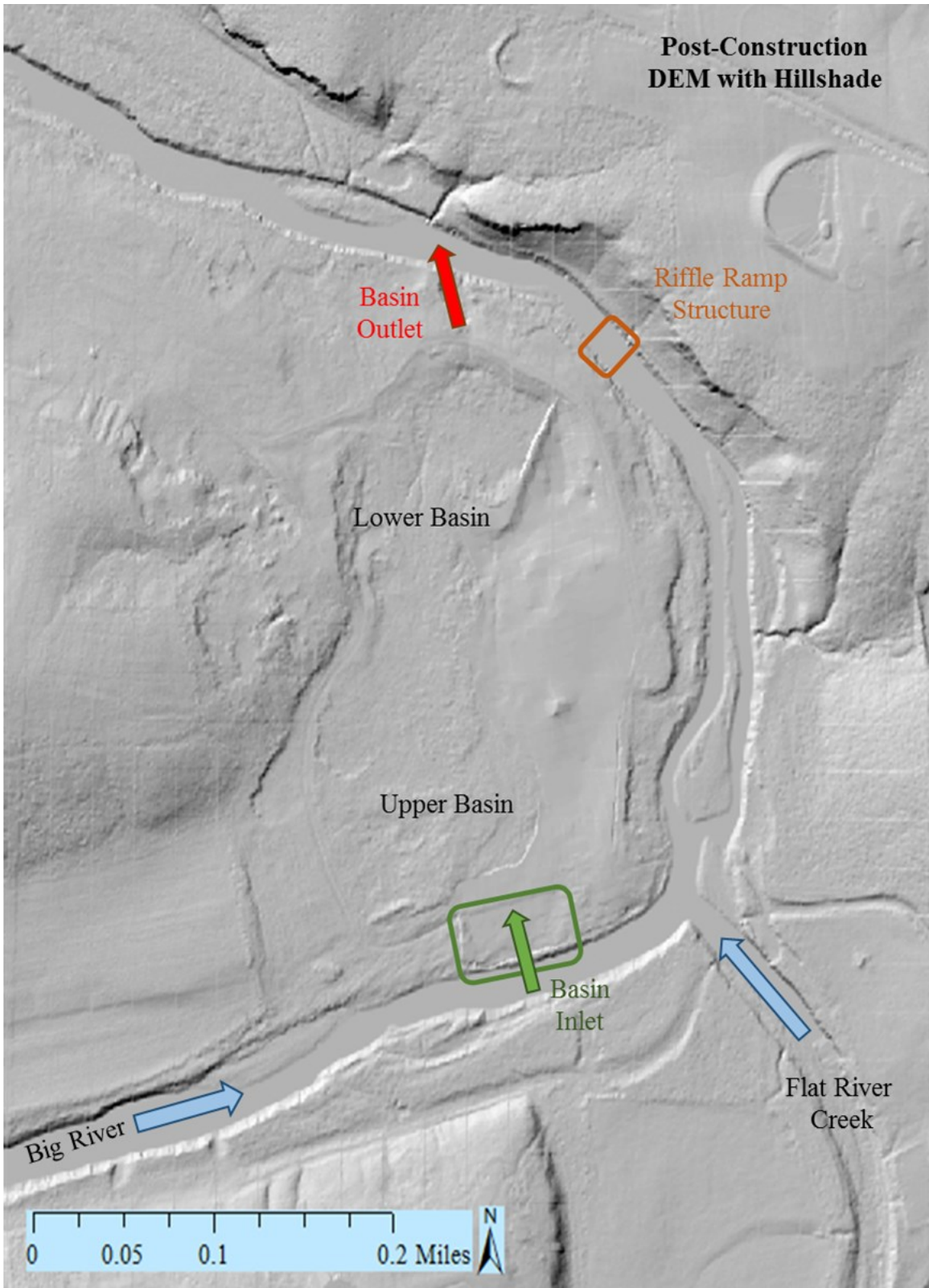


Figure 14 – Post-construction DEM with hillshade.

HEC-RAS Modeling

Flow patterns and velocities within the study area were modeled using HEC-RAS 5.0.3. Two-dimensional (2D) modeling of the Big River required the creation of a terrain layer, creation of a 2D flow area, determination of the most efficient mesh size for the 2D flow area, the addition of a land use layer, and determination of a viable Manning's n for the channel. These components were used to model recurrence interval discharges from PeakFQ interpolations.

Two terrain layers were created from TIFF images produced in GIS: a pre-construction terrain layer and a post-construction terrain layer. To create the pre-construction terrain layer, the before construction TIFF image was imported into HEC-RAS via the RAS Mapper. To create the post-construction terrain layer, the after construction TIFF image was imported into HEC-RAS via the RAS Mapper. Additionally, to create the best representation of the landscape and channel, the survey data for each transect was imported into the post-construction terrain layer. The survey data was used to interpolate the shape of the channel between each transect. These interpolations were exported as their own TIFF image. To create a cohesive terrain layer that included both the basin area and the survey interpolations the TIFF images for both were imported together.

To set parameters of the area that was used in the model, 2D flow areas were added to both TIFF images. These areas work to confine the simulation of water to the channel and surrounding areas defined by that flow area (Figure 15). For a more accurate, realistic representation break lines were added to the model. Break lines represent obstructions to flow such as roads, high ground between the channel and floodplain or

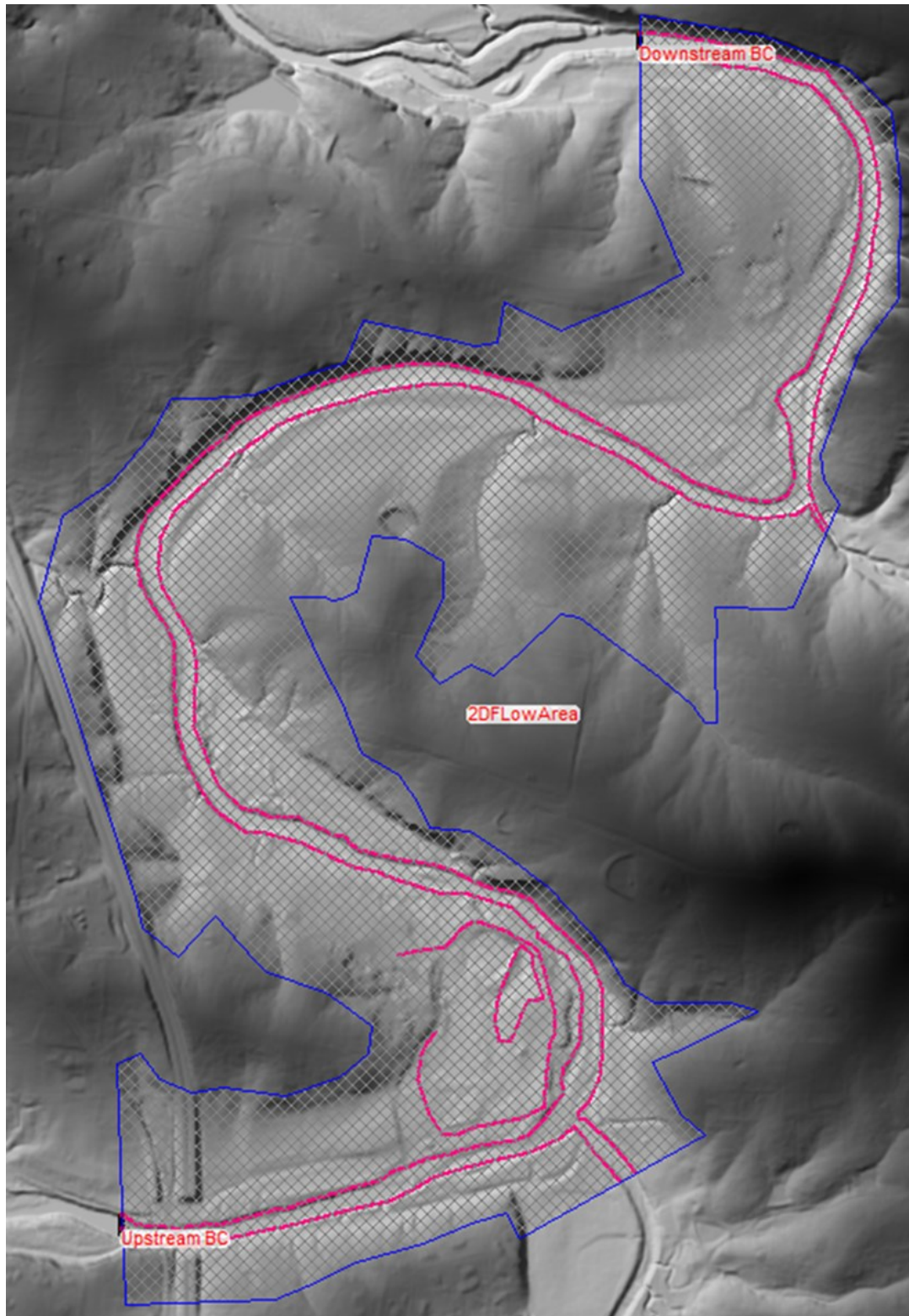


Figure 15 - 2D flow area (blue outline) used in the HEC-RAS modeling of the Big River. Red lines are break lines, which are linear features that are hydraulically important.

natural levees (Brunner, 2016). Using break lines in a 2D flow area forces the cell boundaries to occur along the flow obstructions mentioned above (Figure 16). After the 2D flow area was set, a 2D computation mesh is created for the flow area. The number of cells that compose the mesh are directly related to the processing speed of the model. The use of many cells within the mesh might increase the accuracy of the model, but will take more time to solve. Adding more cells than necessary to does not increase accuracy, but does increase the time of solution. It is important to determine the mesh size that will reduce processing times and produce accurate water surface elevations. Mesh size was determined by running a fixed hydrograph through the post construction 2D area and reducing mesh grid size, from 50, 25, 15, 9, to 5ft² until no significant changes in water surface elevation were observed. Figure 17 shows an example of the varying mesh sizes that were used.

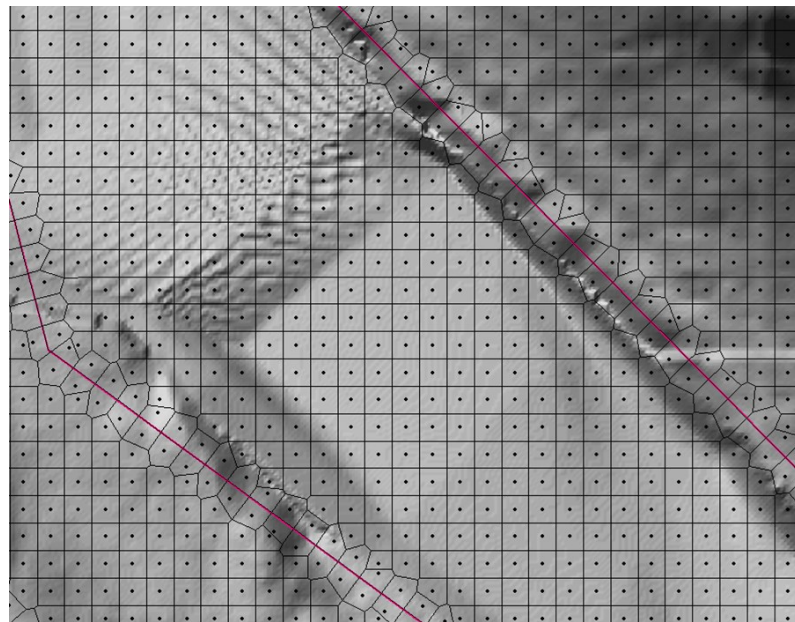


Figure 16 - 9'x9' Mesh shape at the riffle structure. The interaction between the break lines (pink) and the mesh can be seen in how the break lines dictate the shape of the mesh around them. The break lines indicate the location of a natural levee.

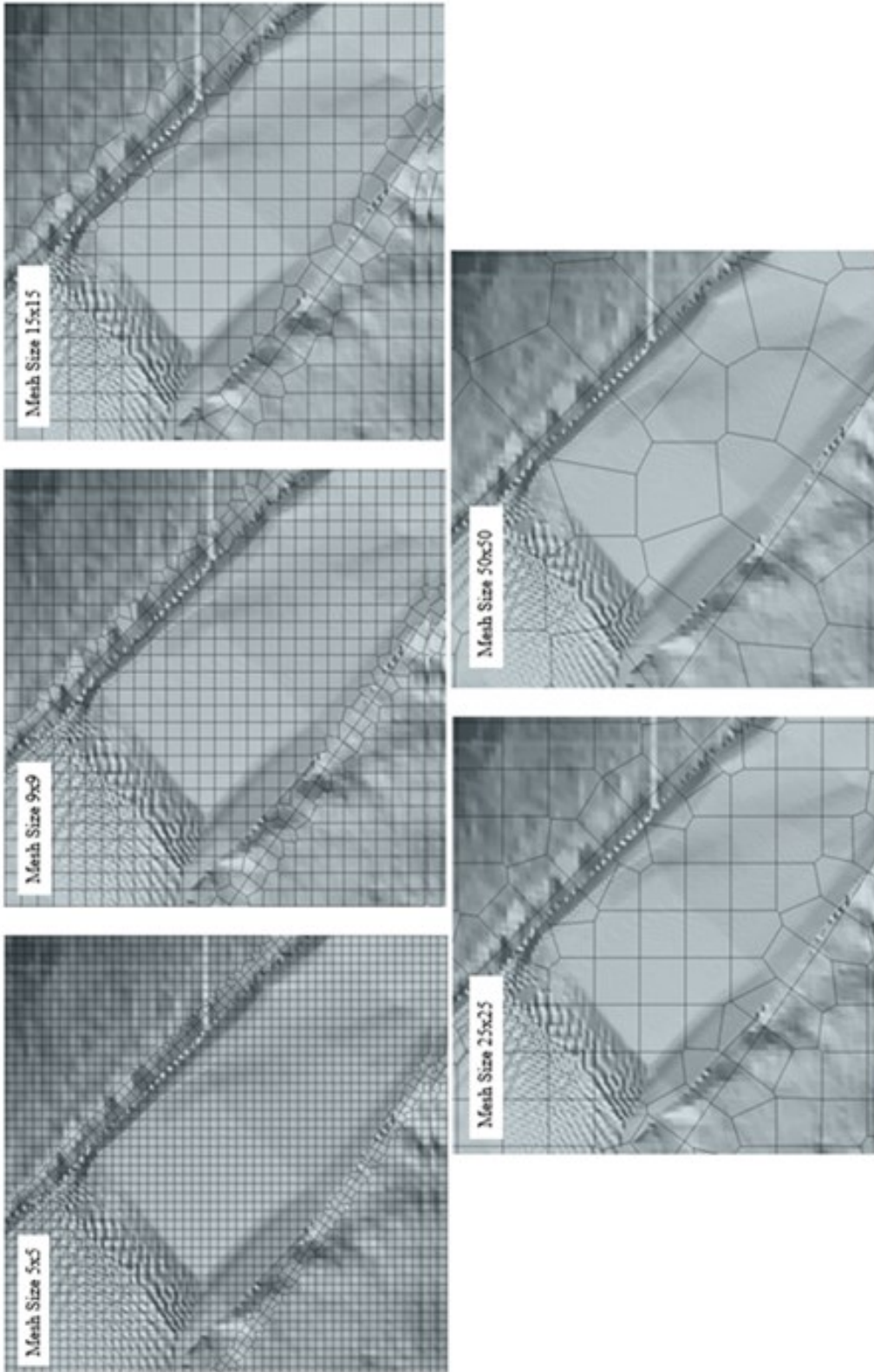


Figure 17 – Mesh sizes used to determine the mesh size for the final model simulations.

To create a model that matched field observations, a land use layer was imported into RAS Mapper (Figure 18). The land use layer allows the user to assign different Manning roughness coefficients according to land uses within the 2D flow area. To determine the Manning's n value that accurately represents what was observed in the field, the model was run with a known discharge corresponding to a measured water elevation while the Manning's n value in the channel was changed from 0.025, 0.030, 0.035, 0.040, to 0.045 to determine the value that most closely represented field measurements. The Manning's n values modeled were chosen from Chow, 1959.



Figure 18 - Land use layer and defined Manning's n layer used for HEC-RAS modeling.

Once the appropriate mesh size and Manning's n value were determined, several flood scenarios were simulated to evaluate the hydraulics of the system. These simulations are helpful in qualitatively and quantitatively evaluating the effectiveness of the lead mine tailings remediation. The 5, 10, 20, 50, and 100-year floods were modeled in HEC-RAS for before and after conditions.

CHAPTER 4 – RESULTS AND DISCUSSION

The purpose of this chapter is to present the survey, geochemical, and modeling findings that are used to answer the questions presented in Chapter 1: Is the riffle structure effective at trapping and storing sediment; is the sediment within the channel contaminated with lead, and if so what are the levels of contamination; and can HEC-RAS modeling be used to model what is happening in the study area. The results from the collected survey data will be grouped to evaluate the change that occurred. The presentation of the survey results will be followed by the discussion of the results and their implications. The results from the geochemical analysis of the sediment samples will be presented, followed by the discussion of the implications. Chapter 4 will end with the presentation of the HEC-RAS modeling results and discussion.

Survey Results

This section of Chapter 4 will evaluate the results of the surveys completed from August 2015 to November 2016. It was hypothesized that Transects 1-5 would undergo little to no change due to their location on or downstream of the riffle structure and that Transects 6-9 would contain the majority of deposition due to their location just upstream of the riffle structure. To evaluate the change that occurred Transects 1 through 22 will be placed in groups that best represent the results from the cross-sectional comparisons. An example figure will be used to represent the changes in each group. These evaluations will be followed by two transects that tell a clear story of how the channel changed

between August 2015 and November 2016. The survey data for each transect can be found in Appendix A.

No change. The results of the comparisons of collected survey data show and field observations show transects 2, 3, 4, 5, 6, 7, 9, and 15 underwent minor to no changes during the time of the study (Figure 19). Transect 2 is downstream of the riffle structure and Transects 3-5 are on the riffle structure. On Transects 2-5 data supported the hypothesis. The data for transects 6-9 did not support the hypothesis made, deposition did not occur as expected.

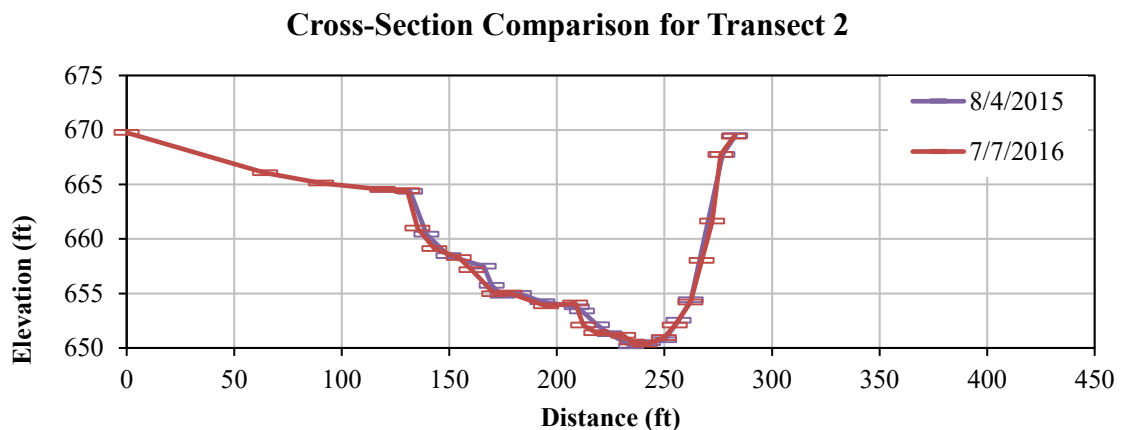


Figure 19 – Example of cross-section survey that showed little to no change along its transect.

Only erosion. The comparisons of the collected survey data show Transects 1, 21, and 22 underwent erosion (Figure 20). Transect 1 was hypothesized to undergo little to no change. Transects 21 and 22 are the most upstream transects. The erosion that occurred on Transect 1 and 22 occurred on the bars along the left bank, while the erosion that occurred on Transect 21 occurred on the toes of both the left and right bank.

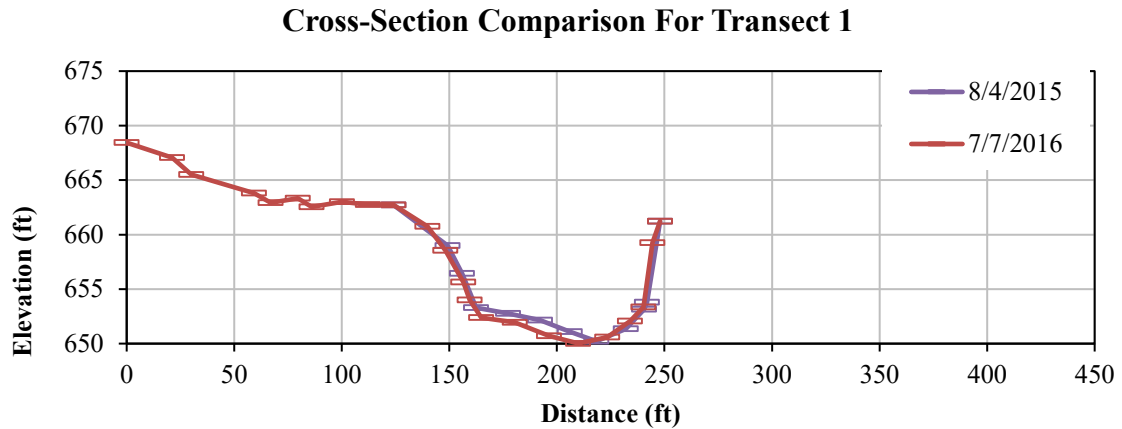


Figure 20 – Example of cross-section survey that showed only erosion along its transect.

Only deposition. Comparisons of survey data and field observations show that Transects 8, 10, 14, 16, and 17 underwent depositional changes along their transects (Figure 21). Transect 8 was hypothesized to undergo deposition, and the results partially confirmed this hypothesis. The deposition on Transect 8 was expected to occur in the channel, however, it occurred as a natural levee on the left bank. The deposition that occurred on transect 10 occurred along the toe of the left bank. On Transects 14 and 17 the deposition occurred on bars, center and right bank, respectively. The deposition that occurred on Transect 16 occurred in the chute along the left bank and on the center bar.

Erosion and deposition. A number of transects underwent both erosion and deposition from August 2015 to November 2016 (Figure 22). These transects were 11, 12, 13, 18, 19, and 20. Transects 11-13 have a chute on the left side channel, a center bar, and the thalweg on the right of the center bar. The deposition that occurred on these transects occurred in the chute and on the bar, while erosion occurred in the thalweg. Transect 18s cross-section is slightly different containing the beginning of the chute on

the left bank, a bar and a natural riffle in the center, and a bar along the right bank. On Transect 18 erosion occurred in the chute while deposition occurred on the bars. Transect 19 and 20 are located on the basin inlet. On both Transect 19 and 20 the top of the left bank was eroded. Transect 19 had deposition along the toe of the left bank and Transect 20 had deposition along the toe of the right bank.

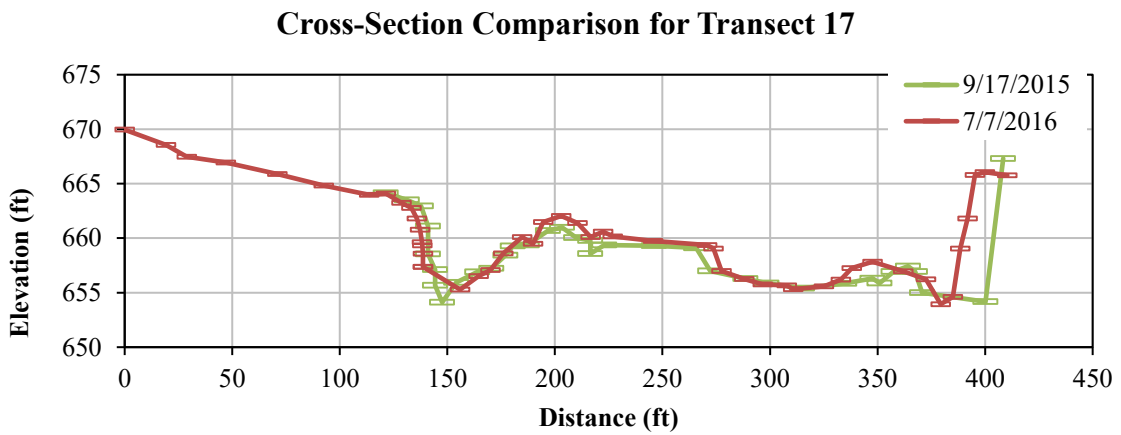


Figure 21 – Example of cross-section survey that showed only deposition along its transect.

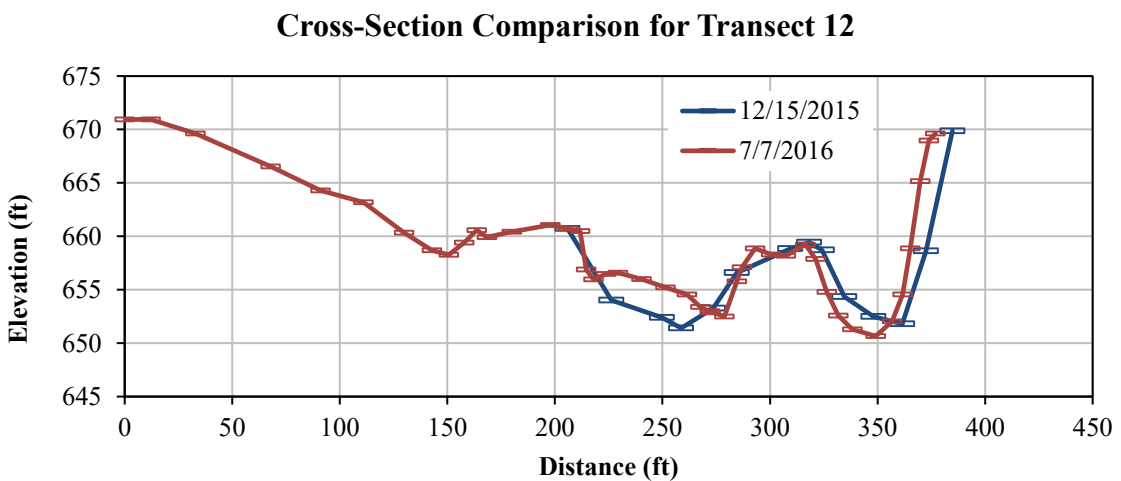


Figure 22 – Example of cross-section survey that showed both erosion and deposition along its transect.

Comparisons of data. Transect 10 and 13 both tell a clear story of changes that occurred over time that matched what was observed in the field. Transect 10 shows deposition in the chute along the left bank (Figure 23). From September 2015 to July 2016 an average depth of 2 ft of deposition occurred in the chute. The change that occurred between September and December 2015 was minor. In late December 2015, after surveying, a large flood (~20,000 cfs) moved through the study area. That flood could be the contributing factor in the deposition observed between December 2015 and July 2016.

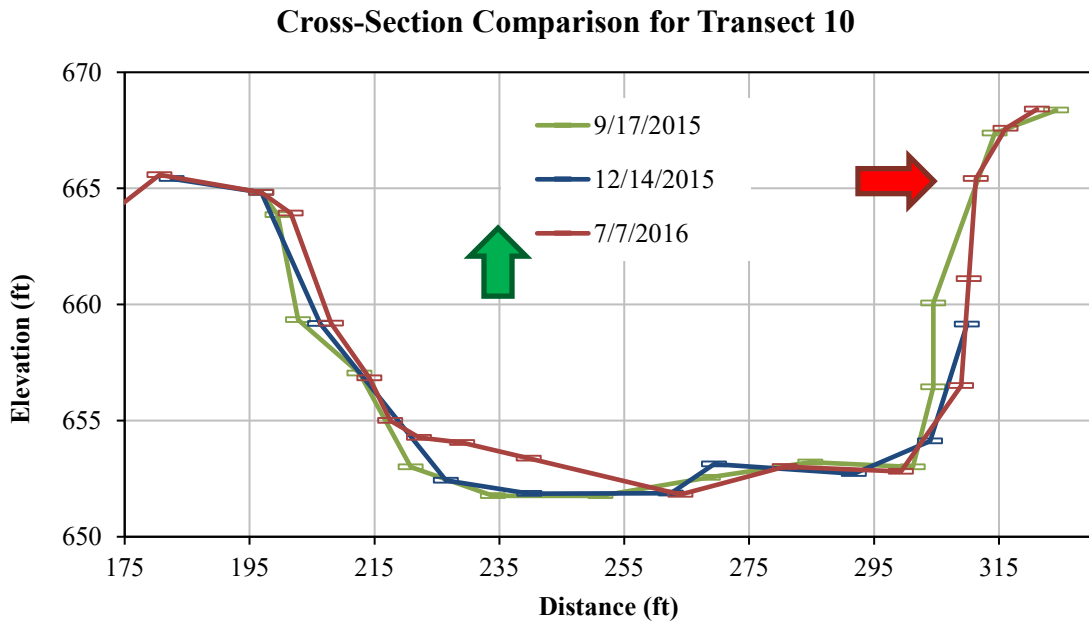


Figure 23 - A comparison of the cross-sectional data used to represent the change that has occurred on Transect 10 where the green arrow indicates deposition and the red arrow indicates erosion.

The cross-sectional comparison of Transect 13 shows a story of both erosion and deposition (Figure 24). The change in the chute on the left side of the channel is primarily deposition with the most deposition occurring between December 2015 and July 2016. On the right side of the channel it can be seen that primarily erosion occurred. The channel seems to have had a proclivity toward depositing in the chute and eroding in the main stem of the channel, and the December flood seems to have aided in this.

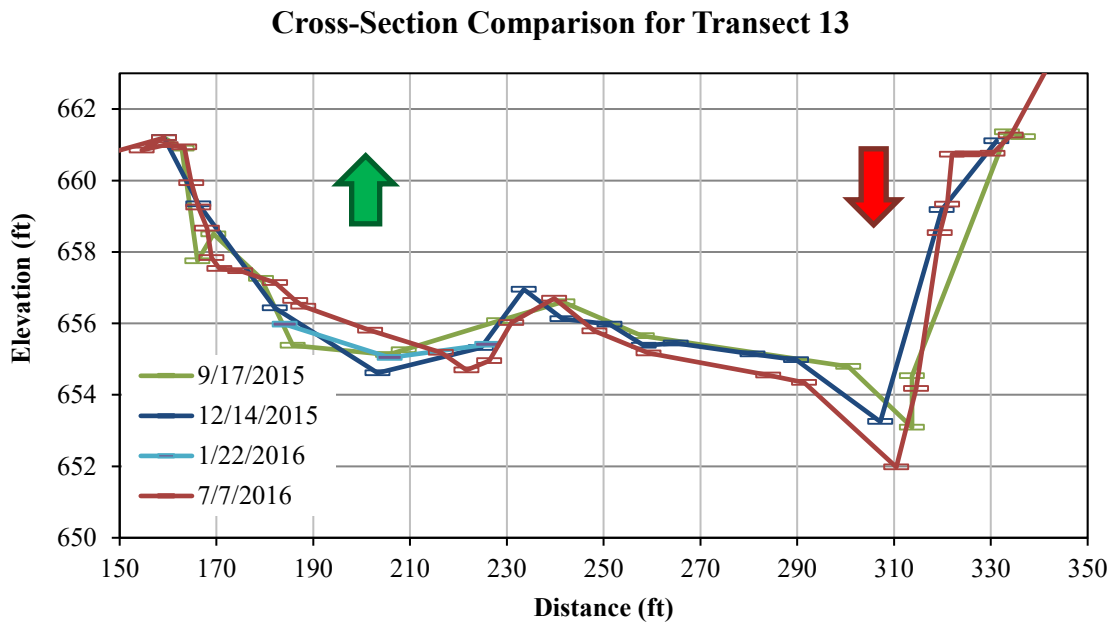


Figure 24 - A comparison of the complete cross-sectional data used to represent the change that has occurred on Transect 13 where the green arrow indicates deposition and the red arrow indicates erosion.

Survey Discussion

Discussion of results. Survey results show the riffle structure has been effective at storing sediment in the channel. The majority of sediment was hypothesized to be stored along Transects 6-8, however the results indicate that approximately 62,000 cubic feet

(ft³) of sediment is being stored in the chute and on bars along Transects 10-16 (Figure 25 and Table 1). It is possible that over a longer period of time deposition would increase downstream toward Transects 6-8. If deposition does not increase downstream, the USEPA will need to adjust dredging plans accordingly. It is possible that significant deposition directly upstream of the structure occurred after construction and installation of the riffle, but before the first round of surveying occurred. Therefore it can be said that the constructed riffle is modestly successful because it is storing sediments, however that storage is not occurring where it was hypothesized to occur. Further monitoring will need to be completed to determine the pattern of deposition and if the riffle structure is a successful remediation technique in the long term.



Figure 25 – Area between Transects 10-16 where the majority of deposition occurred (green circle).

Table 1 – Channel sediment storage within region identified with the most deposition.

Transect #	Area (ft ²)	Length (ft)	Volume (ft ³)
10	50	70	3488
11	165	70	11533
12	133	75	9986
13	18	78	1412
14	5	60	315
15	0	154	0
16	138	255	35165
TOTAL			61898

Discussion of possible error. Survey errors within the datasets could be attributed to a number of things such as human error, surveying at high discharges, or missing poles. Inexperience can play a significant role in causing human error while collecting data. Inexperience of field assistants can lead to missing important geomorphic features while surveying which can lead to errors within the dataset. Inexperience of field assistants while using instruments can also affect the accuracy of data, introducing errors. Examples of this are magnified when using an auto level. Auto levels require surveys to be taken on the line for each transect and they require reading a stadia rod. Surveys taken offline or misreading stadia rods introduce error into datasets.

Survey at high discharges can also introduce errors. When surveying at high discharges, walking transect lines became impossible, and the surveys had to be taken from a canoe. This resulted in important data points being missed and lower accuracy.

Posts were important for maintaining survey consistency. Posts could not be installed after cross-section 17 due to high banks and lack of access to property. Not installing two posts for every transect could contribute to error within the datasets.

Geochemical Results

Thirty-eight sediment samples were collected from the channel and bars of the Big River in September 2015 and November 2016. These samples were analyzed via XRF to determine the concentrations of Pb and Zn. The complete set of these results can be found in Appendix B.

September 2015 Samples. The samples collected in September 2015 were checked for accuracy and precision, as well as analyzed to determine the concentrations of Pb and Zn. The results of the evaluation for accuracy (n=3) showed that the accuracy for Pb was 0.60% and Zn was 5.53%. The check for precision (n=2) revealed that the precision for Pb was 0.85% and Zn was 1.92%. Both the checks for accuracy and precision fell below the limit of 20%, therefore passing.

Through XRF analysis the concentrations of Pb and Zn were found for the September 2015 samples. The maximum concentration of Pb (4955 ppm) being collected from mid-bar on Transect 17 and the minimum concentration of Pb (924 ppm) being collected from the bar tail on Transect 1. The maximum concentration of Zn (2800 ppm) was collected from mid-bar on Transect 22 and the minimum concentration of Zn (658 ppm) was collected from the bar tail on Transect 16 (Figure 26).



Figure 26 – September 2015 minimum and maximum Pb and Zn locations.

November 2016 Samples. The samples collected in November 2016 were evaluated for both accuracy and precision and analyzed via XRF to determine their concentrations Pb, and Zn. The evaluation for accuracy (n=3) showed the accuracy for Pb was 4.48% and Zn was 1.81%. The check for precision (n=2) revealed that the precision for Pb was 1.98% and Zn was 2.09%. Both accuracy and precision for the November 2016 samples fell under the 20% needed to pass.

The concentrations of Pb and Zn for November 2016 were found via XRF analysis. The maximum concentration of Pb (2400 ppm) was collected from the center of the chute on Transect 13 and the minimum concentration of Pb (1214 ppm) was collected from the right side of the chute on Transect 16. The maximum concentration of Zn (3126 ppm) was collected from the center of the chute on Transect 13 and the minimum concentration of Zn (792 ppm) was collected from the right side of the chute on Transect 13 (Figure 27).



Figure 27 – November 2016 minimum and maximum Pb and Zn locations.

Geochemical Discussion

Discussion of errors. The evaluation of precision resulted in the relative percent difference being higher for the September 2015 sample than for the November 2016 samples. Due to relative percent differences between duplicate samples being >20% for multiple XRF analyses, the samples were run multiple times. On the first run the sediment samples for September and November were sieved to <2 (millimeters) mm, and the <2 mm fraction was analyzed with the XRF. The resulted precision was >20%, therefore failing the evaluation for precision. To remedy this, the samples were sieved to < 250 μ m, and the < 250 μ m fraction were run through the XRF. On this run, both the September and November samples passed the precision evaluation.

General Discussion. Through geochemical analysis it can be seen that the sediment within the channel is contaminated with Pb and Zn. The lead-contaminated sediment appears to have the greatest concentrations upstream, around Transect 17 and 18 and slowly decreases downstream (Figure 28). The concentrations of Zn (ppm) found in sediment appears to be highest between Transects 18 and 22 (Figure 29).

High levels of lead were found in sediments that were collected from Transects 11-16, where the majority of deposition is occurring. However, the <250 μ m sample comprises approximately 2.3% of the total sediment stored within the channel. Therefore it appears that deposition and lead concentrations are correlated, but the <250 μ m sample represents a relatively low percentage of the total channel sediment.

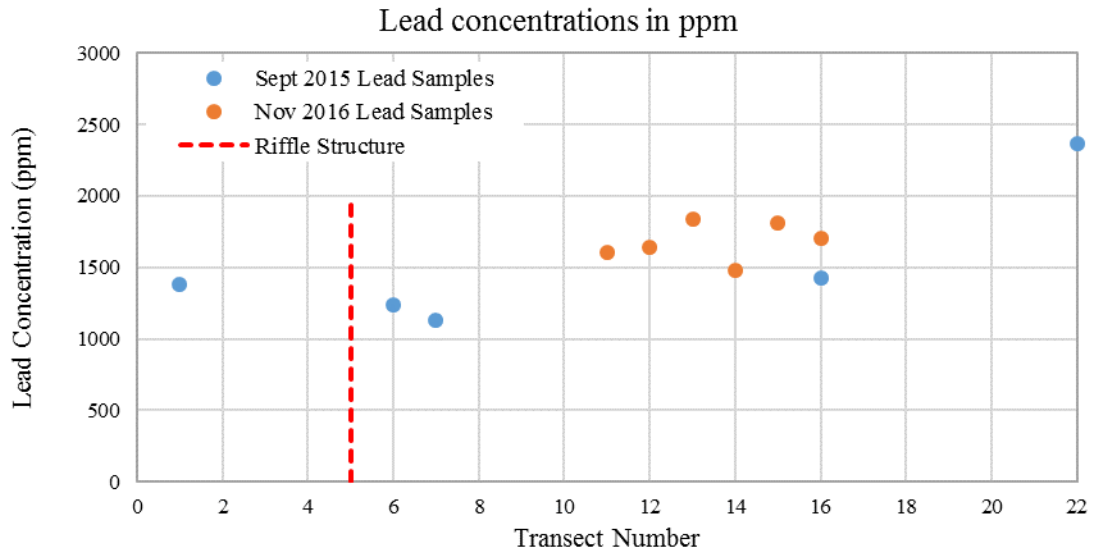


Figure 28 – The concentrations of Pb (ppm) in found in sediment collected from the above transects.

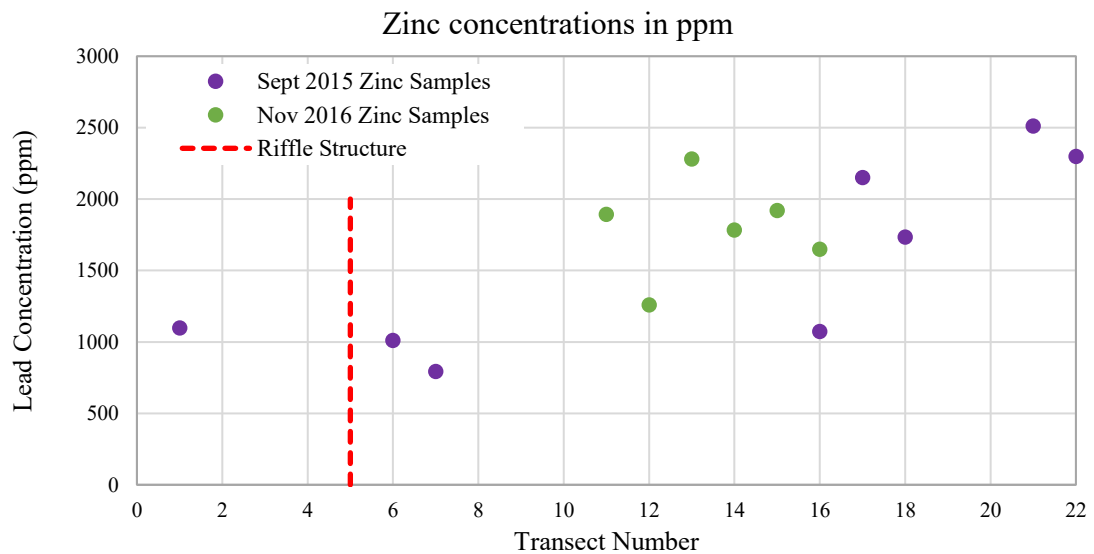


Figure 29 – The concentrations of Zn (ppm) in found in sediment collected from the above transects.

HEC-RAS Results

Mesh size determination. To create an accurate model, two factors, other than ground surface elevation, needed to be considered. The size of the mesh was important in maintaining accuracy as well as enhancing the processing speed, and the determination of the Manning's n was important to create a realistic model. The 2D flow area determined to be most appropriate for further model runs was 9x9ft. This mesh size enhanced processing speeds, as well as maintained the same water surface elevations produced by finer mesh sizes.

Water surface elevation and velocity were evaluated for this determination. The comparison of water surface elevation versus cell size has an asymptotic relationship with the water surface elevation increasing as the cell size increased (Figures 30-33). The comparison of velocity versus cell size has no obvious relationship besides the velocity greatly decreases as the cell size increases (Figures 34-37). The reason for this is that the reported velocity at a specific location is the average velocity within that location's cell. As cell size changes, the center of the cell changes locations and the velocity reported for a specific location is actually the average velocity of various areas that particular location resides in. Even with the observations between velocity and cell size, the water surface elevation was the variable used to determine mesh size.

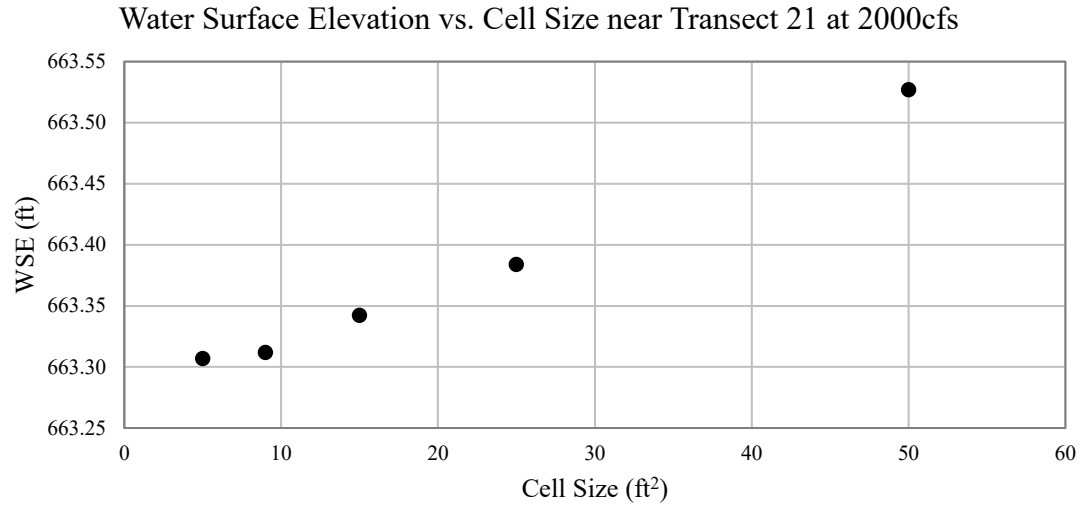


Figure 30 – Water surface elevation and cell size relationship near Transect 21.

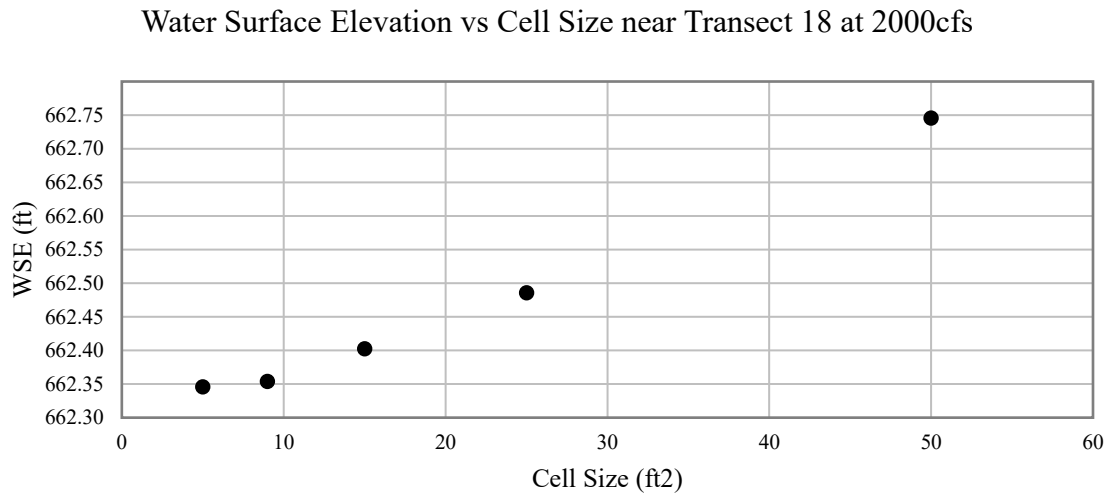


Figure 31 – Water surface elevation and cell size relationship near Transect 18.

Water Surface Elevation vs Cell Size Between Transect 15 and 16 at 2000cfs

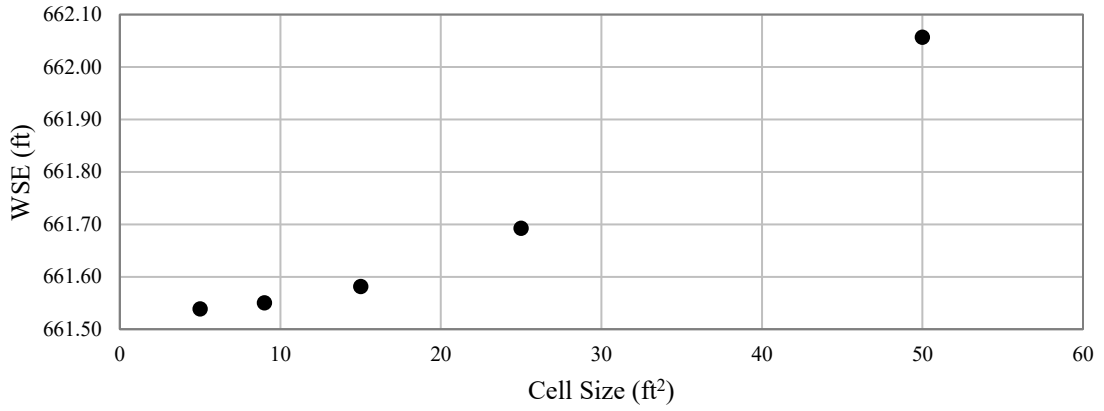


Figure 32 – Water surface elevation and cell size relationship between Transect 15 and 16.

Water Surface Elevation vs. Cell Size near Transect 11 at 2000cfs

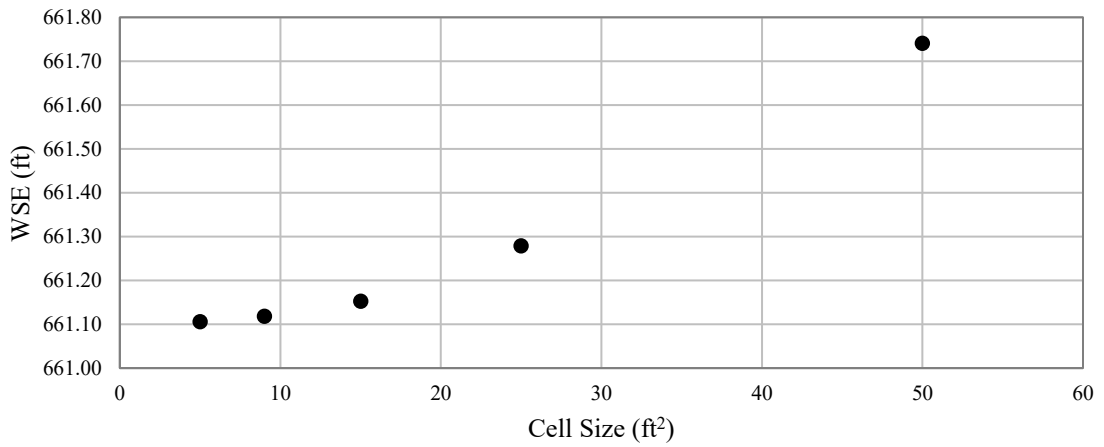


Figure 33 – Water surface elevation and cell size relationship near Transect 11.

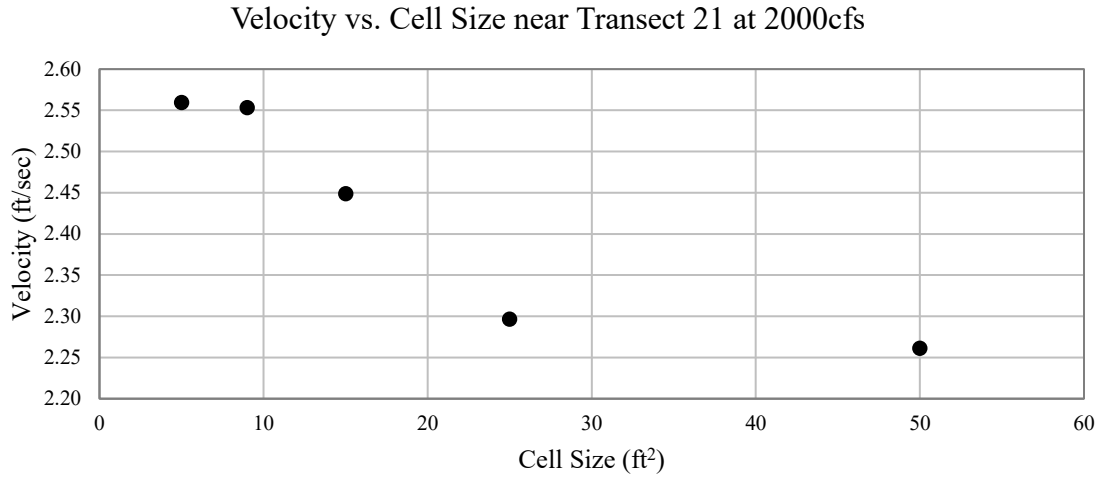


Figure 34 – Velocity and cell size relationship near Transect 21.

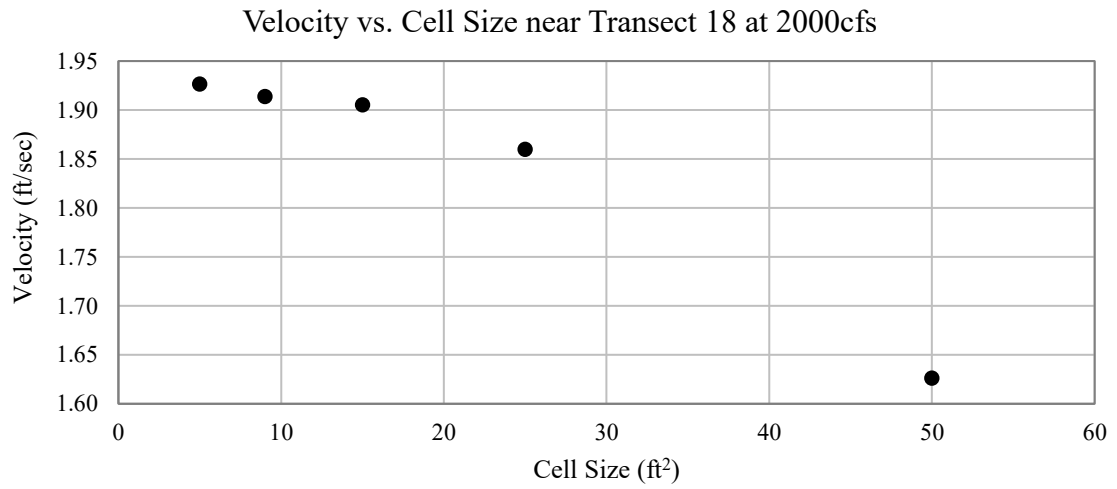


Figure 35 – Velocity and cell size relationship near Transect 18.

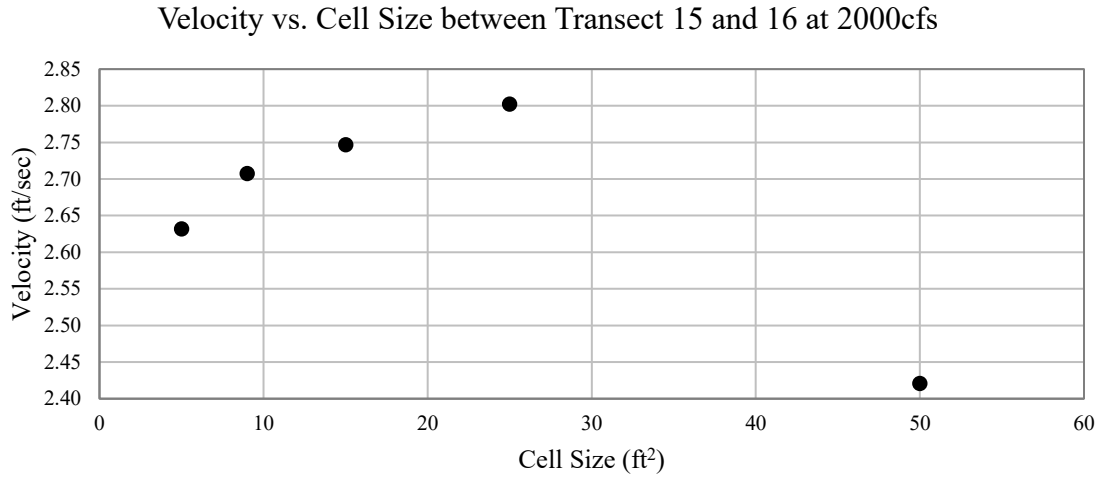


Figure 36 – Velocity and cell size relationship near between Transect 15 and 16.

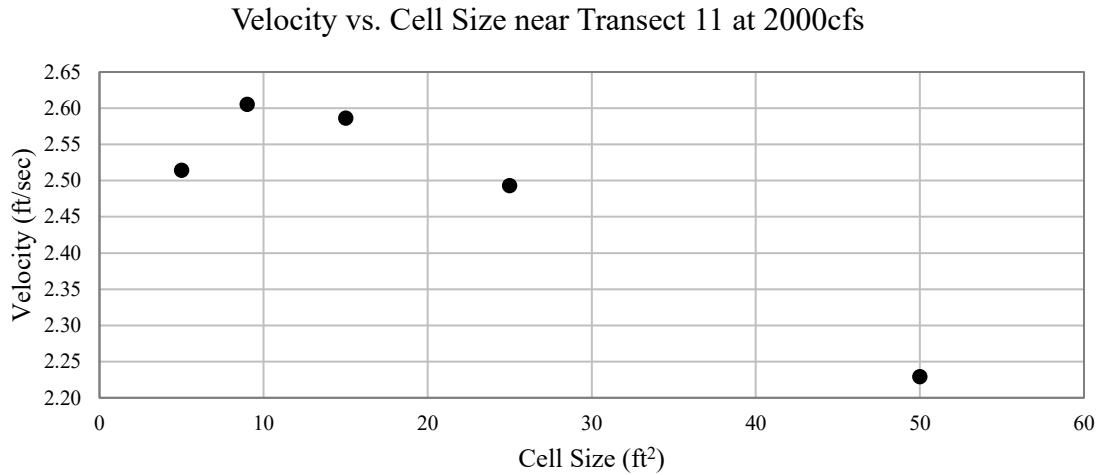


Figure 37 – Velocity and cell size relationship near Transect 11.

Manning’s n determination. By running a hydrograph through the model and comparing the water surface elevation versus varying Manning’s n values and comparing those values to the field measured water surface elevations (Figures 38-41), it was found that the water surface elevation steadily increased as Manning’s n increased. Measured water surface values are relatively close to the different water surface elevations

computed by the model. However, due to the possible surveying errors or incomplete definition of bed geometry, no conclusive results were determined. The Manning's n value of 0.035 was used for further modeling. Several sources suggest 0.035 is appropriate (Chow, 1959; Aldridge and Garrett, 1973; FISRWG, 1998; Bedient et al., 2008).

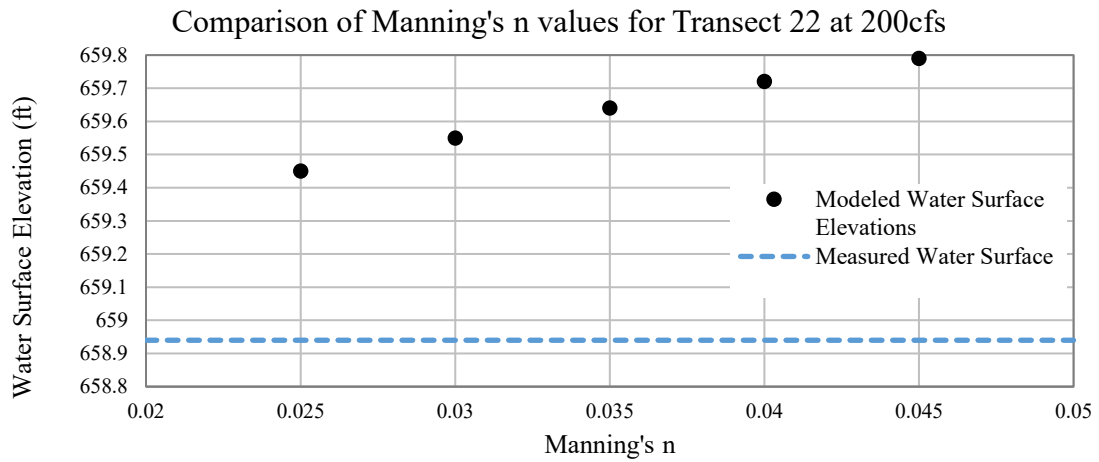


Figure 38 – Water surface elevation and Manning's n relationship at Transect 22.

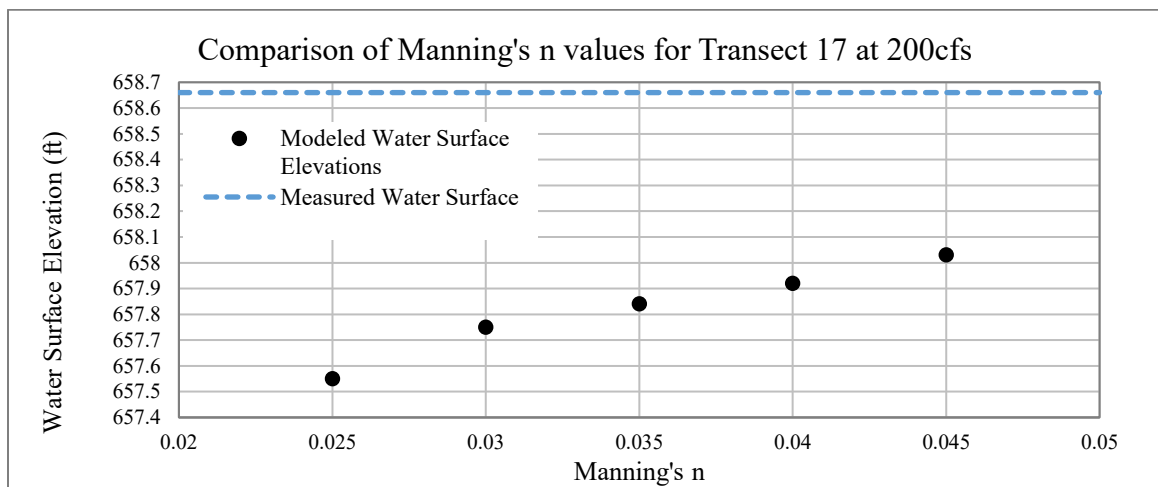


Figure 39 – Water surface elevation and Manning's n relationship at Transect 17.

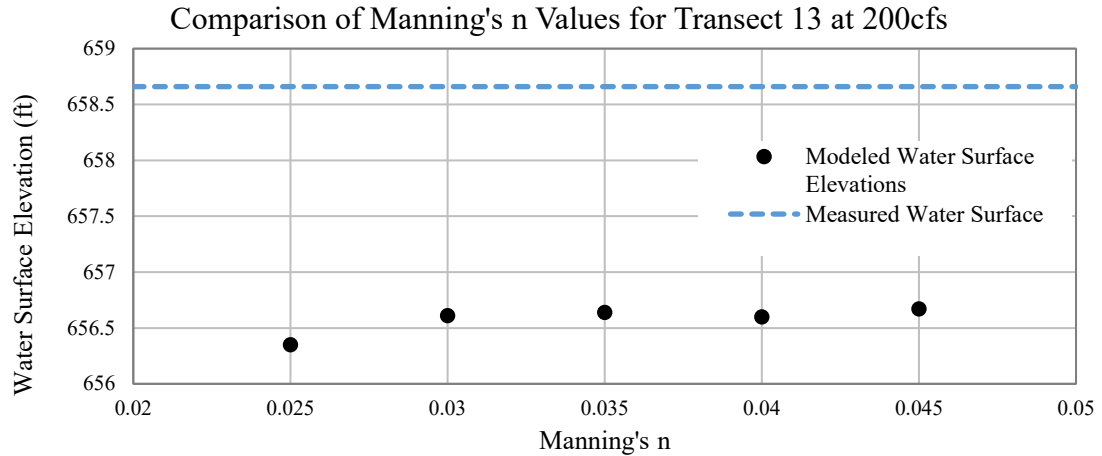


Figure 40 – Water surface elevation and Manning’s n relationship at Transect 13.

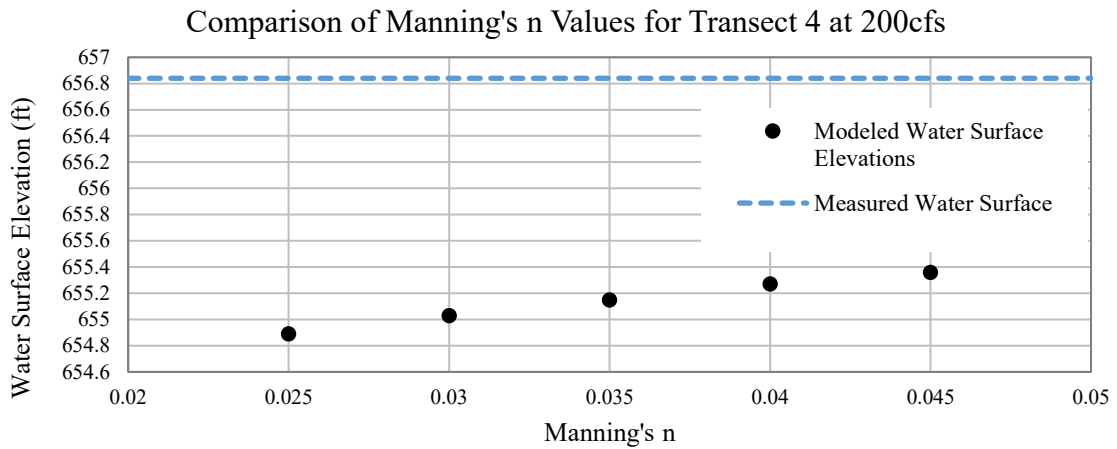


Figure 41 - Water surface elevation and Manning’s n relationship at Transect 4.

Comparison of flood simulations. Using the 9x9ft mesh and a Manning’s n of 0.035 within the channel, the 1.5, 2, 5, 10, 25, 50, and 100-year floods were run through pre and post-construction models. The velocities and water depths for these runs can be found in Appenidces C-D and E-F, respectively. PeakFQ was used to determine the discharge of different flood magnitudes for Irondale, Richwoods, and Byrnesville. This

Table 2 – Discharge of flood recurrence intervals determined from statistical analysis of gage area at various return intervals.

Flood Recurrence Interval (years)	Discharge (cfs)
1.5	11,700
2	15,425
5	25,568
10	32,700
25	41,852
50	48,780
100	55,750

data was used to interpolate the discharge of each flood magnitude for the drainage area below Desloge (Figure 42). The discharges interpolated for the Big River below Desloge were used to model varying flood magnitudes using the pre- and post-construction scenarios (Table 2).

The 1.5-year flood was determined to have a discharge of approximately 11,700 cfs. To compare the models before construction and after construction both models were run with the 1.5-year discharge. The velocity within the channel before construction is greater than the velocity after construction. The pre-construction velocity ranges from 0 feet per second (ft/sec) to 9 ft/sec, comparably the post-construction velocity varies between 0 ft/sec and ~7 ft/sec. The highest velocities occur within the channel boundaries in the pre- and post-construction conditions (Figure 43).

Comparison of Flow Rate vs. Drainage Area at Irondale, Bynesville, & Richwoods

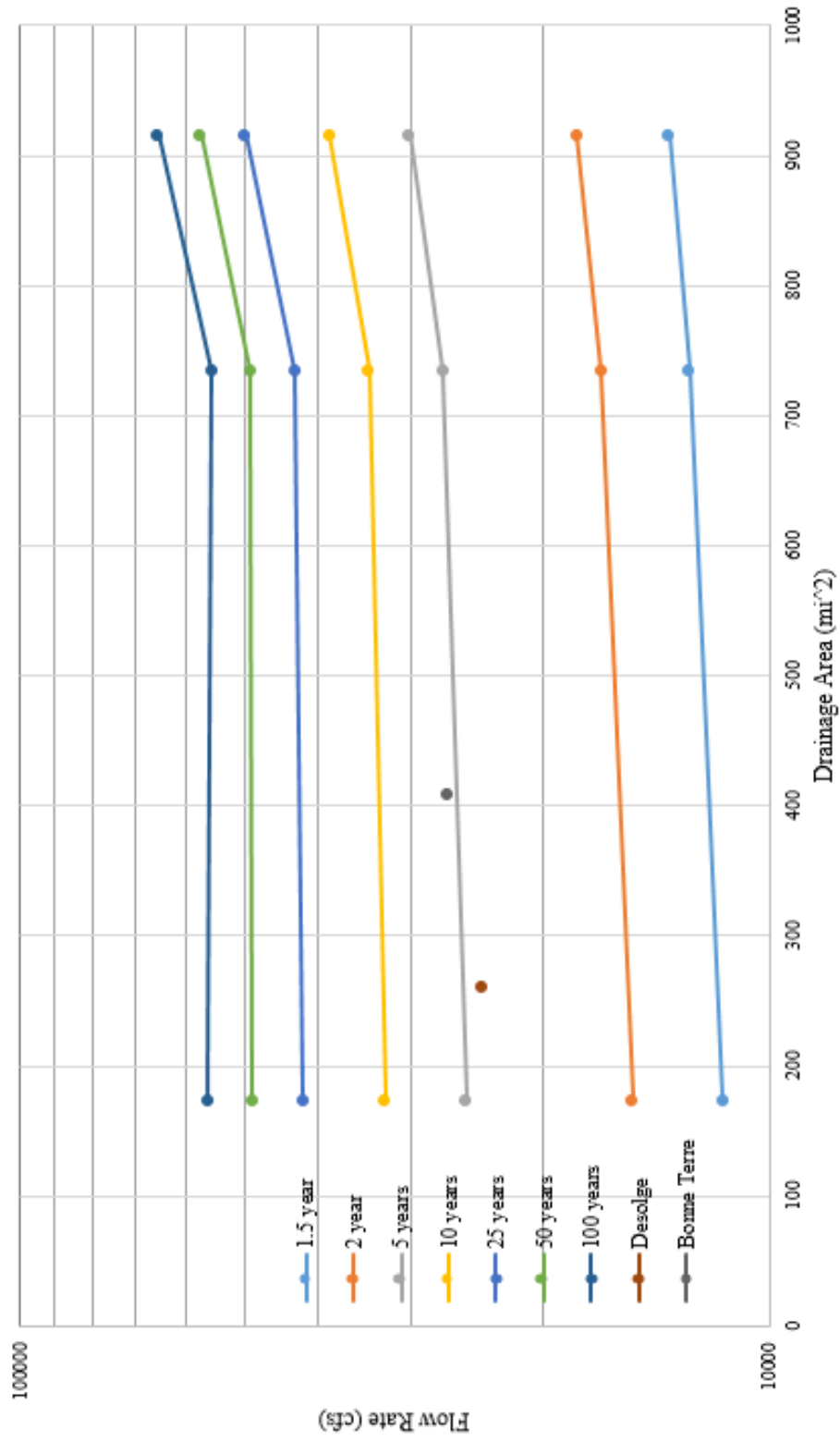


Figure 42 – PeakFQ data used to interpolate the discharge of flood recurrence intervals for the Big River below Desolge.

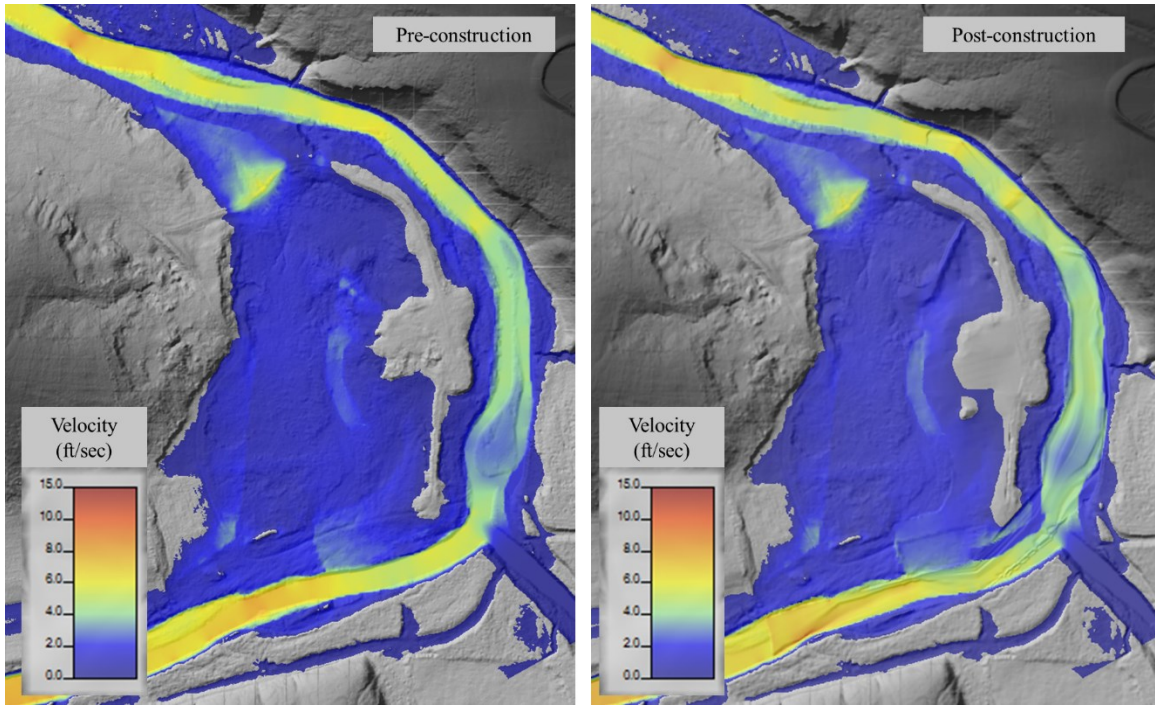


Figure 43 – Pre- and post-construction comparison of the 1.5-year flood (11,700 cfs).

The 2-year flood was determined to have an interpolated discharge of 15,425 cfs. Comparisons of the pre-construction and post-construction simulations of the 2-year discharge do not show prominent differences. The velocities during the 2-year flood for both the pre and post-construction simulations range from 0 to ~11 ft/sec (Figure 44).

Similar to the 1.5-year flood, the velocity appears to be highest within the channel banks. However, a velocity hot spot has appeared outside the channel. The hot spot appears slightly more prominent in the post-construction simulation. This may be due to the lowering of the basin inlet.

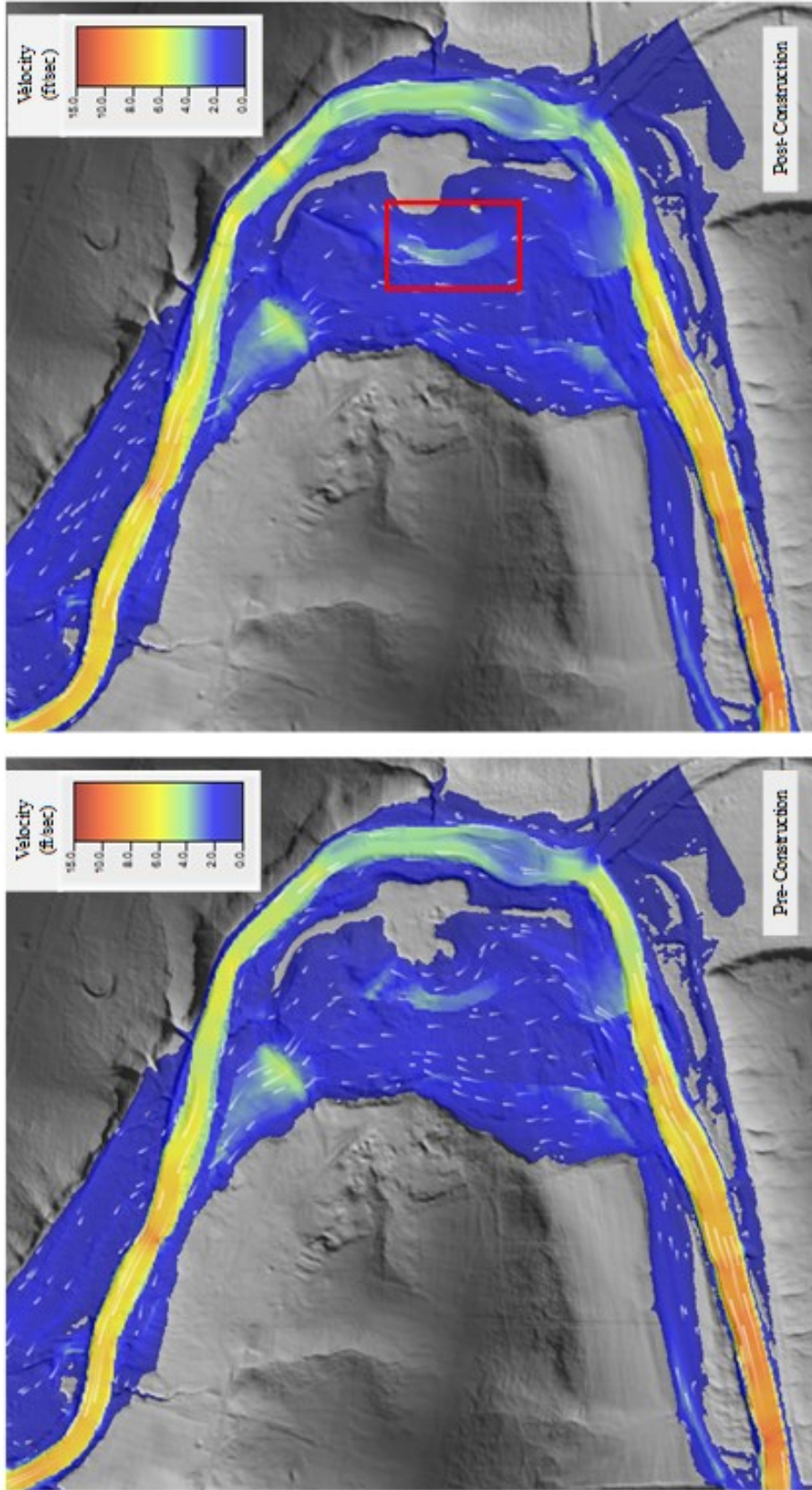


Figure 44 – Pre- and post-construction comparison of the 2-year flood (15,425 cfs). The velocity hotspot appears more prominently in the post-construction simulation

The comparisons of the pre- and post-construction simulations for the 5, 10, 25, 50 and 100-year floods showed little to no significant difference between the pre-and post-construction conditions nor did these simulations show significant difference between flood magnitudes (Figures 45-49). Simulated velocities fall between 0 ft/sec and 15 ft/sec. In all comparisons the velocities within the channel boundaries are higher than outside of the channel boundaries. As the flood magnitude and discharge increase, the velocities increase both inside and outside of the channel.

Comparison of velocities. To understand how the installed riffle and basin changed velocities at the study site, velocities produced from simulations at varying discharges were compared based on the pre- and post-construction terrain. Discharge equaled 600 cfs, 2000 cfs, 15,425 cfs (2-year flood), and 25,568 (5-year flood). A Hjulström curve was used to determine that velocities associated with these discharges have the capacity to transport sand- to gravel-sized material (Figure 50). Areas with velocities low enough for deposition are seen on the left bank between transect 11 and 12.

At 600 cfs, velocities where deposition (Transect 11) and erosion (basin inlet) are occurring were evaluated (Figure 51). The relative percent difference (RPD) was calculated to highlight the change. At the basin inlet, the velocities modeled for the pre- and post-construction simulations were 2.26 ft/sec and 1.12 ft/sec, respectively. The RPD of the pre- and post-construction velocities at the basin inlet is 67%. At Transect 11, the velocities modeled for the pre- and post-construction simulations were 2.12 ft/sec and 1.40 ft/sec, respectively. The RPD of the pre- and post-construction velocities is 50%.

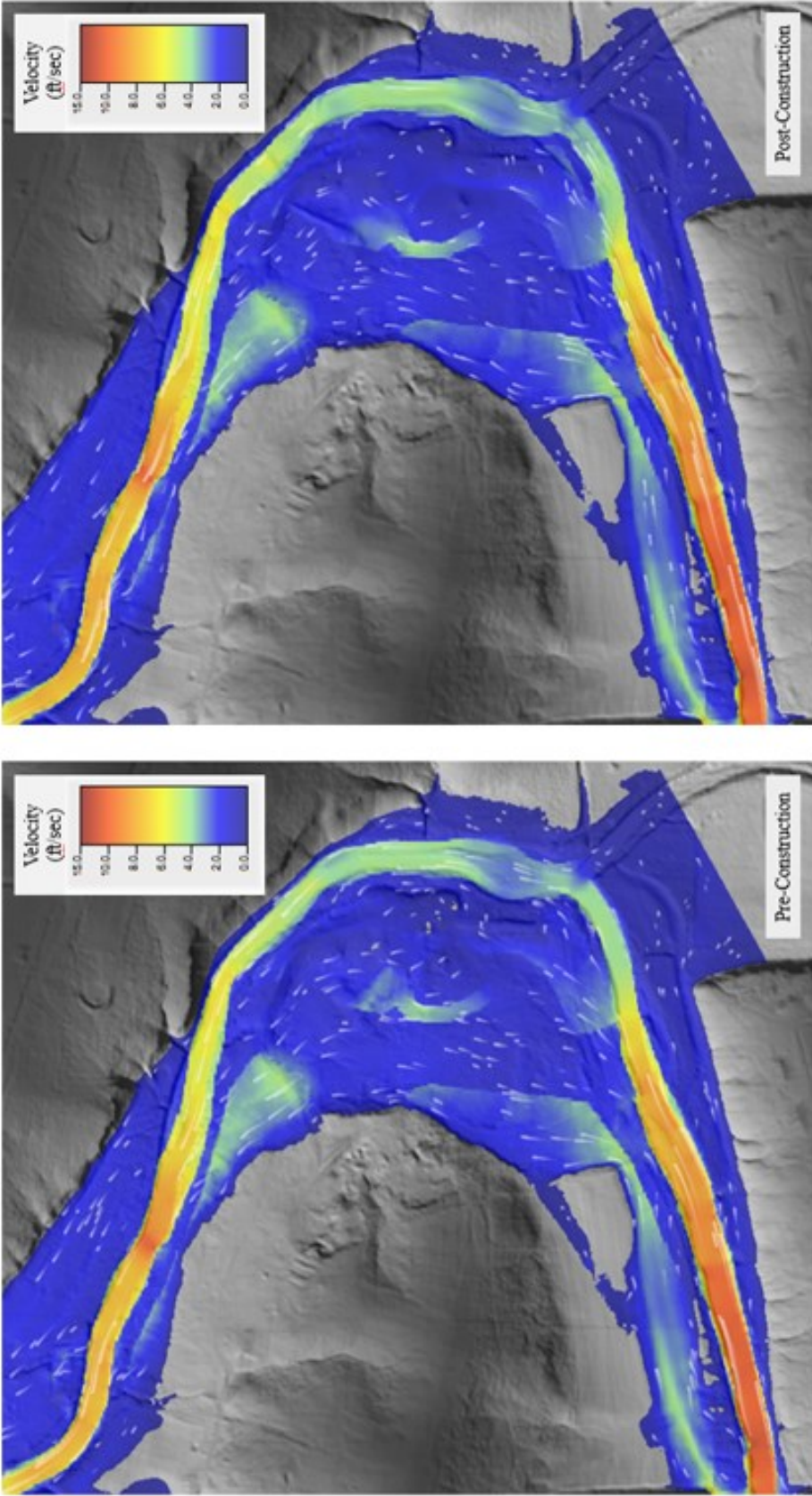


Figure 45 - Pre- and post-construction comparison of the 5-year flood (25,568 cfs)

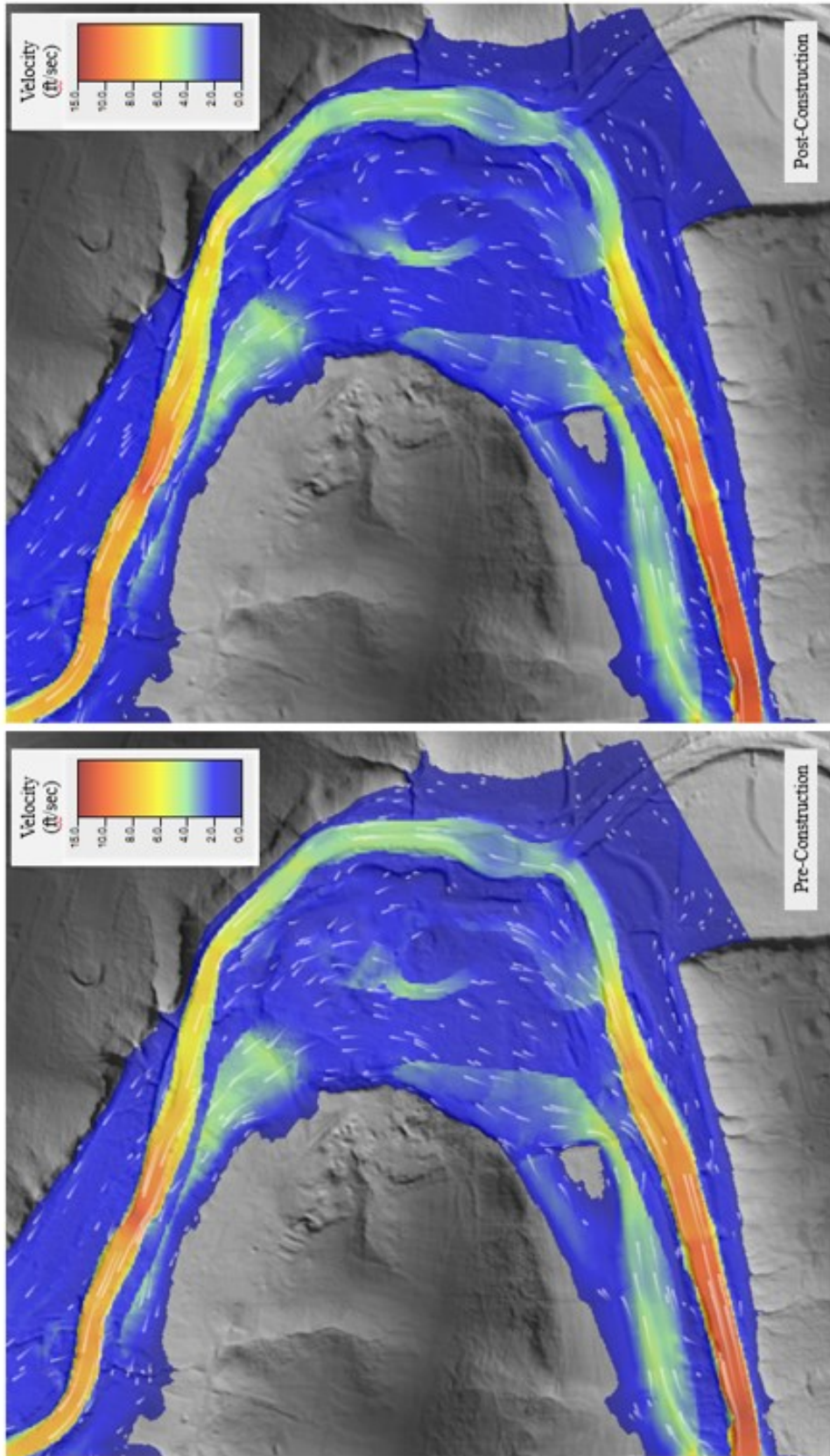


Figure 46 - Pre- and post-construction comparison of the 10-year flood (32,700 cfs)

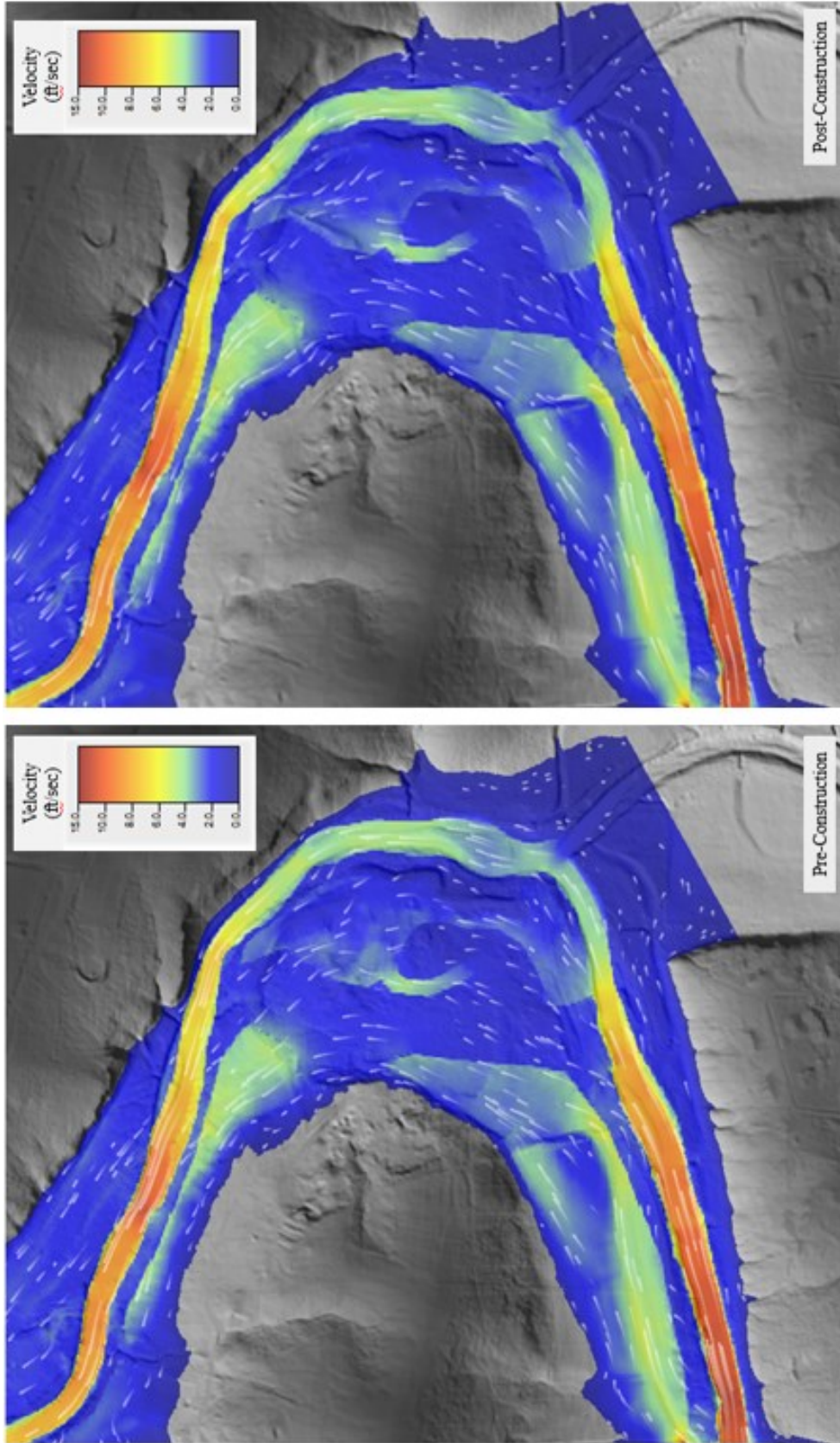


Figure 47 - Pre- and post-construction comparison of the 25-year flood (41,852 cfs)

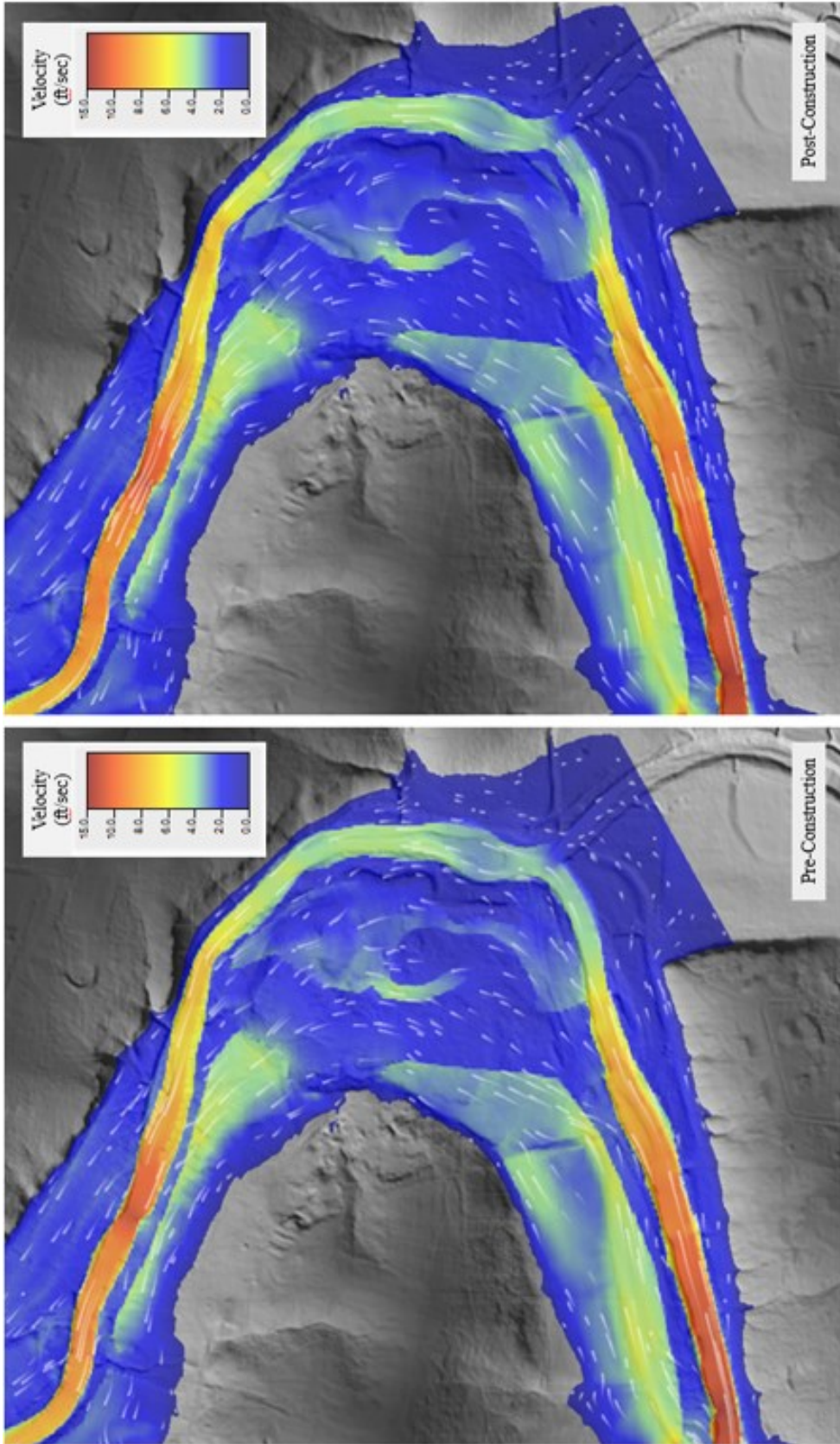


Figure 48 - Pre- and post-construction comparison of the 50-year flood (48,780 cfs)

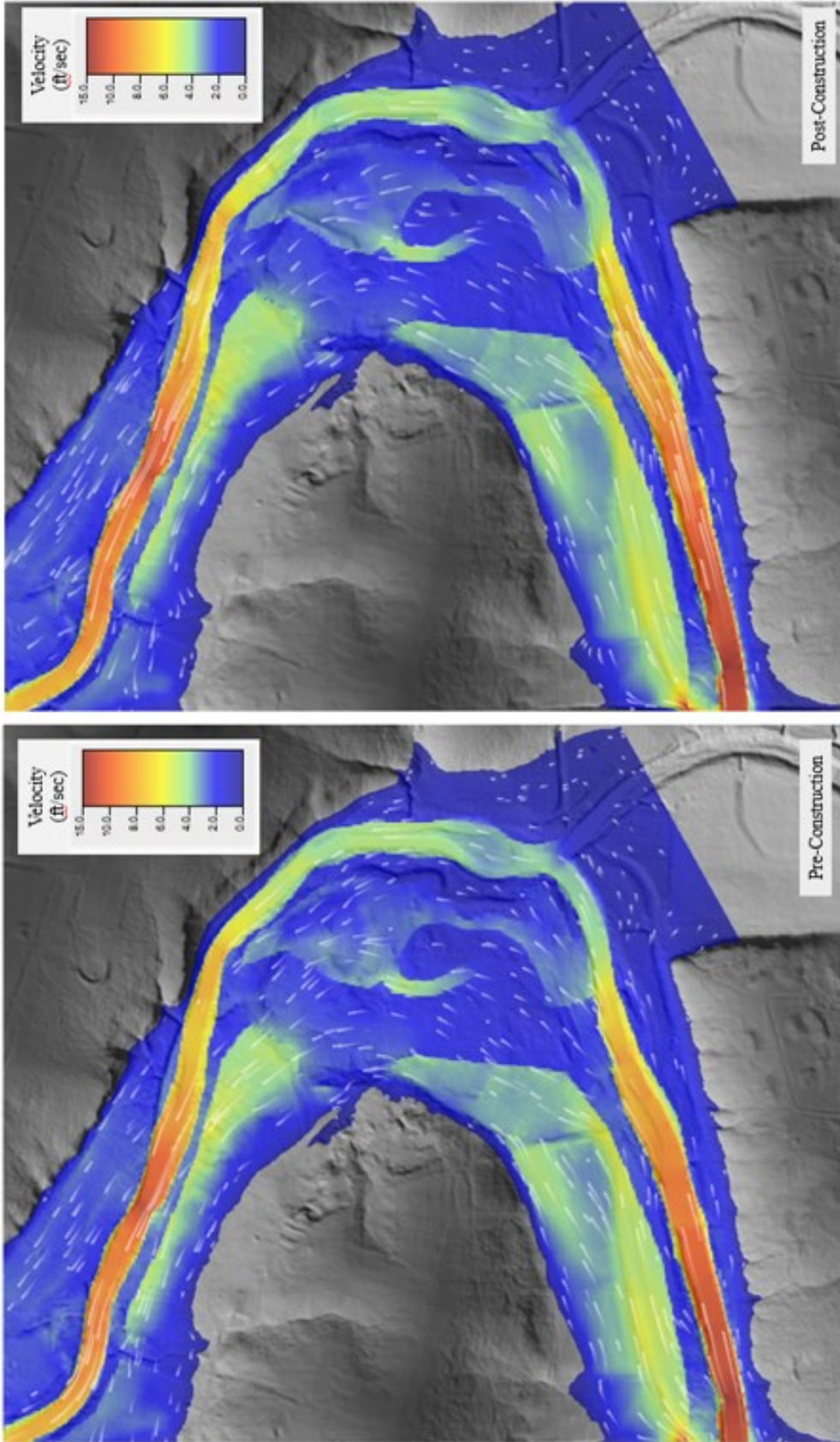


Figure 49 - Pre- and post-construction comparison of the 100-year flood (55,750 cfs)

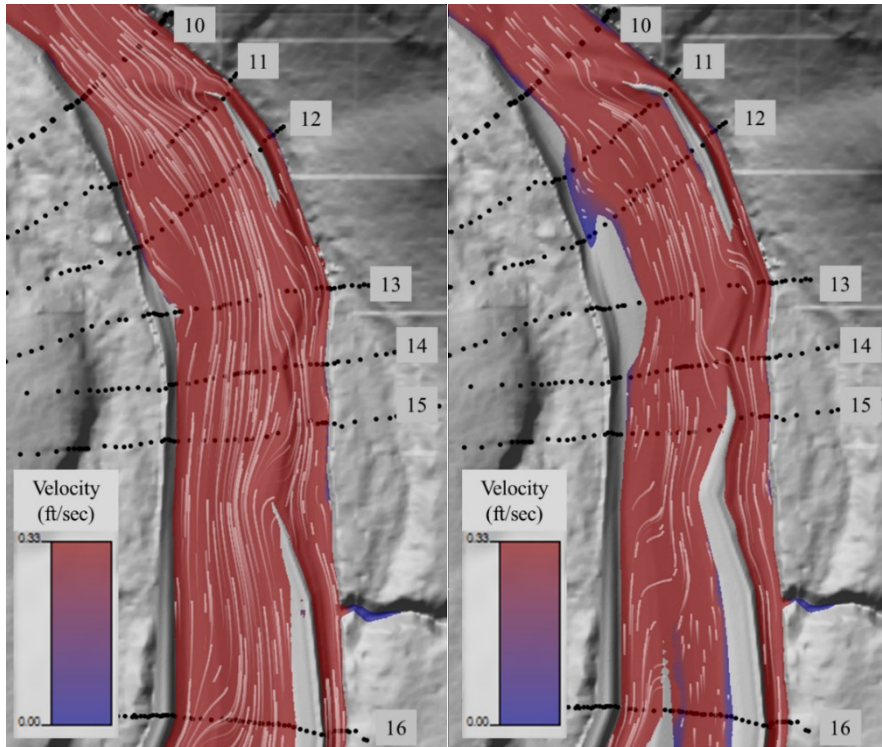


Figure 50 – Simulation of sediment transport capacity at 200 cfs (right) and 600 cfs (left). These simulations depict areas of sediment transport (red) and sediment deposition (blue) based on velocities and grain sizes greater than 2 millimeters (mm).

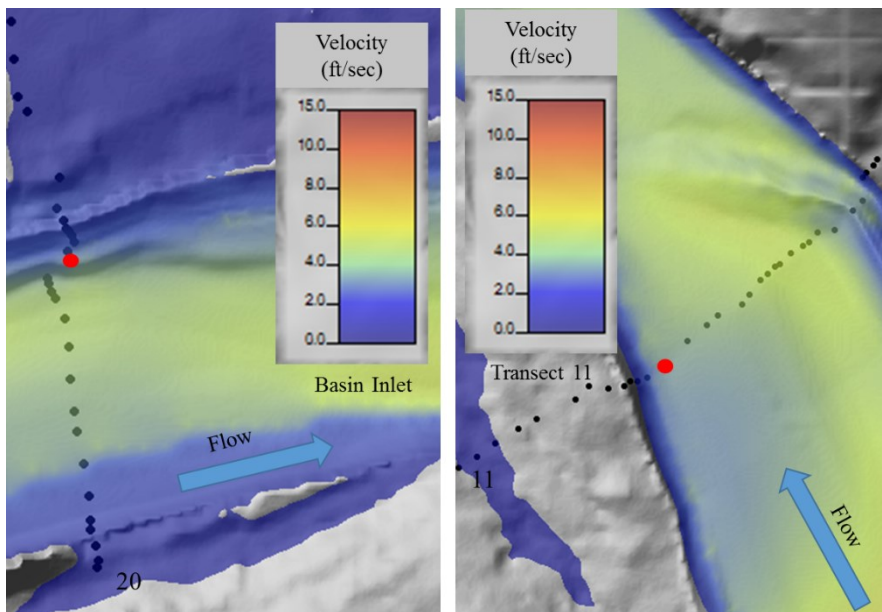


Figure 51 – Velocity measurement locations for pre- & post-construction comparison at 600 cfs taken from basin inlet and Transect 11 for RPD calculations.

At 600 cfs a notable difference is observed at the head of the riffle structure (Figure 52). In the post-construction simulation, a velocity hot spot can be seen at the head of the riffle. From the location of the velocity hot spot and the results of the RPD calculations it can be inferred that the riffle structure is the main control on velocity within the channel when flows are contained within the banks.

At 2000 cfs, the RPD for the basin inlet and Transect 11 was calculated to highlight the change between the pre- and post-construction velocities (Figure 53). At the basin inlet, the velocities modeled for the pre- and post-construction simulations were 3.86 ft/sec and 2.71 ft/sec, respectively. The results of the calculations showed that the RPD of the pre- and post-construction velocities was 35%. Along Transect 11, the velocities modeled for the pre- and post-construction simulations were 3.18 ft/sec and 2.96 ft/sec, respectively. The RPD of the velocities was calculated to be 7.2%. At the basin inlet, the lower velocities are occurring in the post-construction simulation, which could be due to the lowering of the basin inlet. At 2000 cfs the basin begins to fill with water, unlike before construction (Figure 54). The pre-construction shows no flooding in the basin area.

A simulation of the 2-year flood indicates that velocities entering the basin inlet are higher than velocities throughout the basin (Figure 55). High velocities correspond to areas where erosion is occurring, and lower velocities within the basin correspond to areas where deposition is occurring (Figure 56).

To better understand the erosion at the basin inlet the RPDs were calculated for pre- and post-construction simulations. During the 2-year flood simulation (15,425 cfs) the velocities modeled at the basin inlet in the pre- and post-construction simulations

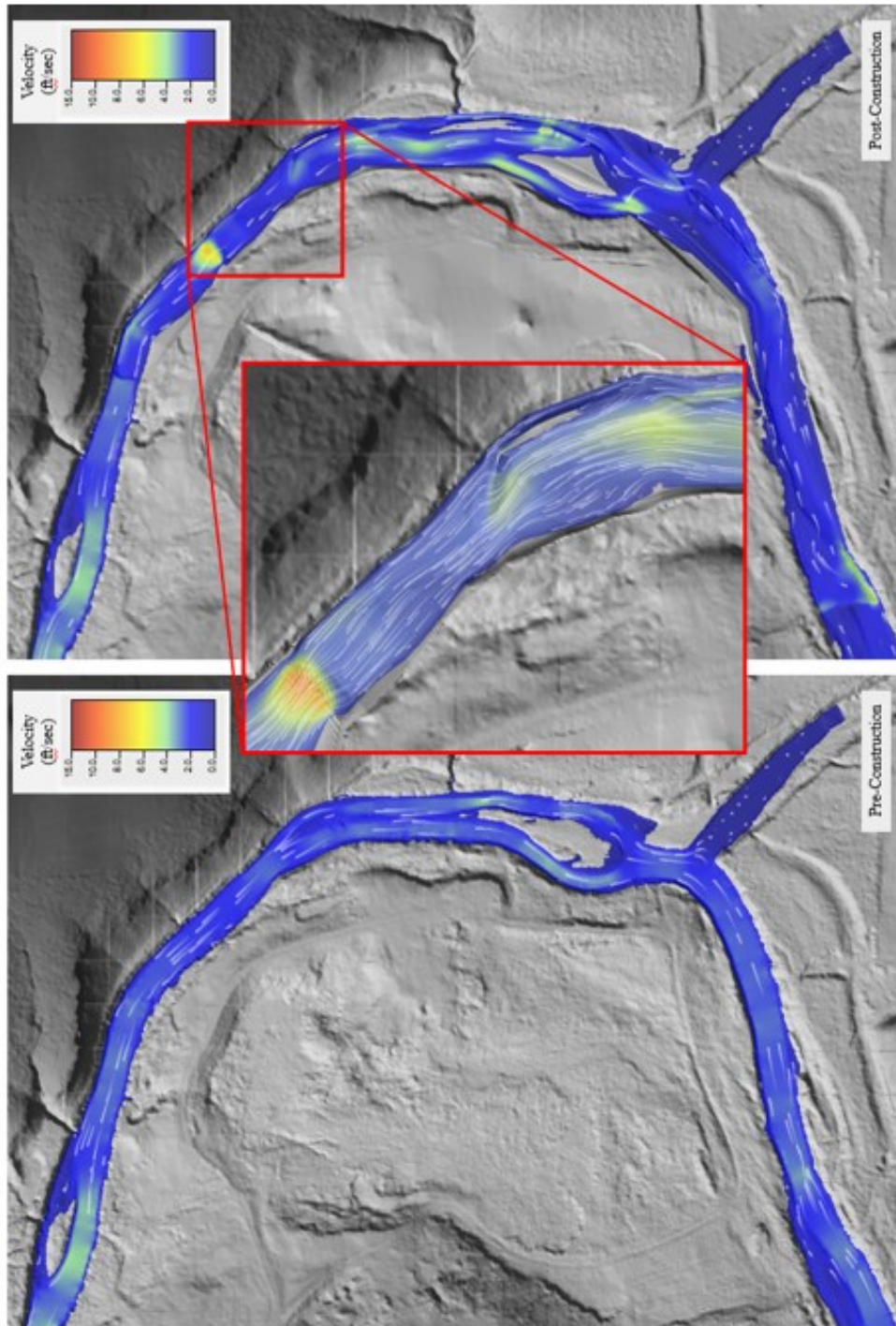


Figure 52 – Simulation highlighting the installed riffle structure is acting as the main control on velocity at 600 cfs in the post-construction simulation.

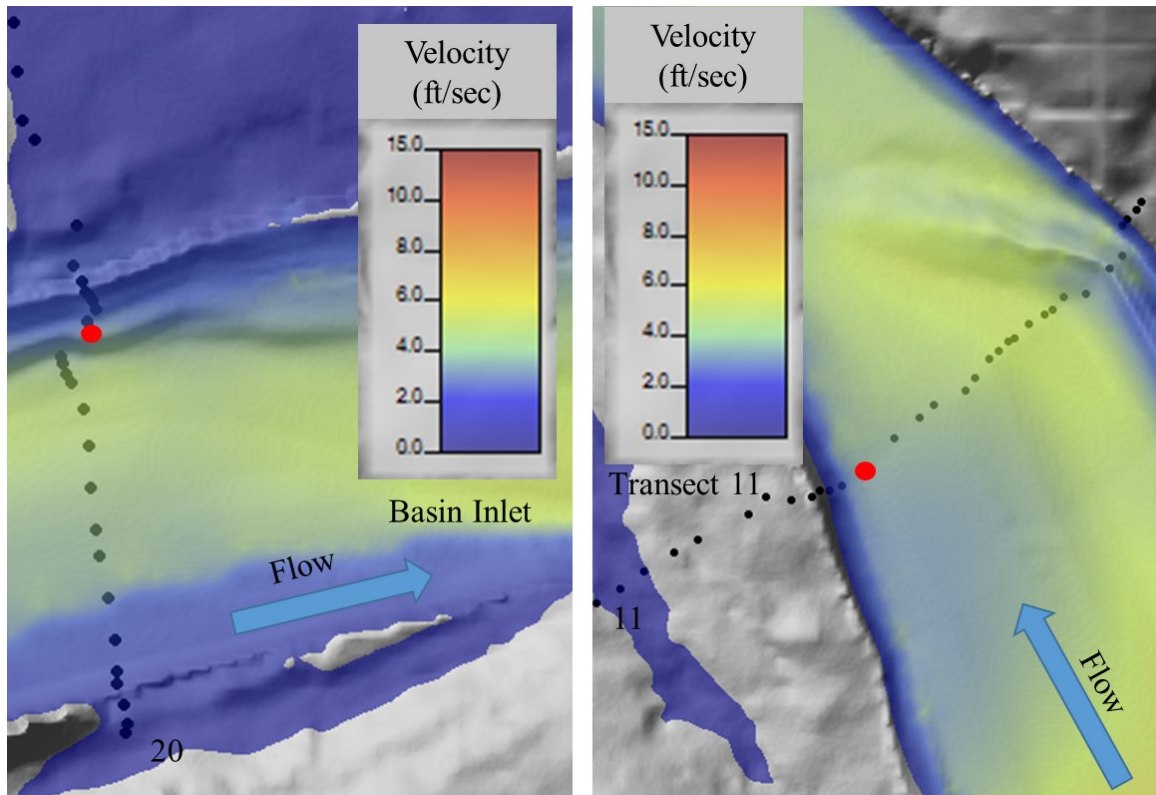


Figure 53 – Velocity measurement locations for pre- & post-construction comparison at 2000 cfs taken from basin inlet and Transect 11 for RPD calculations

were 3.50 ft/sec and 3.75 ft/sec, respectively. The RPD between velocities was 6.9%, with higher velocities occurring during the post-construction simulation. This is most likely a result of the lowering of the basin inlet.

During the 5-year flood (25,568 cfs), the RPD was calculated for pre-and post-construction velocities at the basin inlet. The RPD calculation showed no difference between pre- and post-construction velocities (3.72 ft/sec) at the basin inlet. This may be a result of high discharges being pushed through the area.

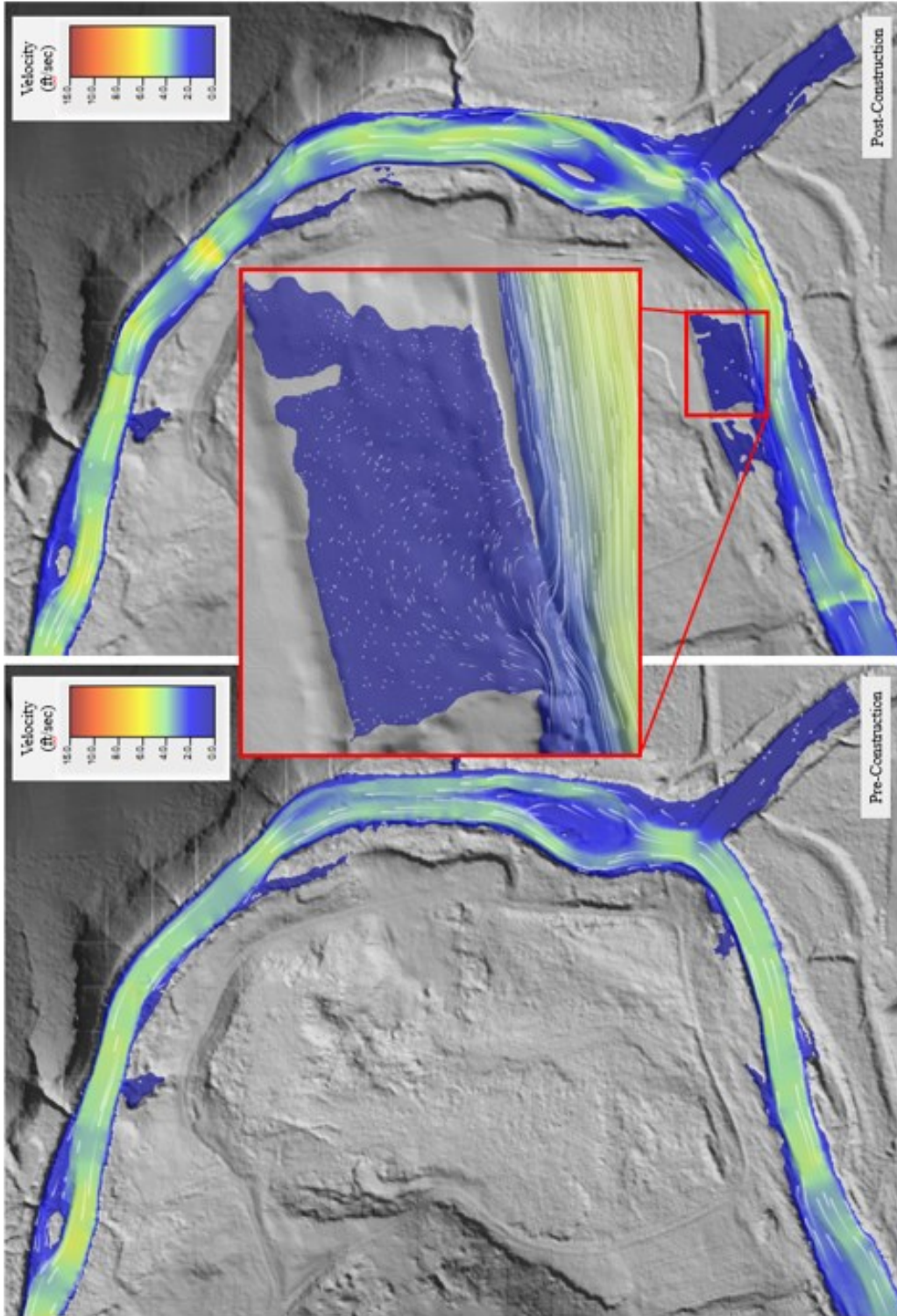


Figure 54 – Simulation highlighting the basin begins flooding at 2000 cfs in the post-construction simulation

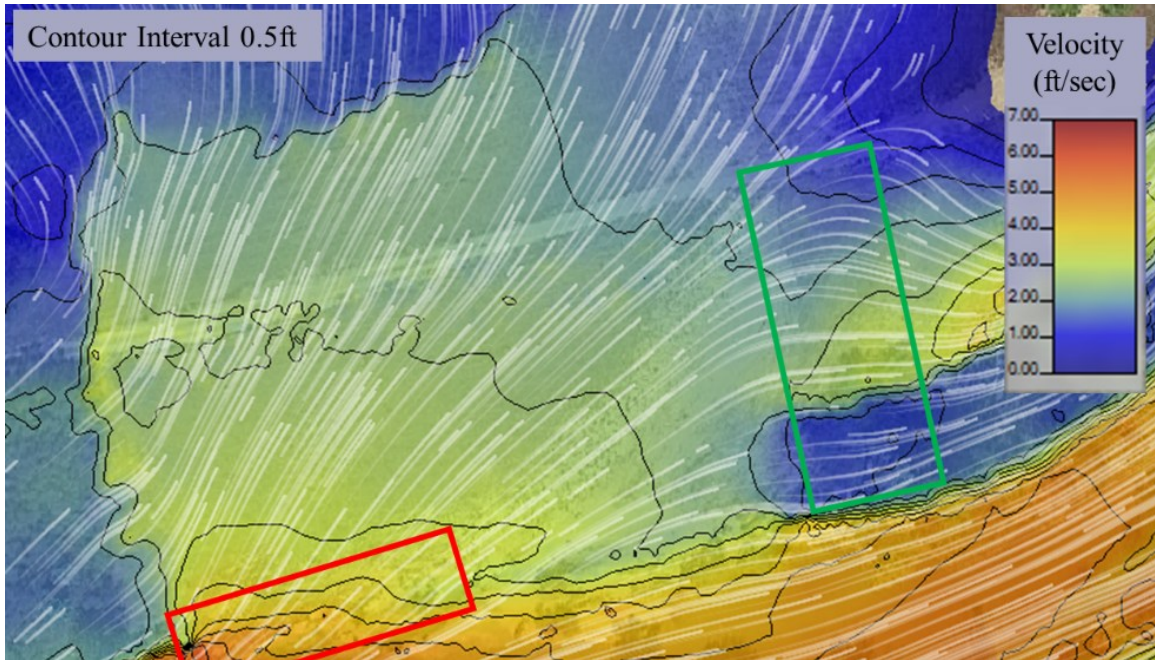


Figure 55 – Simulation of the 2-year flood (15,425 cfs) high velocities at the basin inlet (red square) and lower velocities within the basin (green square).

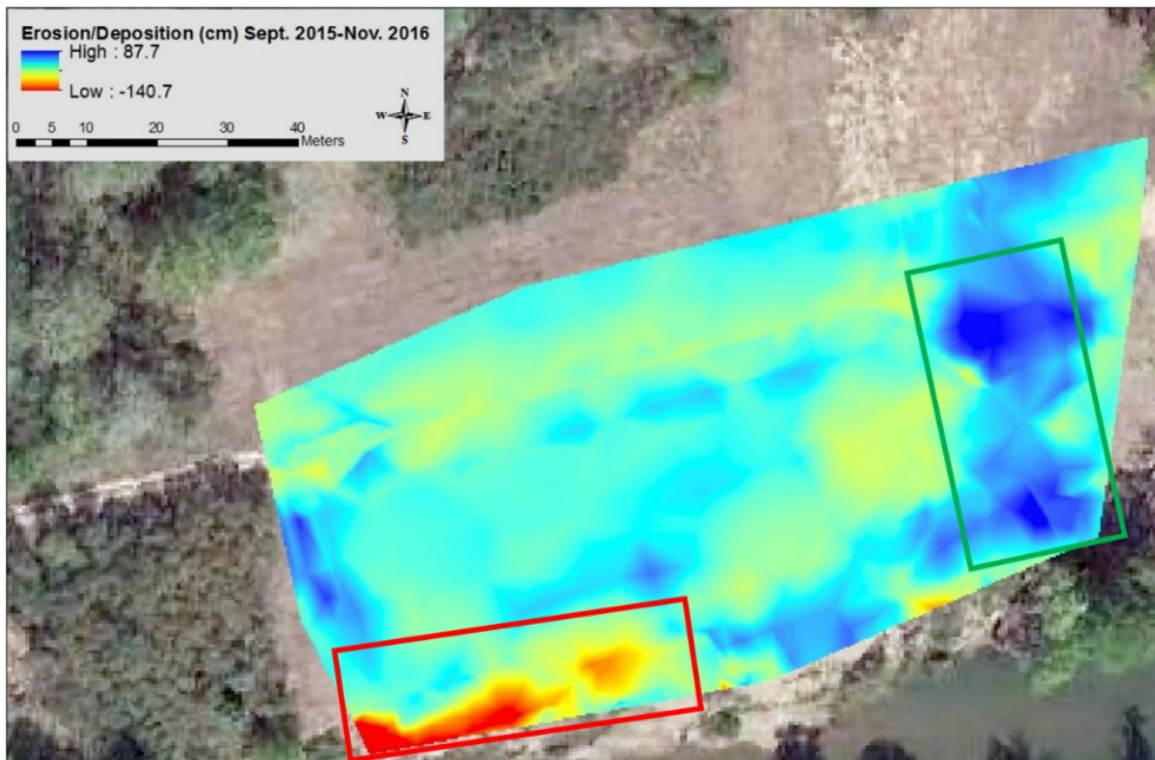


Figure 56 – Voss (2017) survey results of basin indicating erosion at the basin inlet (red square) and deposition within the basin (green square).

Northeast of the basin inlet, deposition is occurring within the basin. To better understand the deposition occurring in this area the velocities were used to determine the RPD between the 2-year and 5-year flood events. The velocity of the 2-year event (15,425 cfs) was 1.94 ft/sec and the velocity of the 5-year event (25,568 cfs) was 2.10 ft/sec. The RPD calculation showed a 7.9% difference in velocities between the 2-year and 5-year floods within the depositional area of the basin.

When comparing velocities of varying flood events, it is easy to see that certain areas are prone to higher velocities than others. This difference is directly related to Manning's n values that were used in flood simulations. In Figure 57, green areas consist

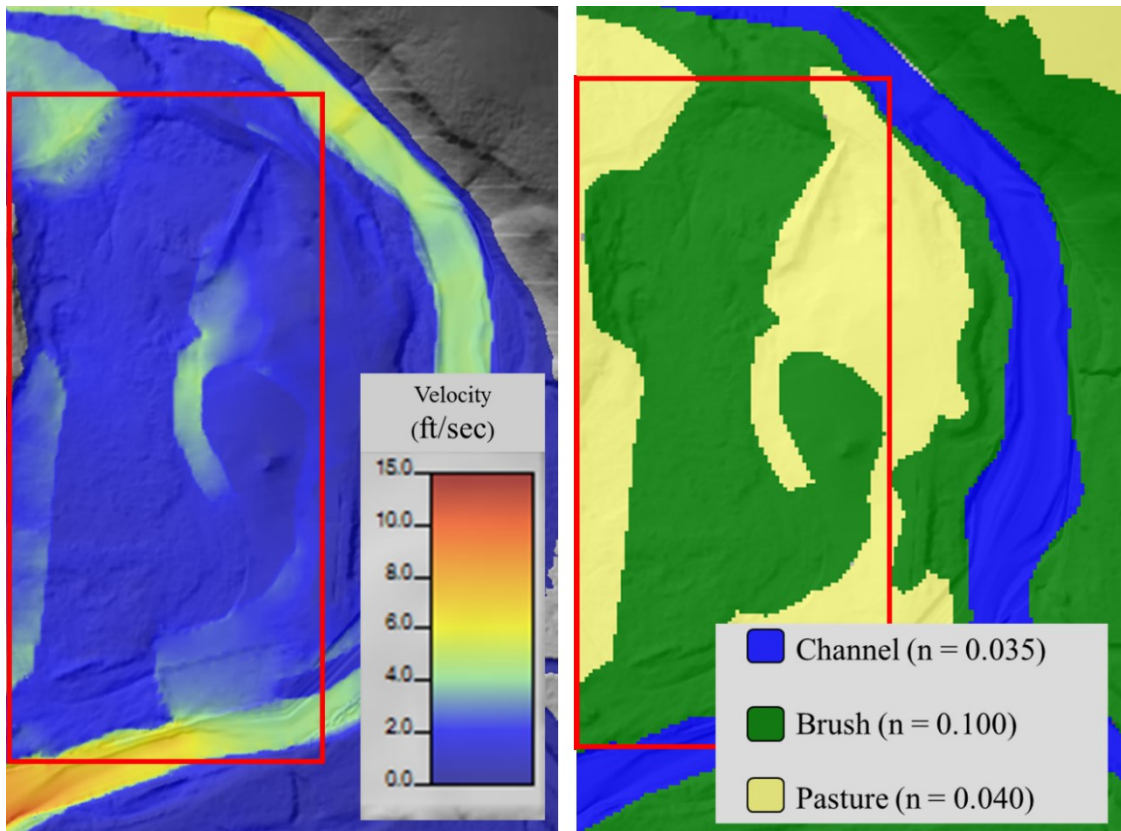


Figure 57 – Effect of land use layer on flood simulations. The red square indicates areas where the Manning's n value (right) is influencing the velocities (left).

of dense trees and brush resulting in a greater roughness coefficient (0.100), yellow areas consist of short to medium length grasses resulting in a lower roughness coefficient (0.040), and the channel, in blue, had the lowest roughness coefficient (0.035). These difference in roughness coefficients directly affect velocity in a given area.

Comparison of model simulations and field observations. Model simulations appear to coincide with field observations within the study area. Within the channel, significant deposition was determined to be occurring around Transects 10-16. During the 2-year flood and 5-year flood velocities are lower in this area than upstream and downstream (Table 3 and Figure 58). Decreased velocity in this area occurred in the 1.5 - 100-year floods, and is likely contributing to deposition occurring in this area of the channel

Table 3 – Velocity comparison in areas of high deposition (Transects 10-16) and the thalweg of transects upstream and downstream.

Transect #	2-year (15,425 cfs) Velocity (ft/sec)	5-year (25,568 cfs) Velocity (ft/sec)
1	5.3	6.0
6	5.0	5.0
10	4.5	4.5
11	3.8	3.8
12	3.7	3.8
13	4.2	3.4
14	4.1	4.3
15	4.1	4.3
16	4.1	4.4
21	7.5	8.3
22	7.1	8.2

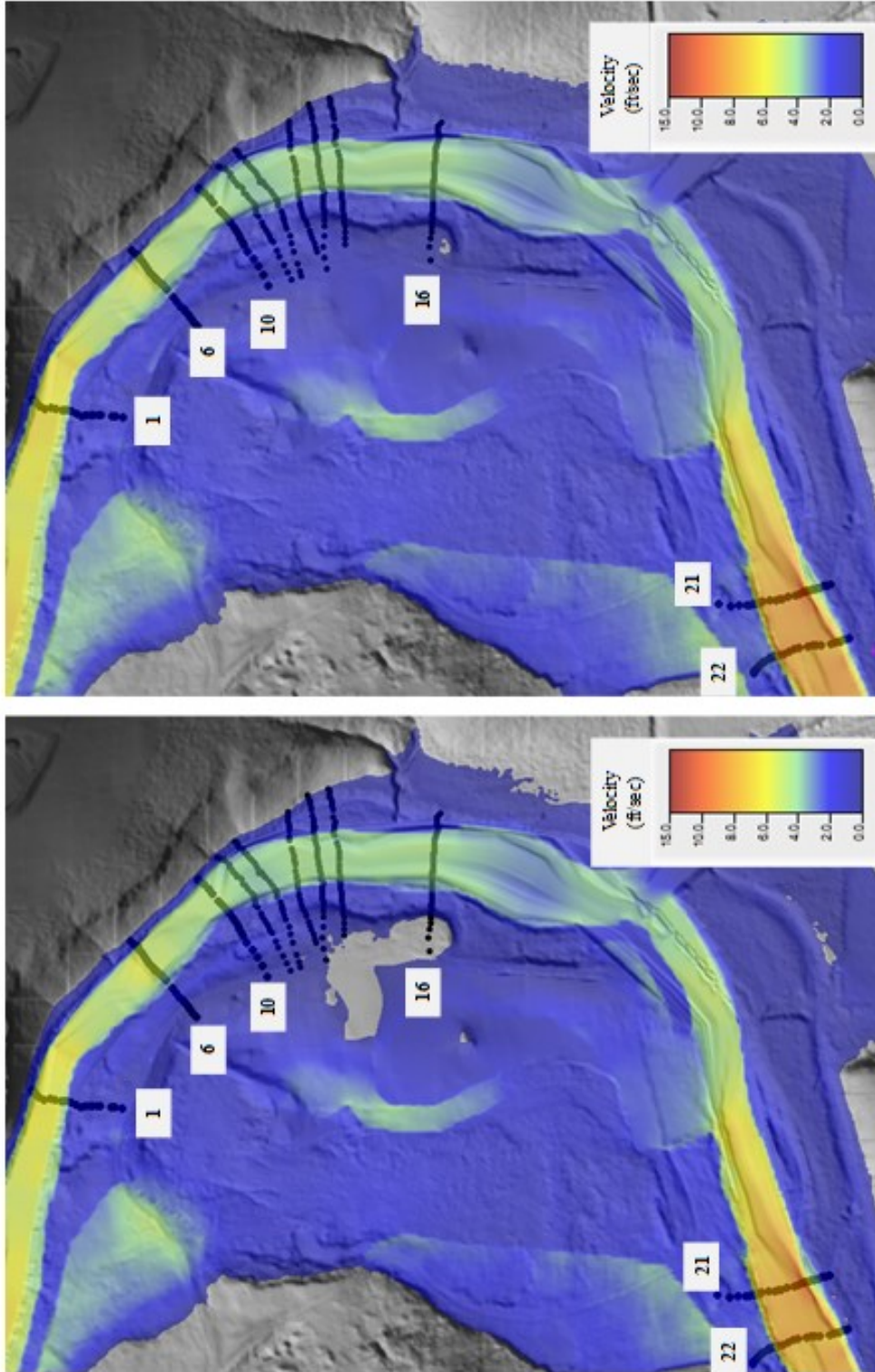


Figure 58 – Simulation highlighting the high velocities upstream and downstream of Transects 10-16 during the 2-year flood (15,425 cfs) (left) and the 5-year flood (25,568 cfs) (right). On Transects 10-16 velocities were taken from the chute near the left bank, on Transects 1, 6, 21, and 22 velocities were taken from the [thalweg](#).

In numerous places outside the channel model simulations matched field observations. High velocities begin to appear on the outlet road during the 1.5-year flood simulation (Figure 59), and are fully apparent during the 2-year through the 100-year floods. This is significant because during the ~5-year flood event the outlet road was washed out and it also washed out during lower events. Wash out of the outlet road is a product of high velocities occurring in this area and the models agree with field observations.

In the upper basin area a headcut development was observed just south of a high-velocity area. This area was designed to route flow from the upper to lower basin. It is hypothesized that this velocity hotspot and the area just south (Figure 60) could be related and the velocity hotspot could be directly influencing the development of the headcut.

After the 5-year flood that occurred in December 2015 a large log jam blocked the road (Figure 61). The simulated water depth for the 5-year flood indicates that a significant decrease in water depth occurred in this area which would account for the large log jam. So again the model behavior matches field observations.

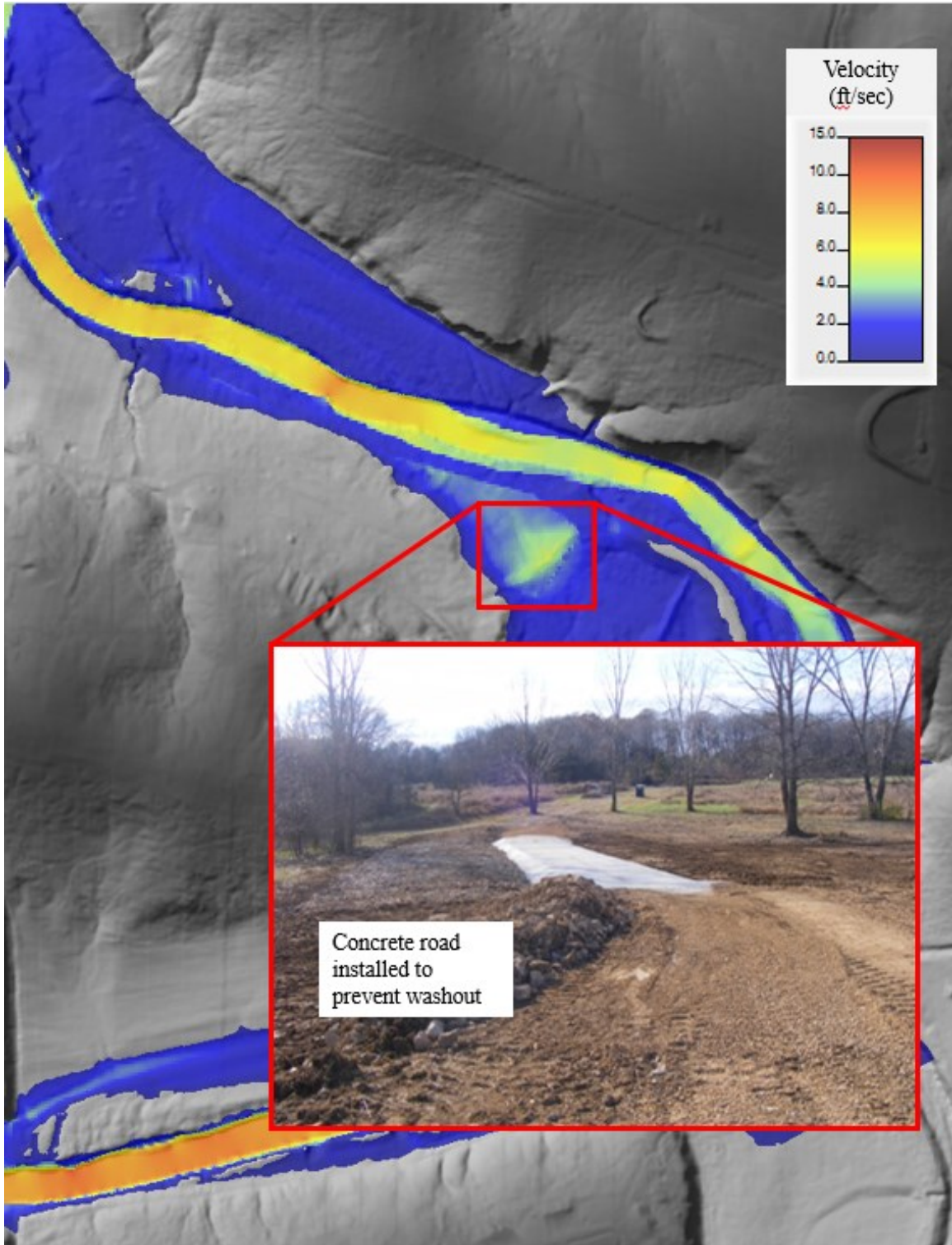


Figure 59 - Simulation of high velocity on outlet road. High velocities during the 2-year flood (15,425 cfs) on the outlet road (seen in red square) is the possible cause of outlet road wash out that occurred after the December 2015 flood.

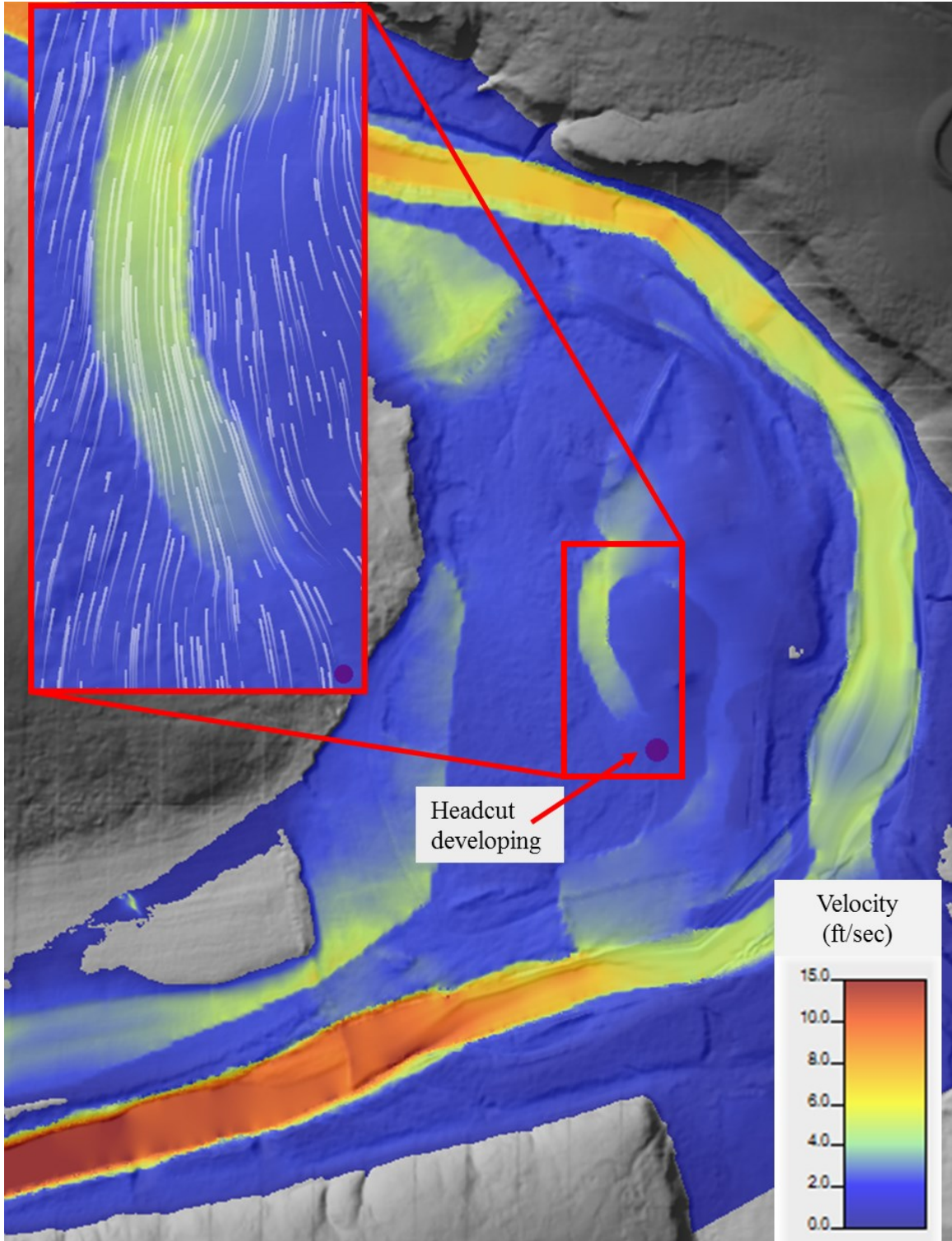


Figure 60 - Simulation of high velocity near developing headcut. The 5-year simulation (25,560 cfs) depicts how a velocity hotspot is hypothesized to be directly related to the developing headcut

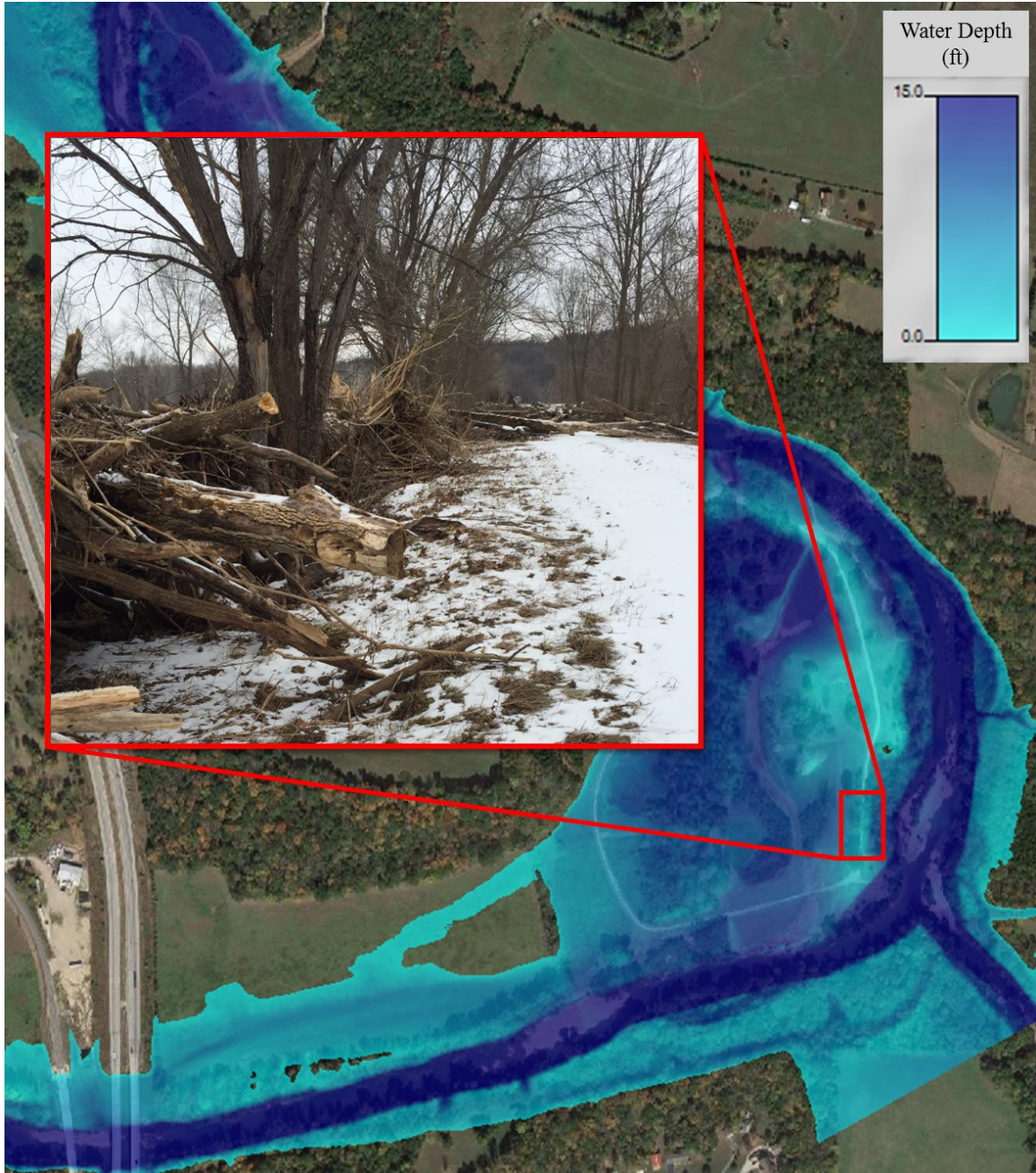


Figure 61 - Simulation of water depth during 5-year flood near large woody debris deposits. Water depth simulation for the 5-year flood (25,560 cfs) shows the location of the log jam that occurred after the December 2015 flood.

HEC-RAS Discussion

Flood simulations. Comparison of pre- and post-construction flood simulations show no significant differences in velocity in the 5, 10, 25, 50, and 100-year floods. Lack of change between the pre- and post-construction simulations at high flows may indicate the constructed riffle and basin have a more substantial affect during smaller flood events.

Velocity comparisons. Comparisons of velocities at relatively low flows show more significant differences in velocities. Differences in velocity at low flows are a result of the installed structures. At low flows the riffle structure appears to be the main control on velocity within the channel, and this may be due to the backwater effect the riffle structure can have on the rest of the channel. Lower velocities at the basin inlet and flow entering the inlet at 2000 cfs also indicate that velocity differences are due to installation of structures within the study area.

Modeling. Velocity simulations have proven to be a useful method for predicting erosion and deposition. Velocity simulations have provided insight into how sediment is being moved within the channel and basin. In many cases, high and low velocities seen within the model correlated with measured and observed erosion and deposition, respectively.

One location where velocity appeared to have dropped due to construction and erosion was measured was the basin inlet. This is an area that may have experienced erosion regardless of construction. However, vegetation removal due to construction is a significant factor enhancing erosion. The removal of vegetation most likely explains why

field observations show erosion even though velocity in this area decreases after construction.

Figure 50 highlights areas of sediment transport and deposition between Transects 10-16. At 200 cfs most of the channel is transporting sediment and at 600 cfs all of the channel is transporting sediment. This trend agrees with what was expected, however sediment was deposited in regions that were indicated within the model as areas of transport. This disagreement is important because it can be explained by three possible scenarios. Scenario one is that this section of channel has reached maximum storage resulting in an increase in velocity. The second scenario may be a failure of the model to characterize flow caused by an incomplete characterization of the channel bed during surveying. The final scenario causing disagreement is the model simulations image only one point in time and the majority of deposition may be occurring at lower flowrates, which does agree with model simulations (Figure 62).

General flow behavior and water surface elevations match, but the intricacies of the bed were not captured well enough to fully support model results. Model simulations do correspond to field observations, and this correlation justifies the model as an accurate analog for events occurring in the field.

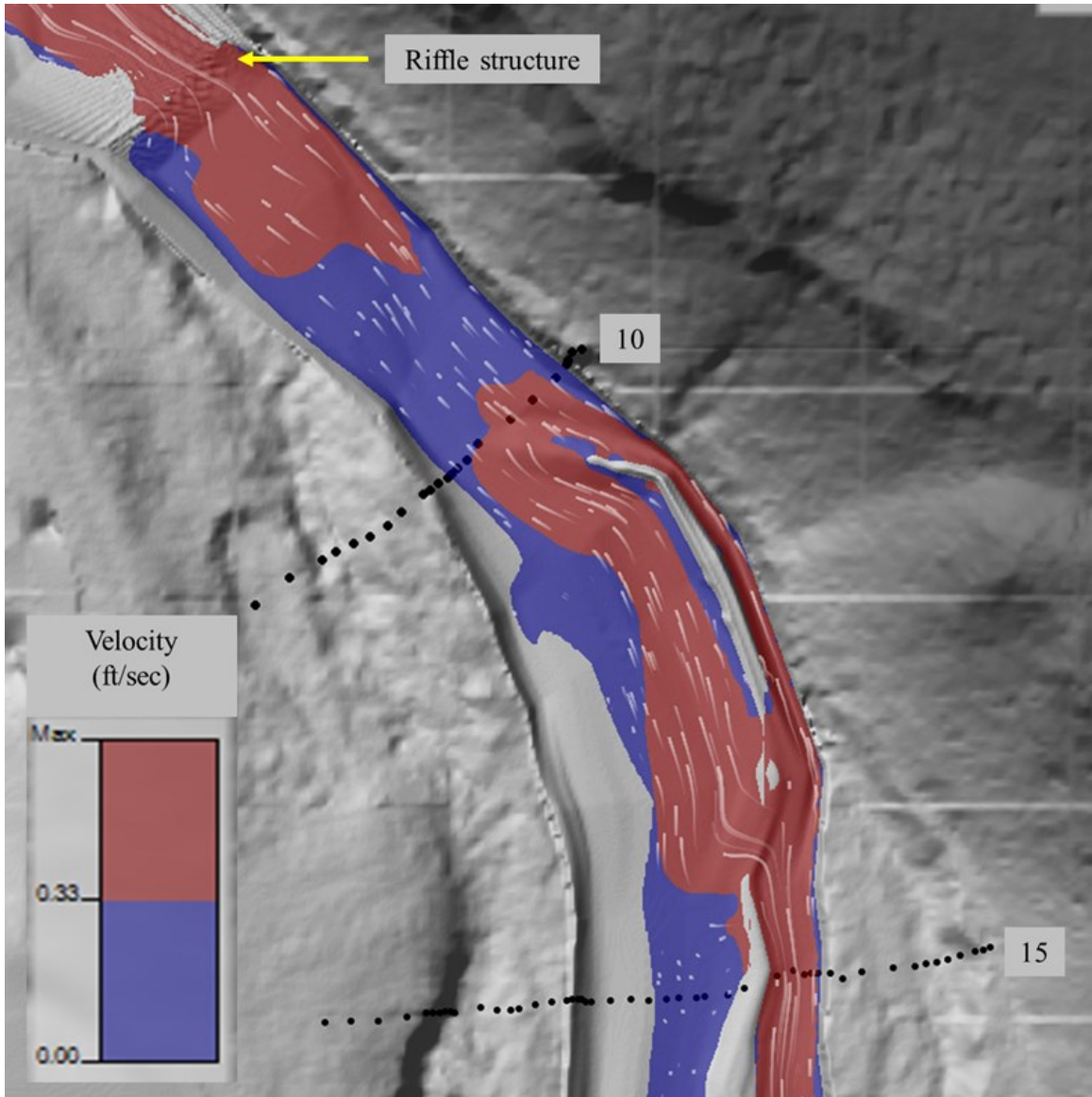


Figure 62 – Simulation at ~100 cfs indicating that deposition should be occurring around Transects 8 and 9 at low flows.

CHAPTER 5 – SUMMARY AND CONCLUSIONS

Due to the extensive lead contamination in the Big River at the Big River Lead Remediation Site, a USEPA Superfund Site, the USACE installed a riffle-ramp structure with the hypothesis that the structure would decrease water velocity just upstream of the structure resulting in deposition and storage of lead-contaminated mining sediments that could be dredged at later dates. Transects were set up, survey data was collected, and sediment samples were analyzed to determine concentrations of Pb and Zn. For a better understanding of flow velocities within the study site HEC-RAS 5.0.3 was used to model conditions during varying flood magnitudes. The model output velocities, water surface elevations, and particle tracing that displayed flow direction.

Significant Results

The most significant results of this study include:

- 1) Survey results indicated that the riffle ramp structure is modestly successful.
- 2) Geochemical analysis showed that sediment within the channel and on bars has a range of 673 ppm to 4955 ppm, well above the USEPA standard for lead.
- 3) The model proved to be a useful tool for representing high- and low-velocity areas that correlated with erosion and deposition that was observed in the field. This correlation between high velocities and erosion seen in the thalweg and low velocities and deposition in the chute around Transects 10-16 aids in the understanding of sediment movement within the channel and provides insight to potential dredging activities, including the capability to predict dredging consequences.

Future Work

Although this study improved the understanding of the successfulness of riffle ramp remediation structures and created a model that can be used as an analog for actual flood events, or alternative structure geometries, it is important to look at what more could be done to better understand and represent the Big River Lead Remediation Site. For better understanding and representation of the site the main goals of the study should be expanded upon.

Evaluation of the success of the riffle ramp structure required collection of survey data to account for changes that occurred within the channel over time, however, monitoring the channel for ~1.5 years only shows short-term changes within the channel. To understand if riffle remediation structures could be a useful remediation technique, monitoring channel changes through the collection of survey data would need to be continued to understand longer term effects. To better understand how the riffle structure is storing sediment it would be beneficial to collect survey data for creating a profile representing sediment deposition within the channel. Continued surveys would benefit from the addition of posts on the right bank as well as consistency of instruments used for data collection.

During this study no dredging had occurred. However, the effect of dredging on sediment transport is an important part of the project that has not been studied.

Through geochemical analysis it was determined that sediment within the channel and on bars of the Big River at the Big River Lead Remediation Site contain both Pb and Zn contaminants. The level of contaminants seemed to be highest within the area of deposition, however due to the few number of samples collected the exact location of

contaminants was inconclusive. In the future, collecting samples from all places where deposition is occurring and running a geochemical analysis of those samples may help determine if the channel is storing Pb and Zn contaminants of the highest concentrations.

Although the model has proved to be a sufficient analog for representing varying velocities and depths of water within the site, the model can always be improved. In the future it may be beneficial to add the culverts installed by the UASCE to better represent how flow is routed through the basin area. HEC-RAS 5.0.3 also has the capabilities of modeling sediment transport. For dredging purposes, modeling sediment transport could be beneficial to the USEPA and the USACE. Further studies could also be done to assess the effect Flat River Creek has on the hydraulics or sediment load of the Big River. Long-term comparison of computer modeling and field behavior will improve understanding of sediment transportation and modeling of sediment transport, resulting in a more accurate model.

REFERENCES CITED

- Agency for Toxic Substances and Disease Registry, 2010, Case studies in environmental (CSEM) lead toxicity: Center for Disease Control (paper copy, 71 p.).
- Aldridge, B.N., and Garrett, J.M., 1973, Roughness coefficients for stream channels in Arizona. U.S. Geological Society Open-File Report 73-3 (online pdf, 87 p.).
- Bedient, P.B., Huber, W.C., and Vieux, B.E., 2008, Hydrology and Floodplain Analysis Fourth Edition: Upper Saddle River, New Jersey, Prentice Hall, 795 p.
- Brown, B.L., 1981. Soil survey of St. Francois County, Missouri. United States Department of Agriculture, Soil Conservation Service and Forest Service in cooperation with the Missouri Agricultural Experiment Station, 142p.
- Brunner, G.W., 2016A, HEC-RAS, River Analysis System, 2D Modeling User's Manual Version 5.0: U.S. Army Corps of Engineering Hydrologic Engineering Center, 171 p.
- Brunner, G.W., 2016B, HEC-RAS, river analysis system hydraulic reference manual: U.S. Army Corps of Engineering Hydrologic Engineering Center, 547 p.
- Chow, V.T., 1959, Open Channel Hydraulics: New York, McGraw-Hill, 680 p.
- Ervine, D.A, MacLeod, A.B., 1999, Modelling a river channel with distant floodbanks, Proceedings of the Institution of Civil Engineers – Water and Maritime Engineering, vol. 136, p. 21-33, doi:10.1680/iwtme.1999.31265.
- Fan, C., Wang, W., Liu, K. F., and Yang, T., 2012, Sensitivity analysis and water quality modeling of a tidal river using a modified Streeter-Phelps Equation with HEC-RAS-calculated hydraulic characteristics: Environmental Modeling and Assessment, v. 17, p. 639-651.
- Federal Interagency Stream Restoration Working Group (FISRWG), 1998, Stream corridor restoration: principles, processes, and practices: U.S. Department of Agriculture (online pdf, 637 p.)
- Ferguson, R.M., Lyness, J.F., Myers, W.R.C., and O'Sullivan, J.J., 1998, Hydraulic performance of environmental features in rivers: Water and Environment Journal, v. 12, p. 268-291, doi:10.1111/j.1747-6593.1998.tb00187.x.
- Fischenich, J.C., 1994, Instream and streambank environmental feature guidelines, in Proceedings, 1994 National Conference on Hydraulic Engineering, Buffalo, New York, p. 406-410.

- Gibson, S., and Boyd, P., 2016, Monitoring, measuring, and modeling a reservoir flush on the Niobrara River in the Sandhills of Nebraska, in Proceedings, International Symposium on River Sedimentation: Stuttgart, Germany, p. 1-8.
- Goodell, C. R., and Brunner, G. W., 2004, Watershed analysis with the Hydrologic Engineering Center's River Analysis System (HEC-RAS): Army Engineer Research and Development (paper copy, 20 p.).
- Hassanzadeh, Y., 2012, Hydraulics of sediment transport, *in* Zheng, J., ed., Hydrodynamics- Theory and Model: European Union, InTech, p. 23-58.
- Interstate Technology Regulatory Council, 2010, Case study as part of a web-based technical and regulatory guidance, Big River Mine Tailings Site, St. Francois County, Missouri: http://www.itrcweb.org/miningwaste-guidance/cs62_big_river.htm (accessed November 2016).
- Keller, E.A., 1978, Pools, riffles, and channelization: *Environmental Geology*, v. 2, p. 119-127.
- Keller, E.A., and Melhorn, W.N., 1978, Rhythmic spacing and origin of pools and riffles: *Geological Society of America Bulletin*, v. 89, p. 723-730.
- Knight, D.W., and Shiono, K., 1996, Channel and floodplain hydraulics, *in* Anderson, M.G., Walling, D.E., Bates, P.D., ed., *Floodplain Processes*: New York, Wiley, 668 p.
- Kondolf, G.M., 1998, Lessons learned from river restoration projects in California: *Aquatic Conservation: Marine and Freshwater Ecosystems*, v. 8, p. 39-52.
- Lagasse, C.R., Ou, W., Honka, L. D., Atlas, W. I., Hutton, C. N., Kotaska, J., Hocking, M. D., 2014, Design considerations for community-based stream monitoring to detect changes in Pacific salmon habitats: *Ecology and Society*, v. 19, p. 1-15.
- Leopold, L.B., Wolman, M.C., and Miller, J.P., 1964, *Fluvial Processes in Geomorphology*: New York, Dover Publications, 522 p.
- Lisle, T.E., 1982, Effects of aggradation and degradation on riffle-pool morphology in natural gravel channels, Northwestern California: *Water Resources Research*, v. 18, p. 1643-1651.
- Lutgens, F.K., and Tarbuck, E.J., 2015, *Essentials of Geology*: New Jersey, Pearson, 574p.
- Maeder, C., 2015, The road to HEC-RAS: <http://www.civilgeo.com/the-road-to-hec-ras/> (accessed March 2016).

- Missouri Department of Natural Resources, 2016A, Mine maps – St. Francois County: <http://dnr.mo.gov/geology/geosrv/geores/minemapsstfrancois.htm> (accessed May, 2016).
- Missouri Department of Natural Resources, 2016B, Big River Mine Tailings Site: <https://dnr.mo.gov/env/hwp/sfund/bigriver.htm> (accessed November 2016).
- Moby, D.E., Weber, J.S., and Klahr, F., 2009, Final phase I damage assessment plan for Southeast Missouri Lead Mining District: Big River Mine Tailings Superfund Site, St. Francois County and Viburnum Trend Sites, Reynolds, Crawford, Washington, and Iron Counties: MDNR and FWS, (paper copy, 77 p.)
- Newbury, R.W. and Gaboury, M.N., 1993, Stream Analysis and Fish Habitat Design, a Field Manual: British Columbia, Newbury Hydraulics Ltd., 261p.
- Owen, M.R., Pavlowsky, R.T., and Martin, D.J., 2012, Big River borrow pit monitoring project: The Ozarks Environmental and Water Resources Institute Missouri State University (electronic copy, 82 p.).
- Ozarks Environmental and Water Resources Institute, 2007, Standard operating procedure for X-MET3000TXH+ Handheld XRF Analyzer: Missouri State University (paper copy, 32 p.).
- Pappenberger, F., Beven, K., Horrit, M, and Blazkova, S., 2004, Uncertainty in the calibration of effective roughness parameters in HEC-RAS using inundation and downstream level observations: *Journal of Hydrology*, v. 308, p. 46-69, doi:10.1016/j.jhydrol.2004.06.036
- Radspinner, R. R., 2009, Development of design guidelines for in-stream flow control structures [Masters thesis]: Virginia Polytechnic Institute and State University, 98 p.
- Roy, A.G., and Abrahams, A.D., 1980, Rhythmic spacing and origin of pools and riffles: *Geological Society of America Bulletin*, v. 91, p. 248-250.
- Sellin, R.H.J., Ervine, D.A., Willets, B.B., 1993, Behavior of meandering two-stage channels: *Proceedings of the Institution of Civil Engineers – Water, Maritime, and Energy*, v. 101, p. 99-111.
- U.S. Environmental Protection Agency, 2001, Lead; identification of dangerous levels of lead; final rule: *Federal Register*, v. 66, p. 1206-1240.
- U.S. Environmental Protection Agency, 2016, Superfund site: Big River Mine Tailings/St. Joe Minerals Corp., Desloge, Mo:

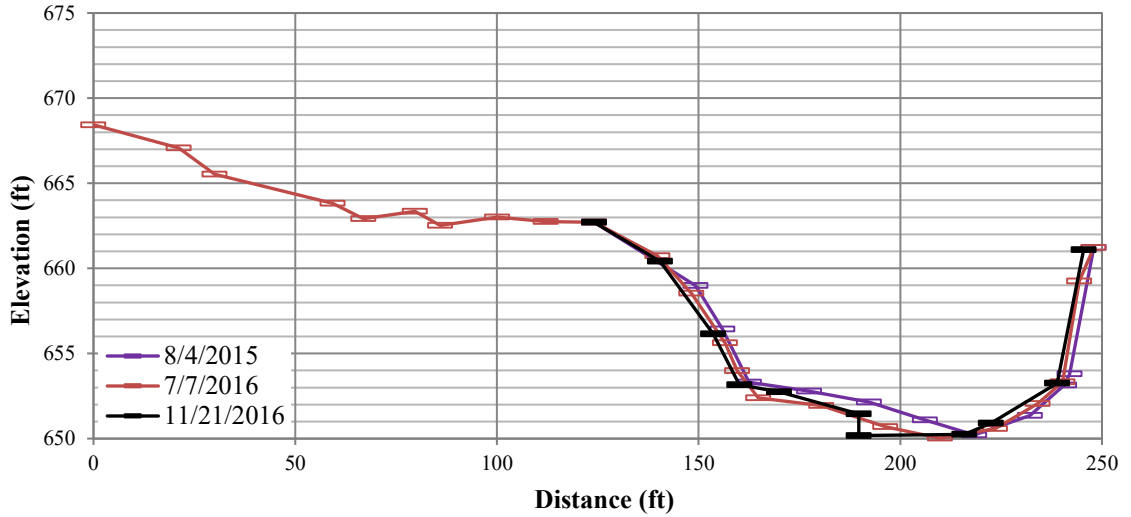
<https://cumulis.epa.gov/supercpad/cursites/csinfo.cfm?id=0701639> (accessed November 2016).

- U.S. Environmental Protection Agency Region 7, 1993, Engineering evaluation/cost analysis for the Big River Miner Tailings Site, Desloge, Missouri: U.S. Environmental Protection Agency, p. 1-2
- U.S. Environmental Protection Agency Region 7, 2011, Record of Decision: Big River Mine Tailings Superfund Site, St. Francois County, Missouri: U.S. Environmental Protection Agency, p. 1-26.
- U.S. Fish and Wildlife Service, 2008, Preassessment screen and determination Big River Mine Tailings Site, St. Francois County, Missouri: Missouri Department of Natural Resources, p. 1-20.
- U.S. Geologic Survey, 2017, USGS 07017260 Big River below Desloge, Mo: https://nwis.waterdata.usgs.gov/mo/nwis/uv/?cb_00060=on&cb_00065=on&format=gif_default&site_no=07017260&period=&begin_date=2015-08-01&end_date=2016-11-30 (accessed March 2017).
- Van Rijn, L.C., 1984, Sediment transport, part I: bedload transport: *Journal of Hydraulic Engineering*, v. 110, p. 1431-1456.
- Voss, J. 2017, Deposition patterns and rates of mining-contaminates sediment within a sedimentation basin system, Big River, S.E. Missouri [Masters Thesis]: Missouri State University, 157p.
- Walker, D.R., Millar, R.G., and Newbury, P.E., 2004, Energy profiles across constructed riffles: *Journal of Hydraulic Engineering*, v. 130, p. 199-207, doi:10.1061/(ASCE)0733-9429(2004)130:3(199).
- Wilcock, P.R., and DeTemple, B.T., 2005, Persistence of armor layers in gravel-bed streams: *Geophysical Research Letters*, v. 32, p. 1-4.
- World Atlas, 2016, Missouri –county map: <http://www.worldatlas.com/webimage/countrys/namerica/usstates/counties/mocounty.htm> (accessed May, 2016).

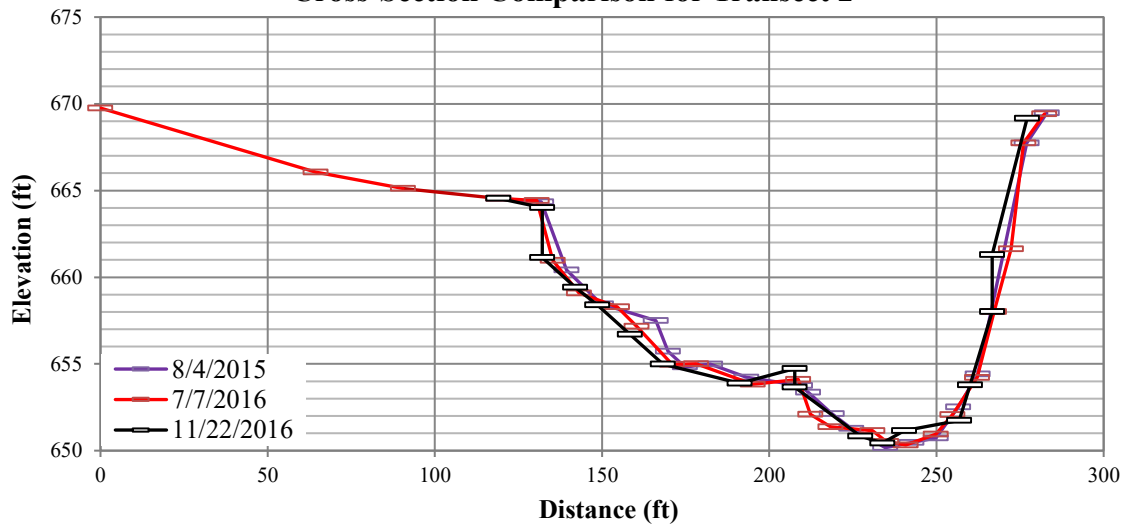
APPENDICES

Appendix A – Compilation of all survey data collected from August 2015 to November for Transects 1-22

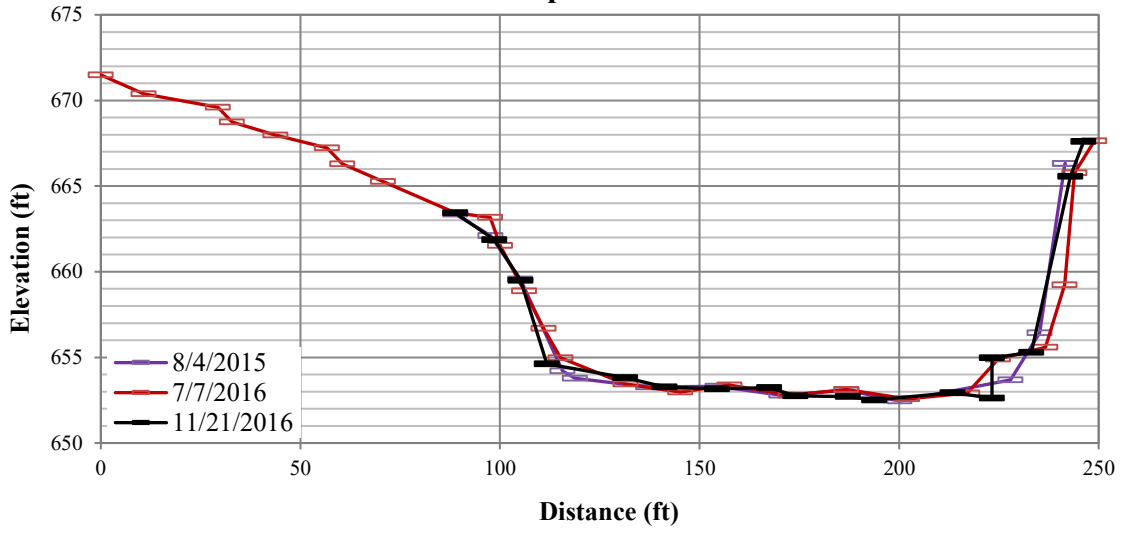
Cross-Section Comparison For Transect 1



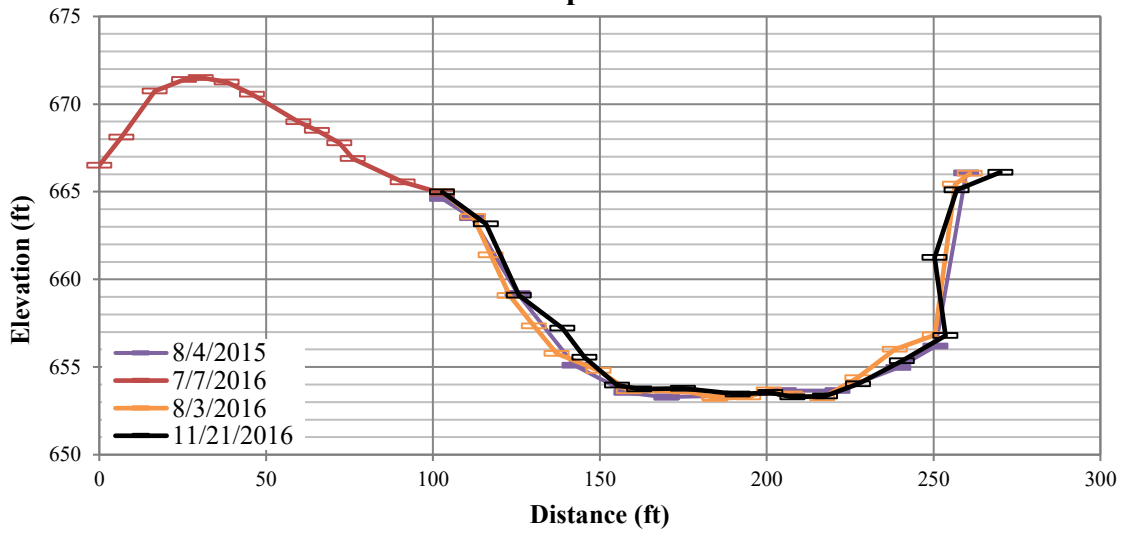
Cross-Section Comparison for Transect 2



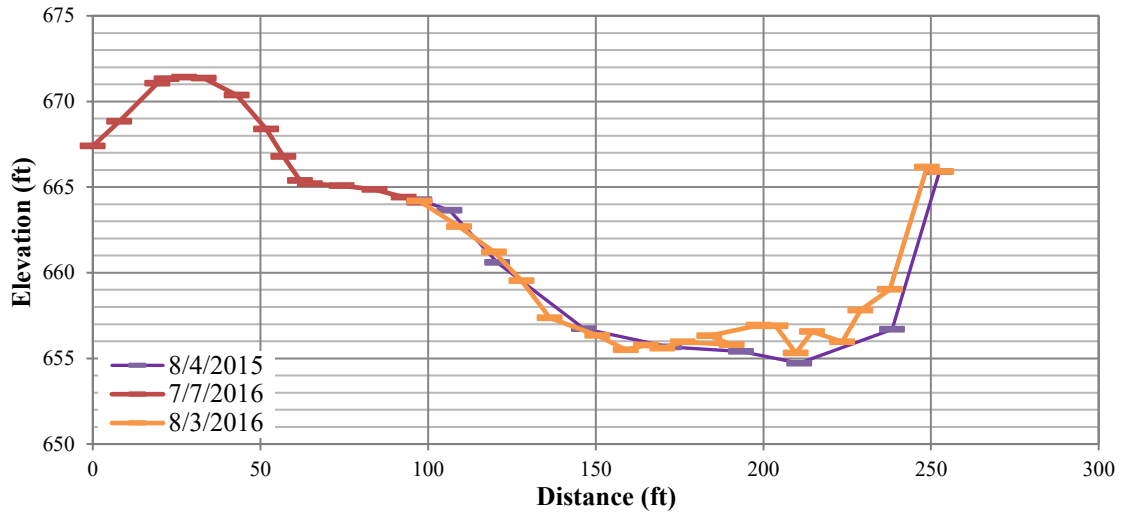
Cross-Section Comparison for Transect 3



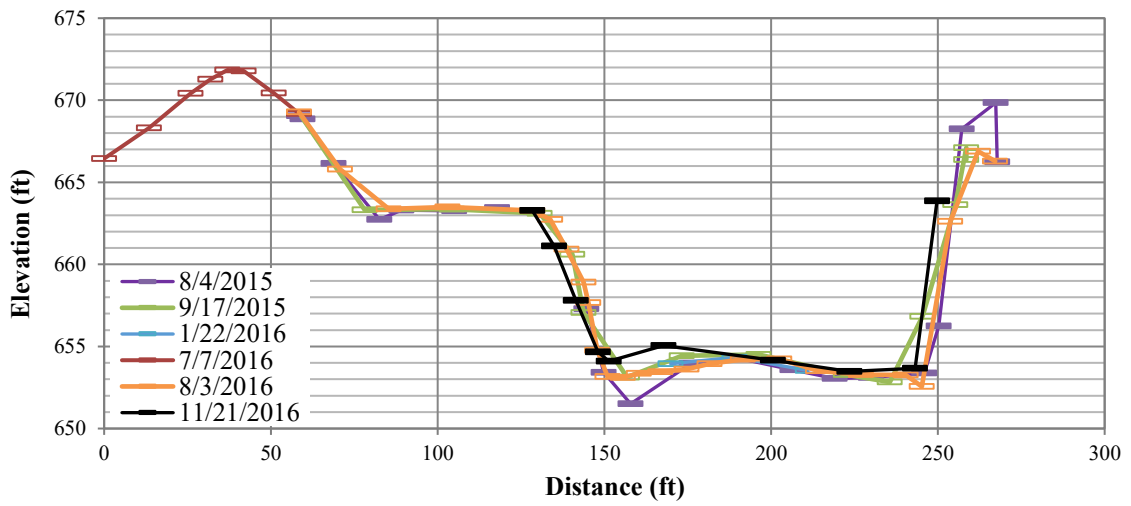
Cross-Section Comparison for Transect 4



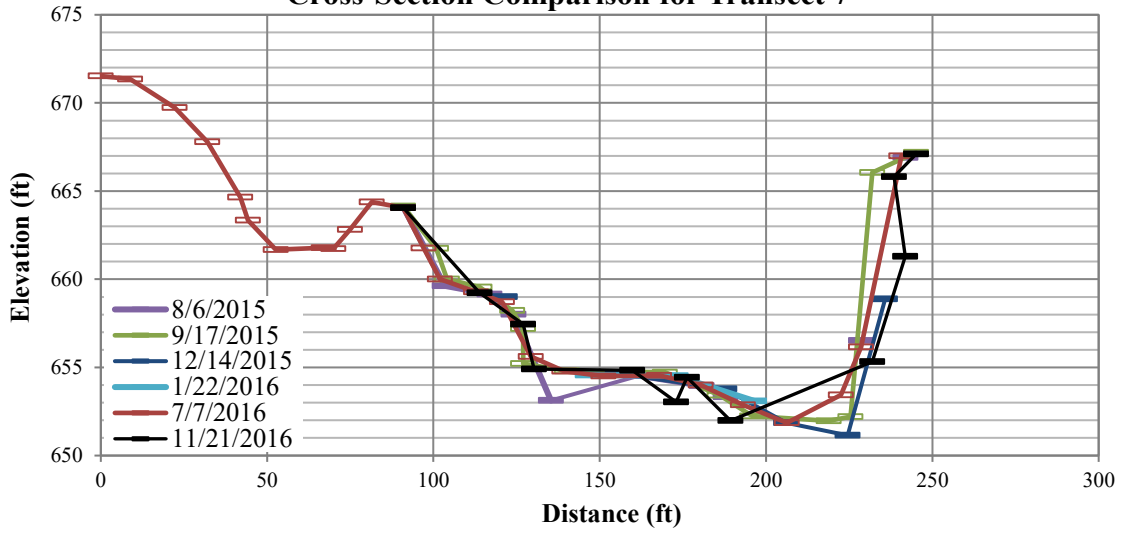
Cross-Section Comparison for Transect 5



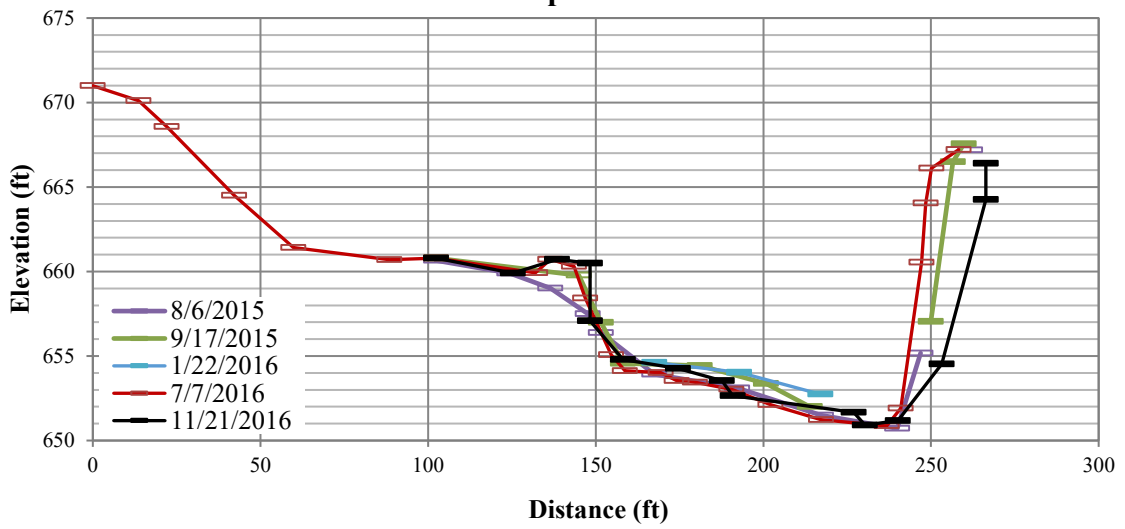
Cross-Section Comparison for Transect 6



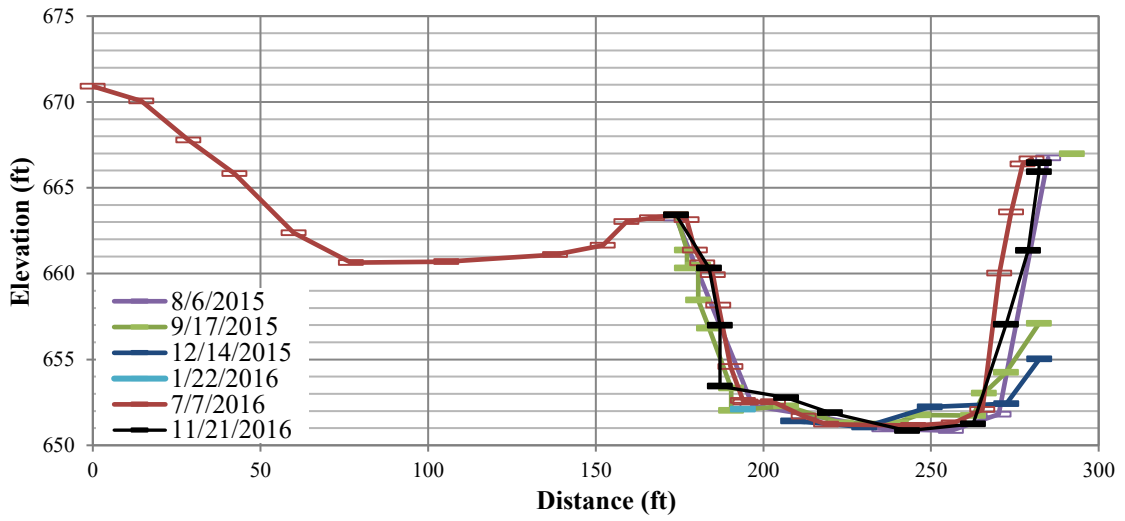
Cross-Section Comparison for Transect 7



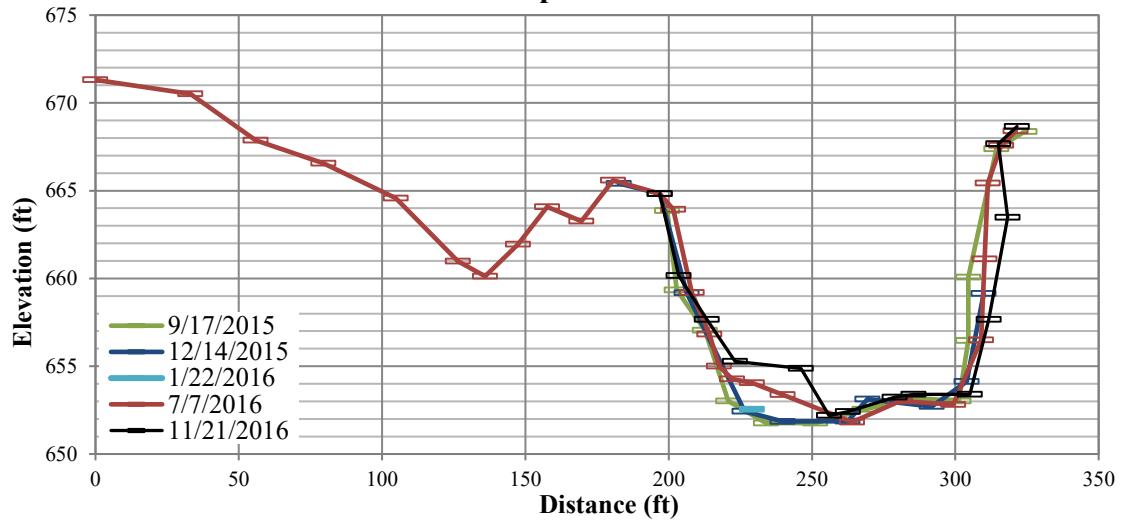
Cross-Section Comparison for Transect 8



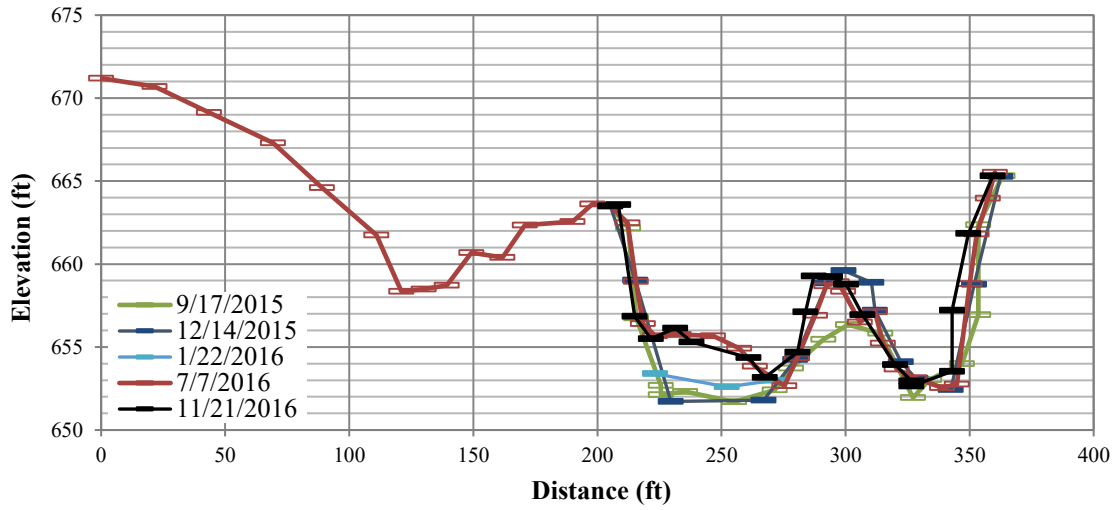
Cross-Section Comparison for Transect 9



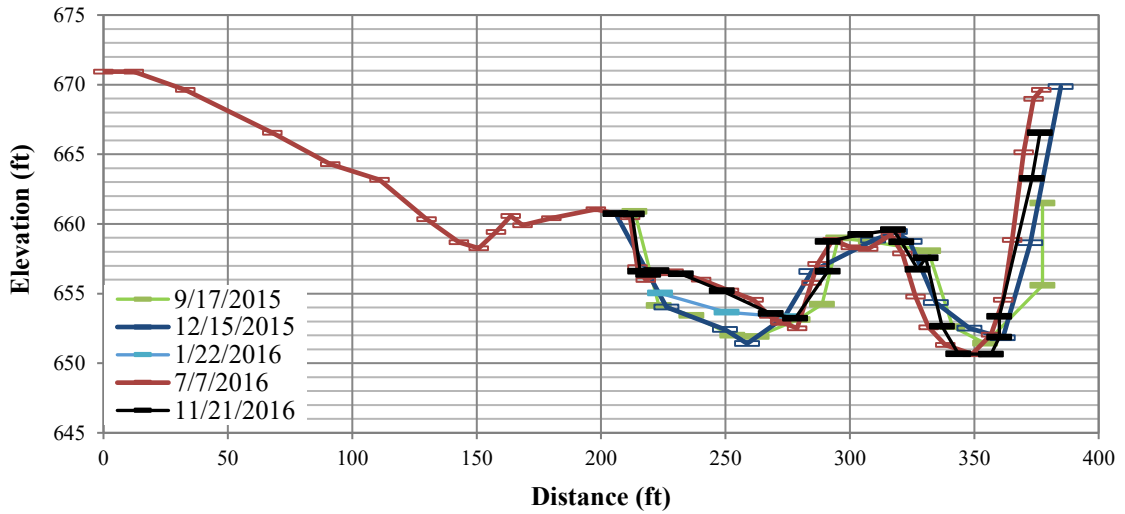
Cross-Section Comparison for Transect 10



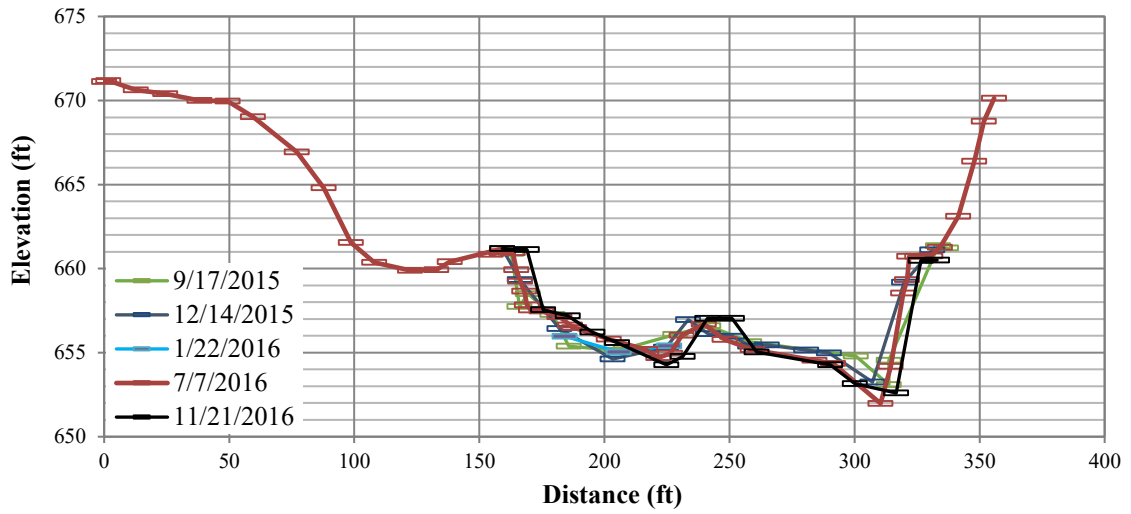
Cross-Section Comparison for Transect 11



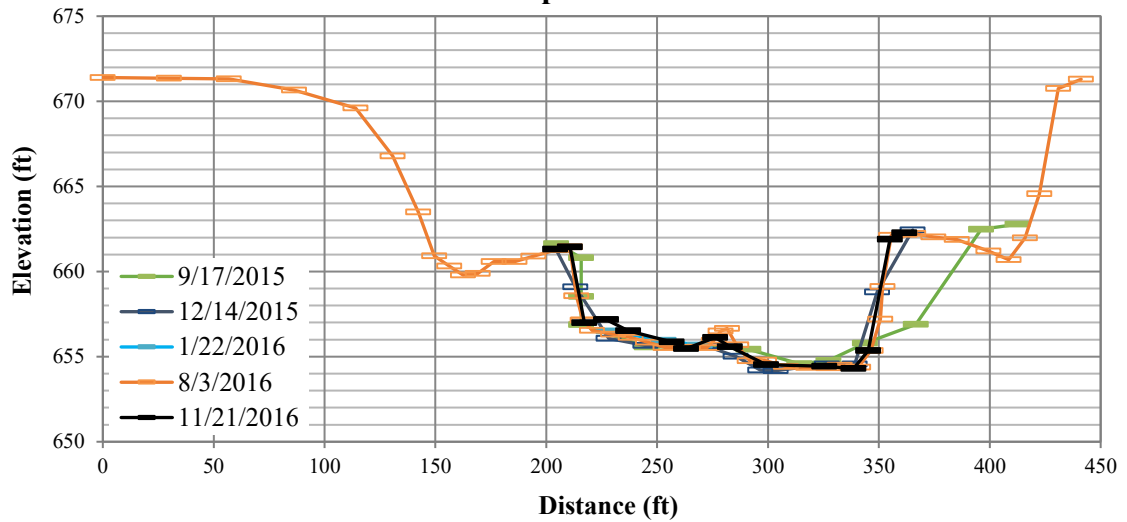
Cross-Section Comparison for Transect 12



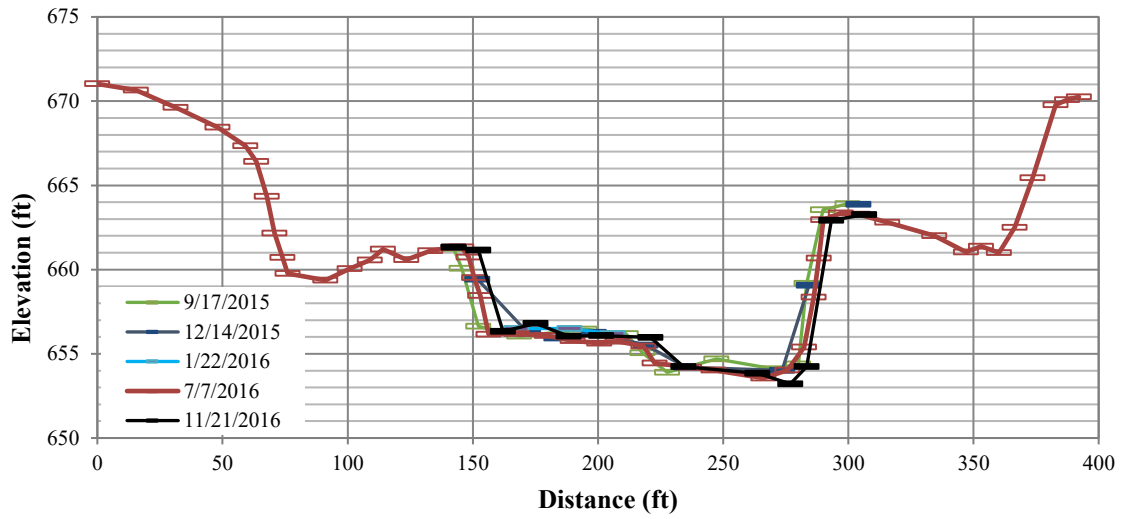
Cross-Section Comparison for Transect 13



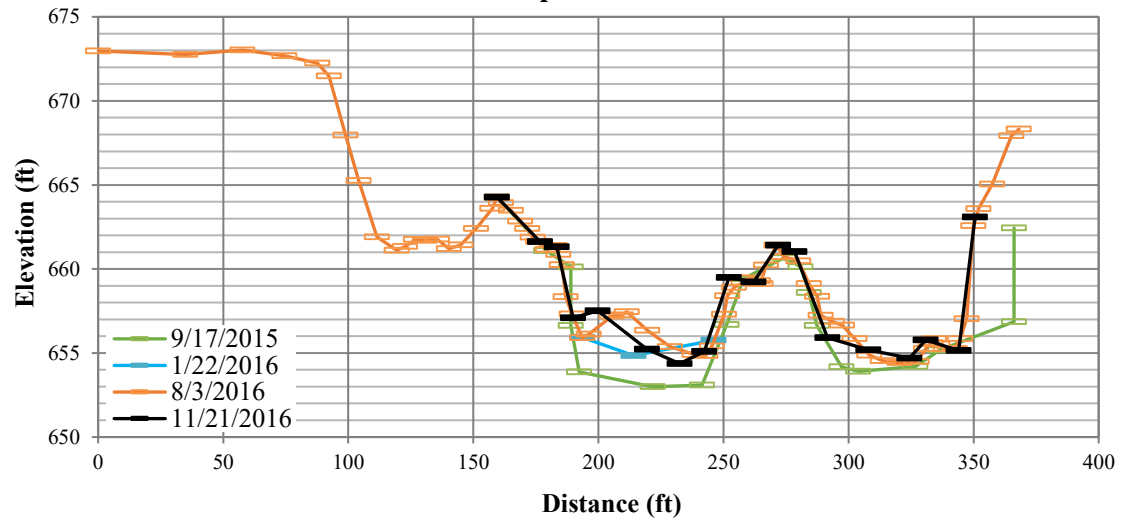
Cross-Section Comparison for Transect 14



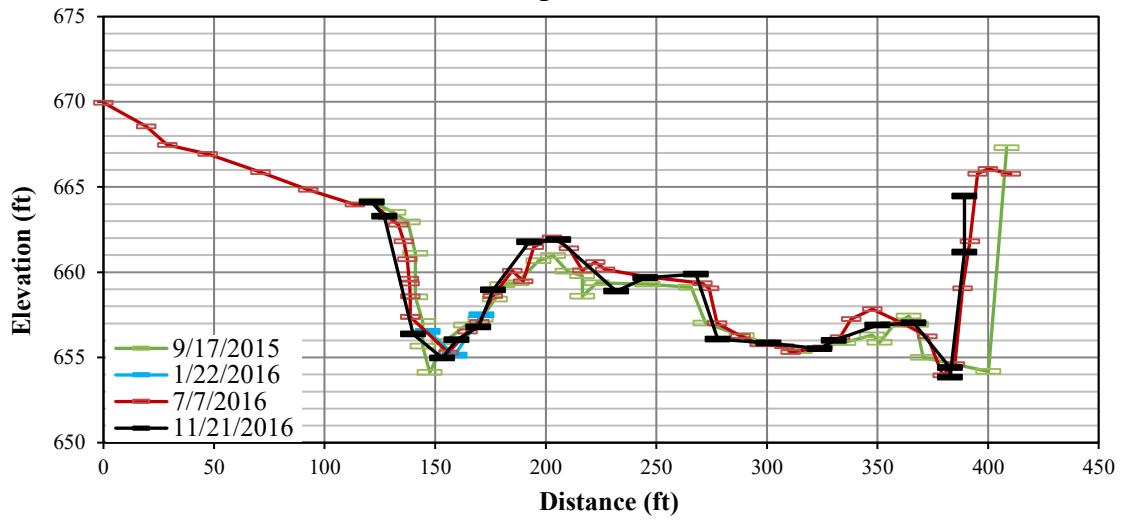
Cross-Section Comparison for Transect 15



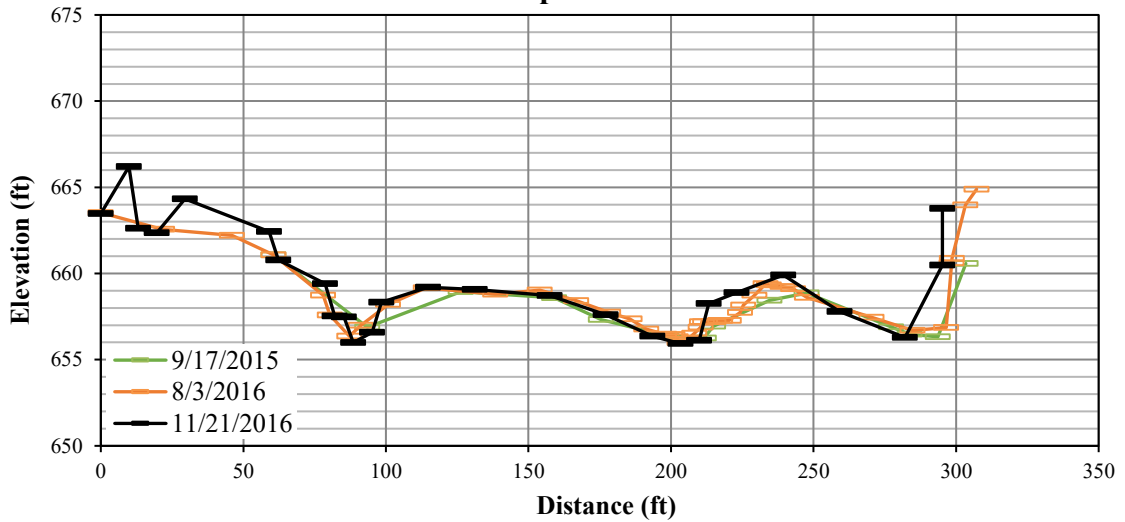
Cross-Section Comparison for Transect 16



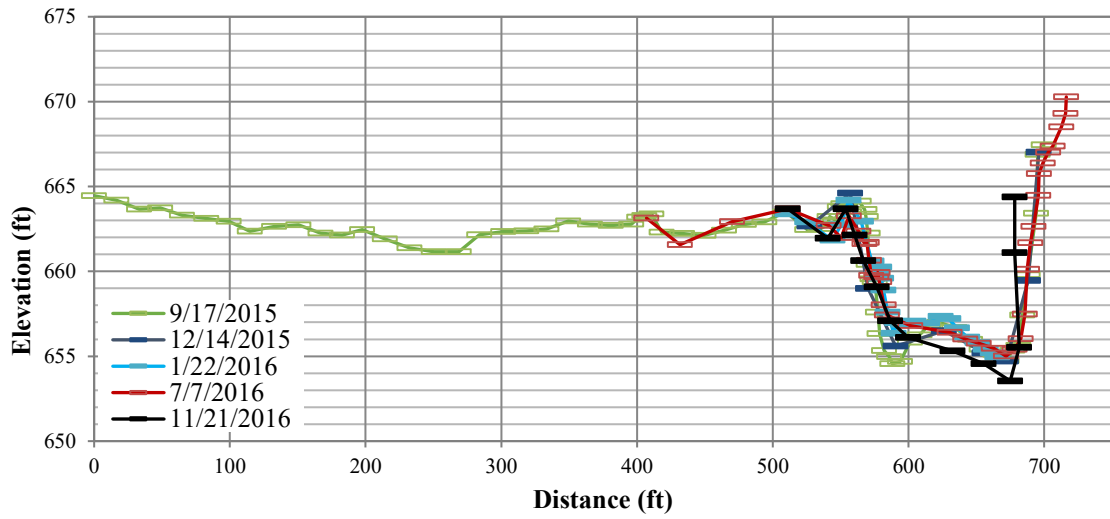
Cross-Section Comparison for Transect 17



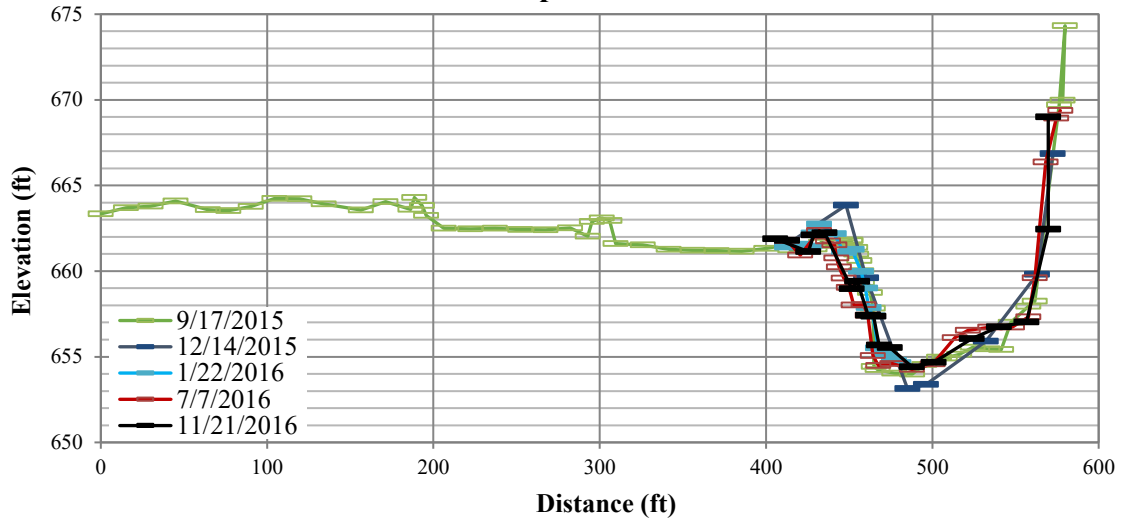
Cross-Section Comparison for Transect 18



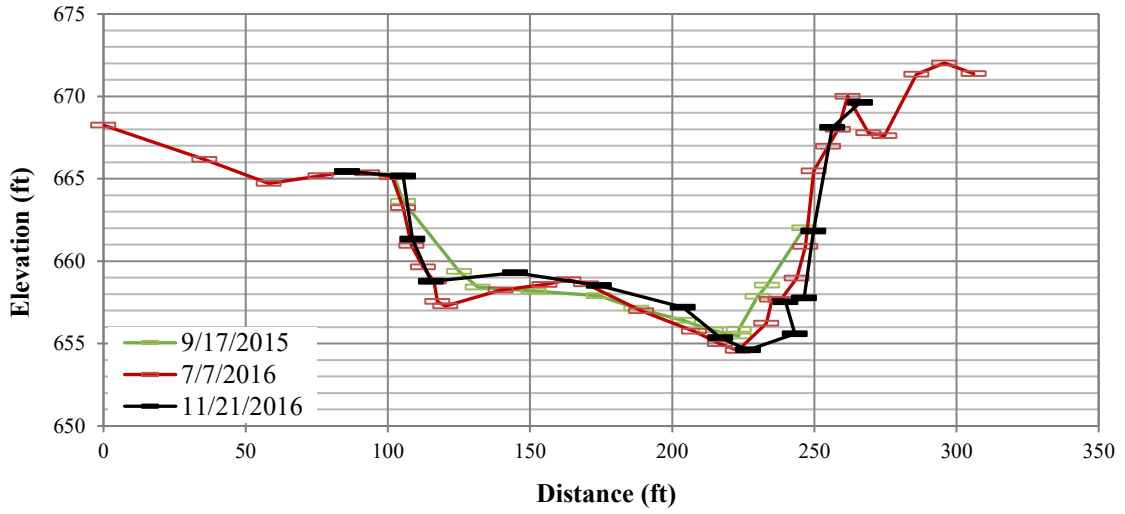
Cross-Section Comparison for Transect 19



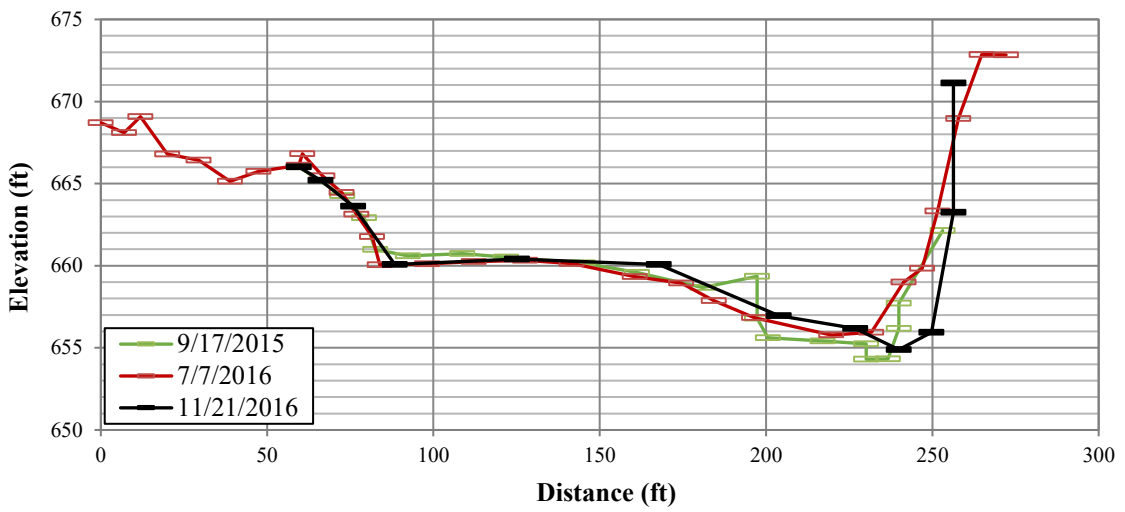
Cross-Section Comparison for Transect 20



Cross-Section Comparison for Transect 21



Cross-Section Comparison for Transect 22



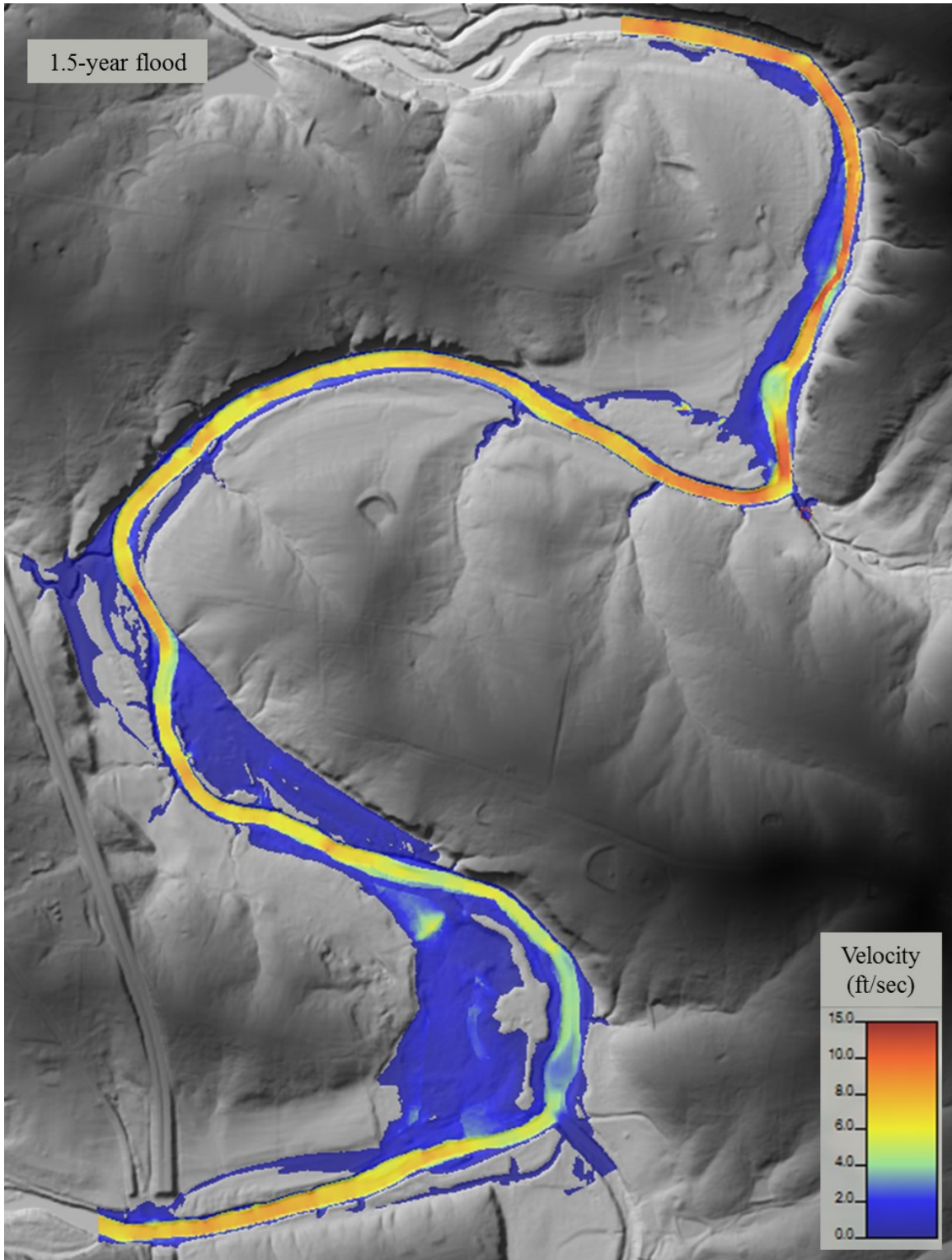
Appendix B – Geochemical Data**September 2015 Samples**

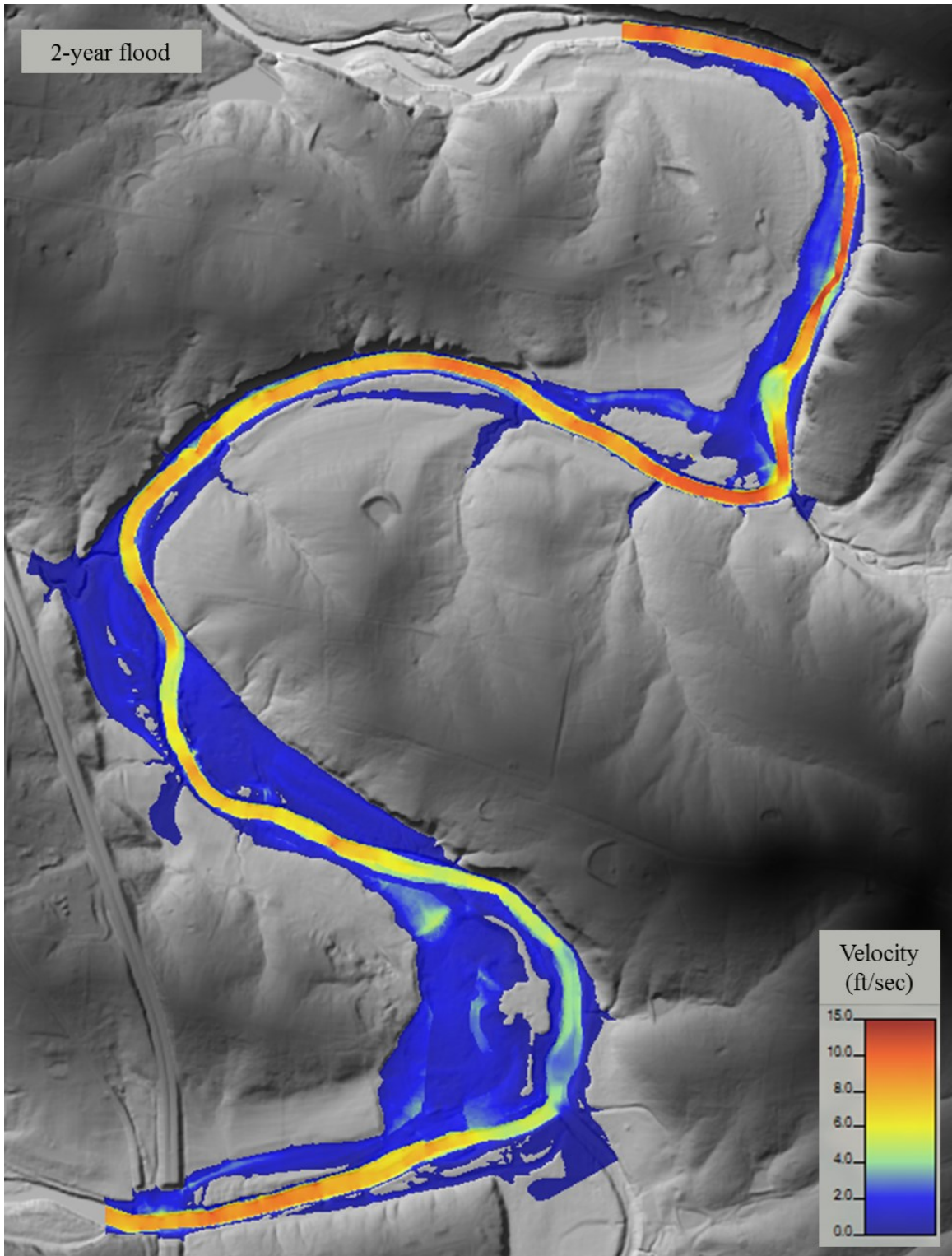
Sample Name	Pb (ppm)	Zn(ppm)
Standard 1 (jasperoid)	897	860
Blank 1	ND	7
1-3 -- Transect 22	1680	1797
2-4 -- Transect 22	3049	2800
3-5 -- Transect 21	2983	2313
4-6 -- Transect 21	3348	2710
5-9 --Transect18	3469	1320
6-10 --Transect 18	3076	2146
7-11 --Transect 17	4955	2373
8-12 --Transect 17	2143	1928
9-17 -- Transect 16	1458	1423
10-18 -- Transect 16	1699	1235
10-18 duplicate	1720	1257
Standard 2 (jasperoid)	801	824
Blank 2	ND	6
11-19 -- Transect 16	1301	658
12-20 -- Transect 16	1259	973
13-21 -- Transect 6	1064	1200
14-22 -- Transect 6	1407	822
15-23 -- Transect 7	924	791
16-24 --Transect 7	1344	795
17-27 --Transect 1	1900	1267
18-28 --Transect 1	1458	1026
19-29 --Transect 1	1217	1032
20-30 --Transect 1	954	1068
20-30 duplicate	949	1090
Standard 3 (jasperoid)	854	797
Blank 3	ND	ND

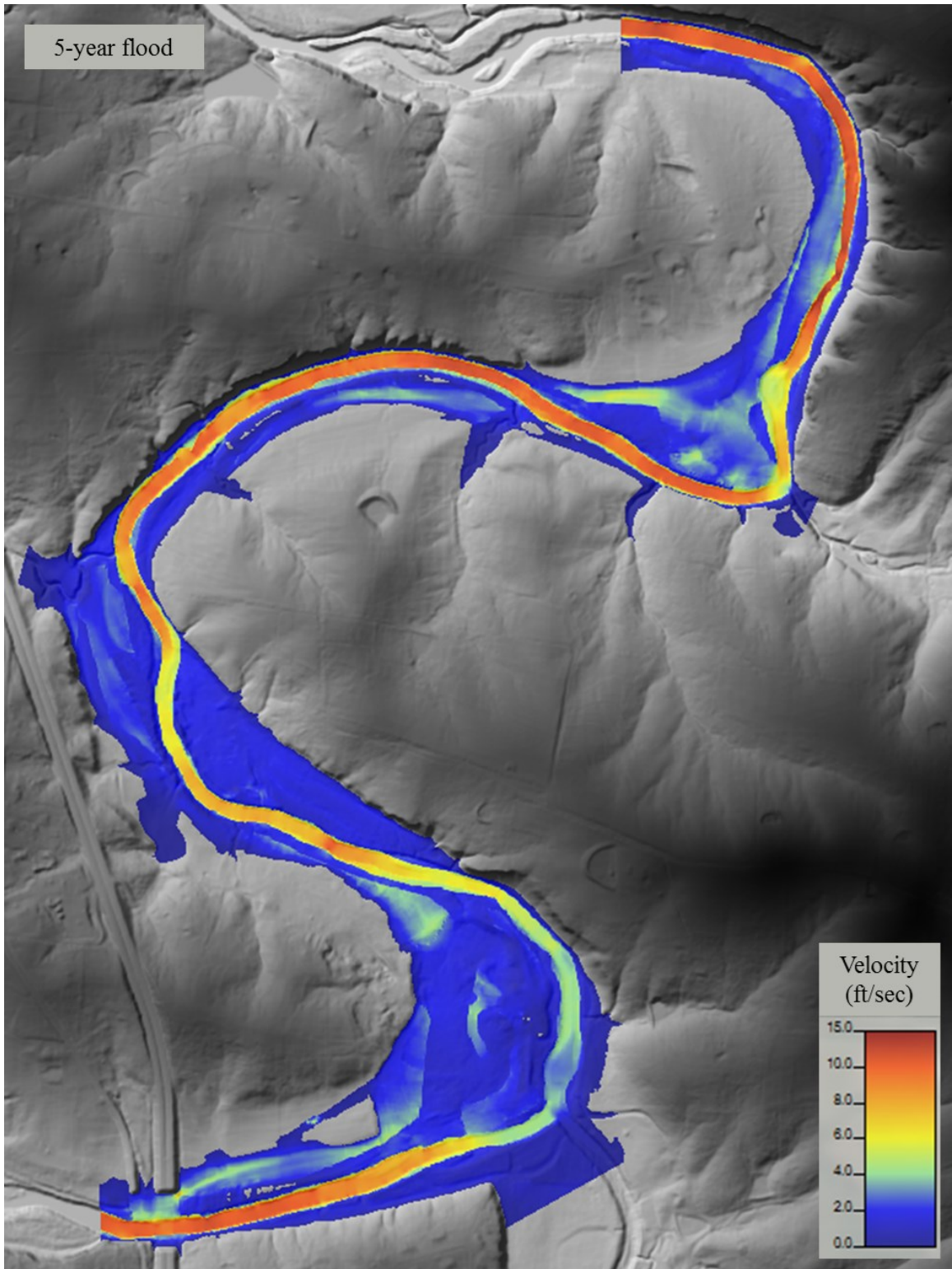
November 2016 Samples

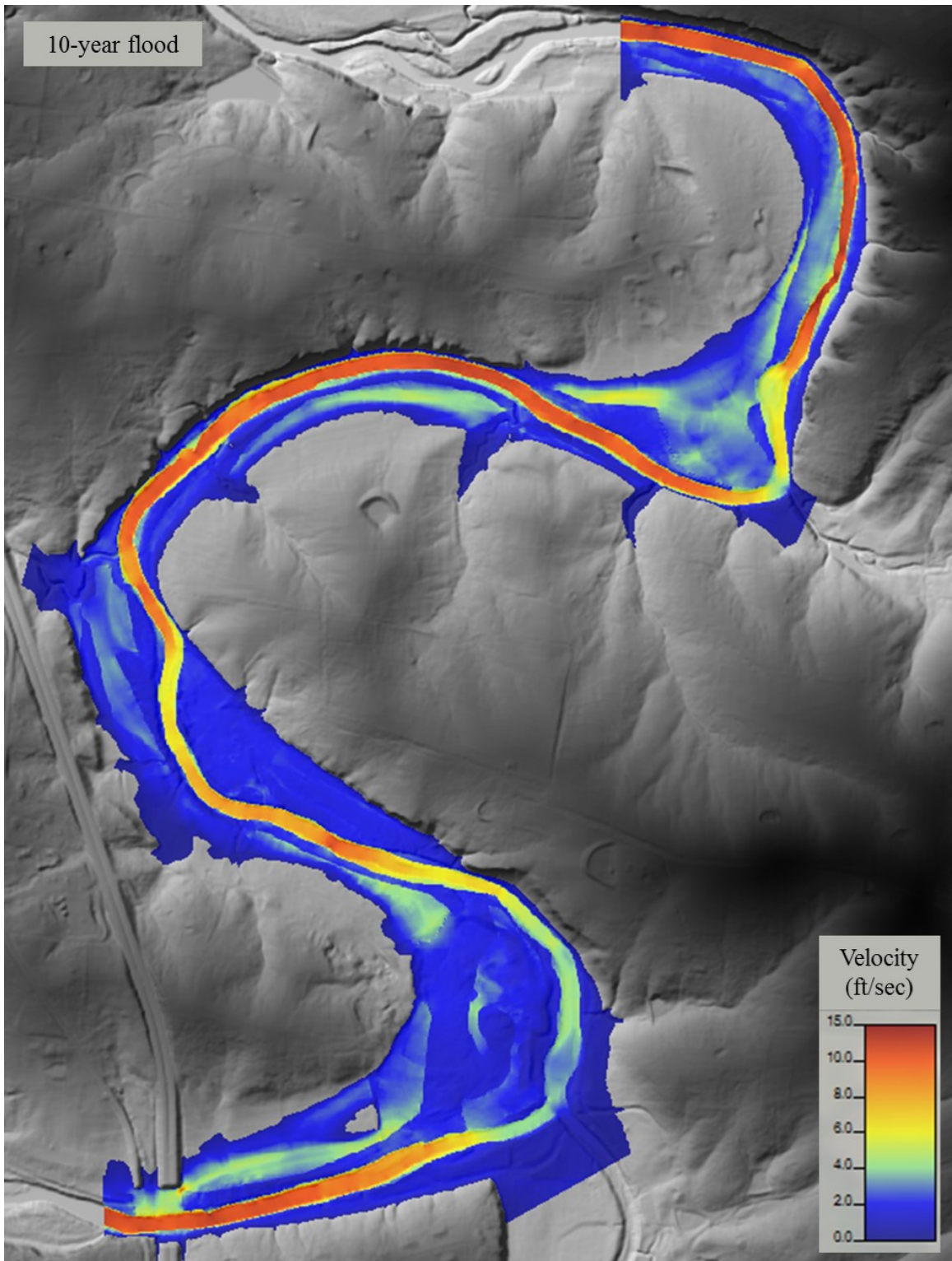
Sample Name	Pb (ppm)	Zn(ppm)
Standard 1 (jasperoid)	927	856
Blank 1	ND	ND
T11-1 Transect 11	1821	2904
T11-2 Transect 11	1463	1722
T11-3 Transect 11	1528	1051
T12-1 Transect 12	1421	1680
T12-2 Transect 12	1521	895
T12-3 Transect 12	1983	1200
T13-1 Transect 13	1883	2926
T13-2 Transect 13	2400	3126
T13-3 Transect 13	1247	792
T13-3 Duplicate	1235	797
Standard 2 (jasperoid)	899	848
Blank 2	ND	8
T14-1 Transect 14	1456	1608
T14-2 Transect 14	1328	1957
T14-3 Transect 14	1656	1784
T15-1 Transect 15	1887	2027
T15-2 Transect 15	1567	1861
T15-3 Transect 15	1987	1872
T16-1 Transect 16	2283	1956
T16-2 Transect 16	1614	1802
T16-3 Transect 16	1214	1187
T16-3 Duplicate	1251	1230
Standard 3 (jasperoid)	859	871
Blank 3	ND	14

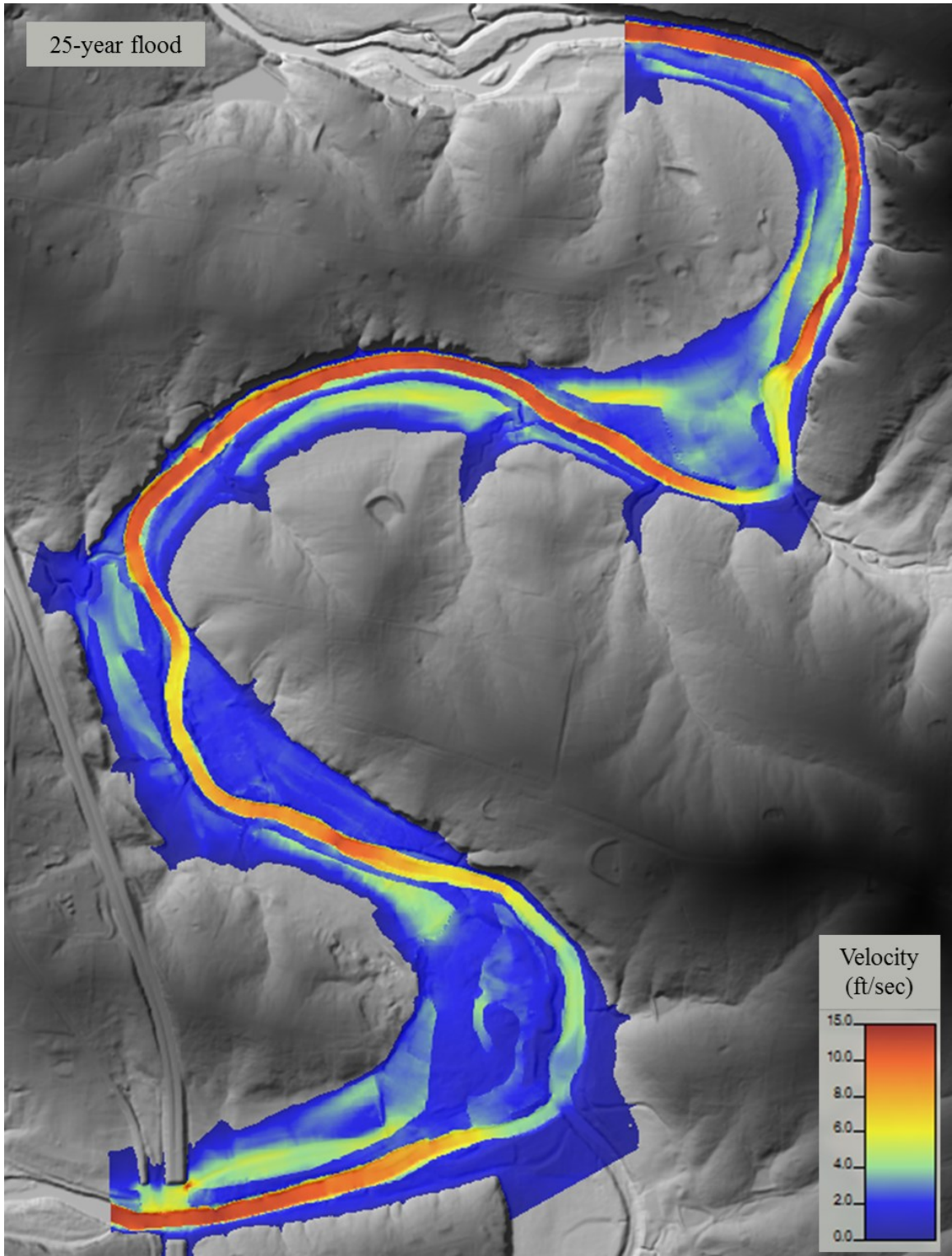
Appendix C – Pre-construction velocity models.

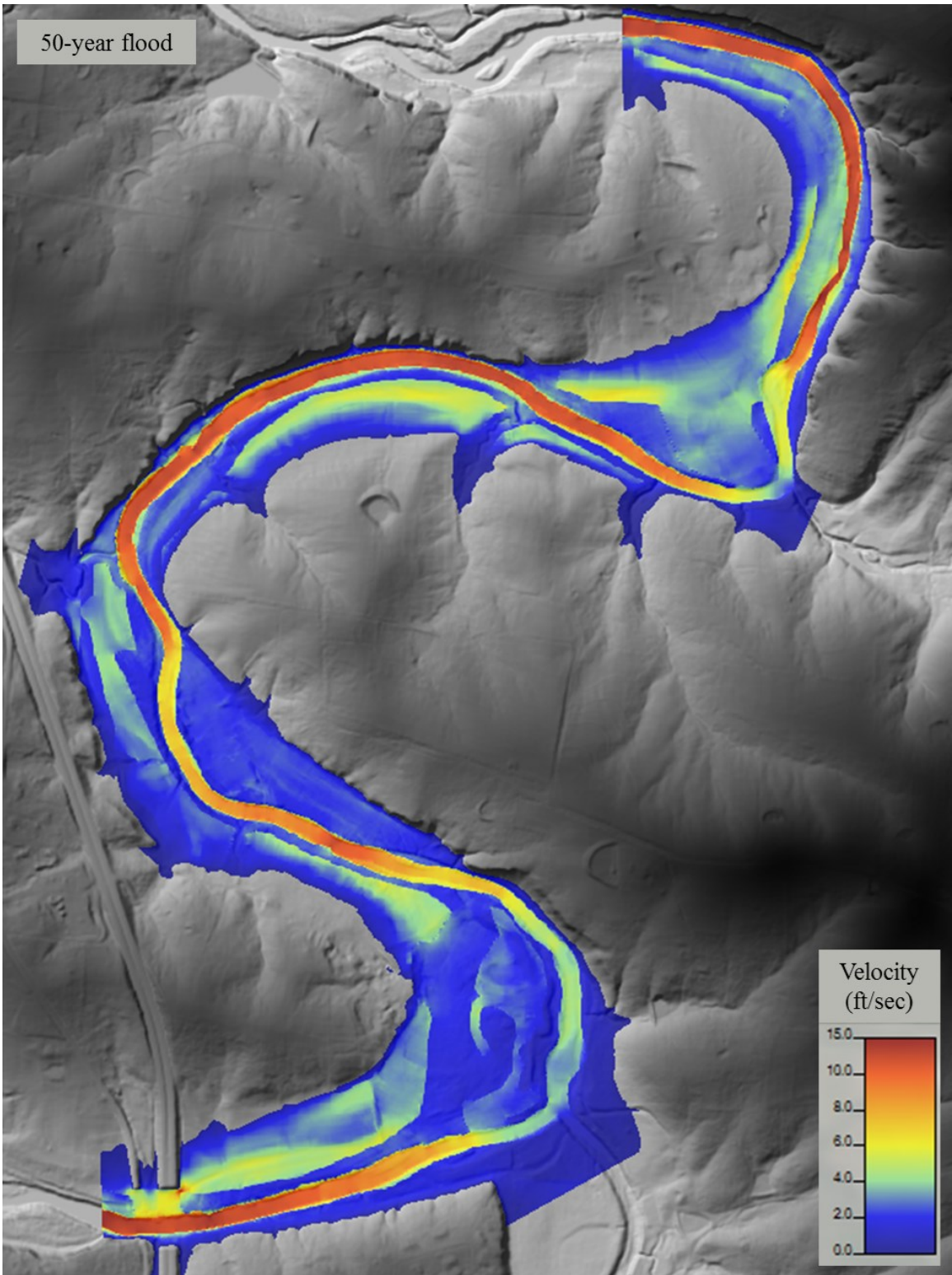


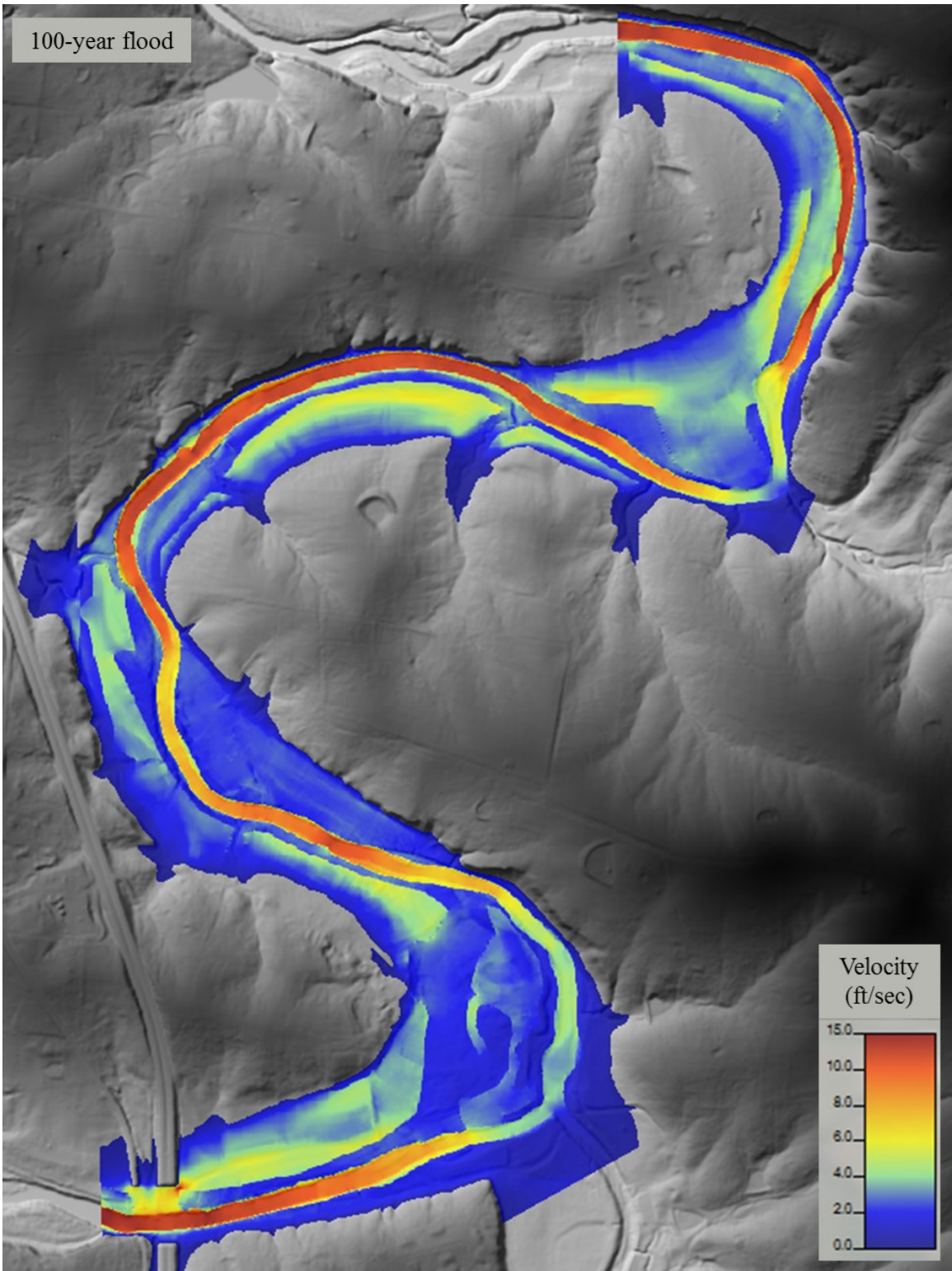




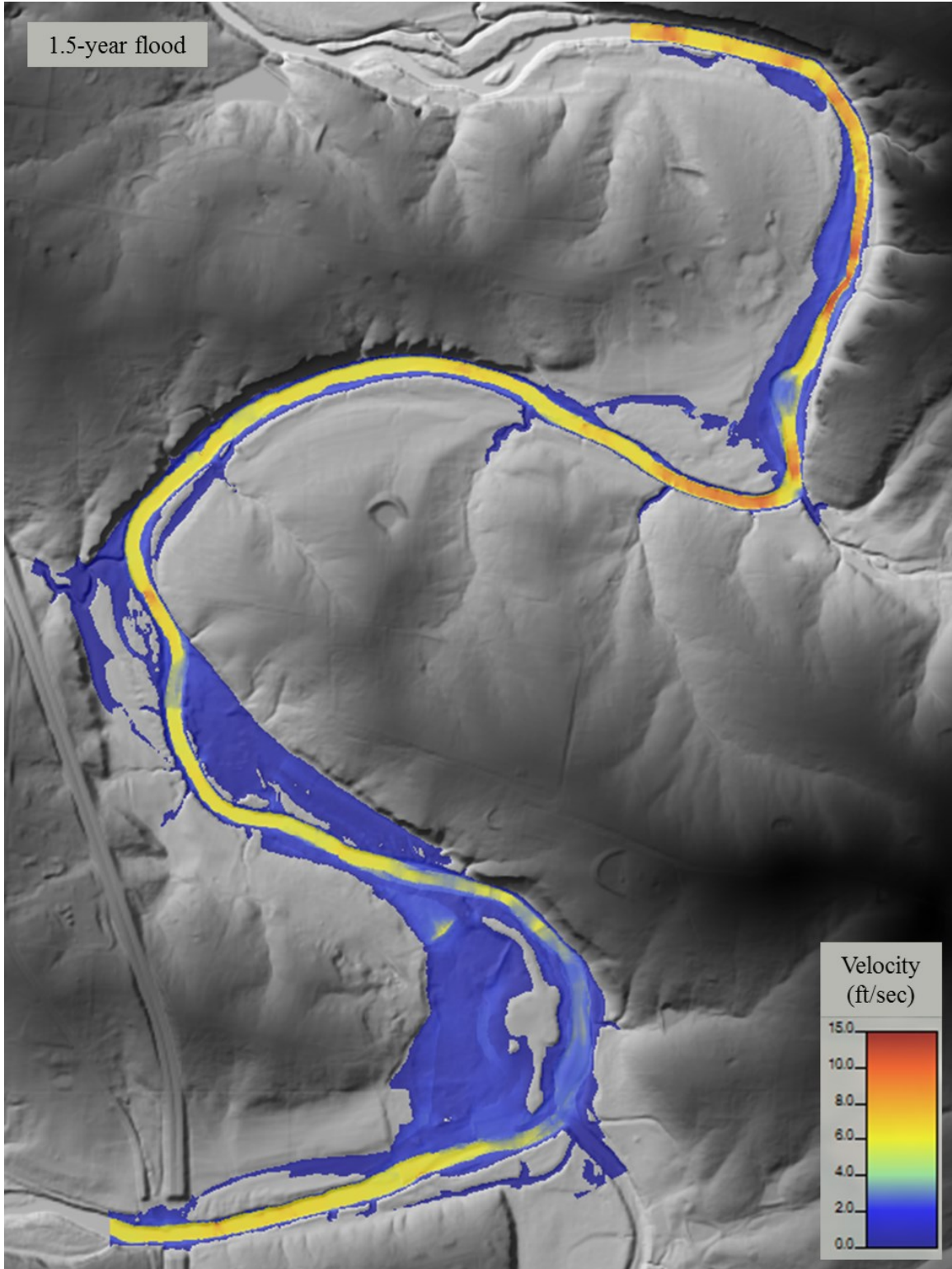


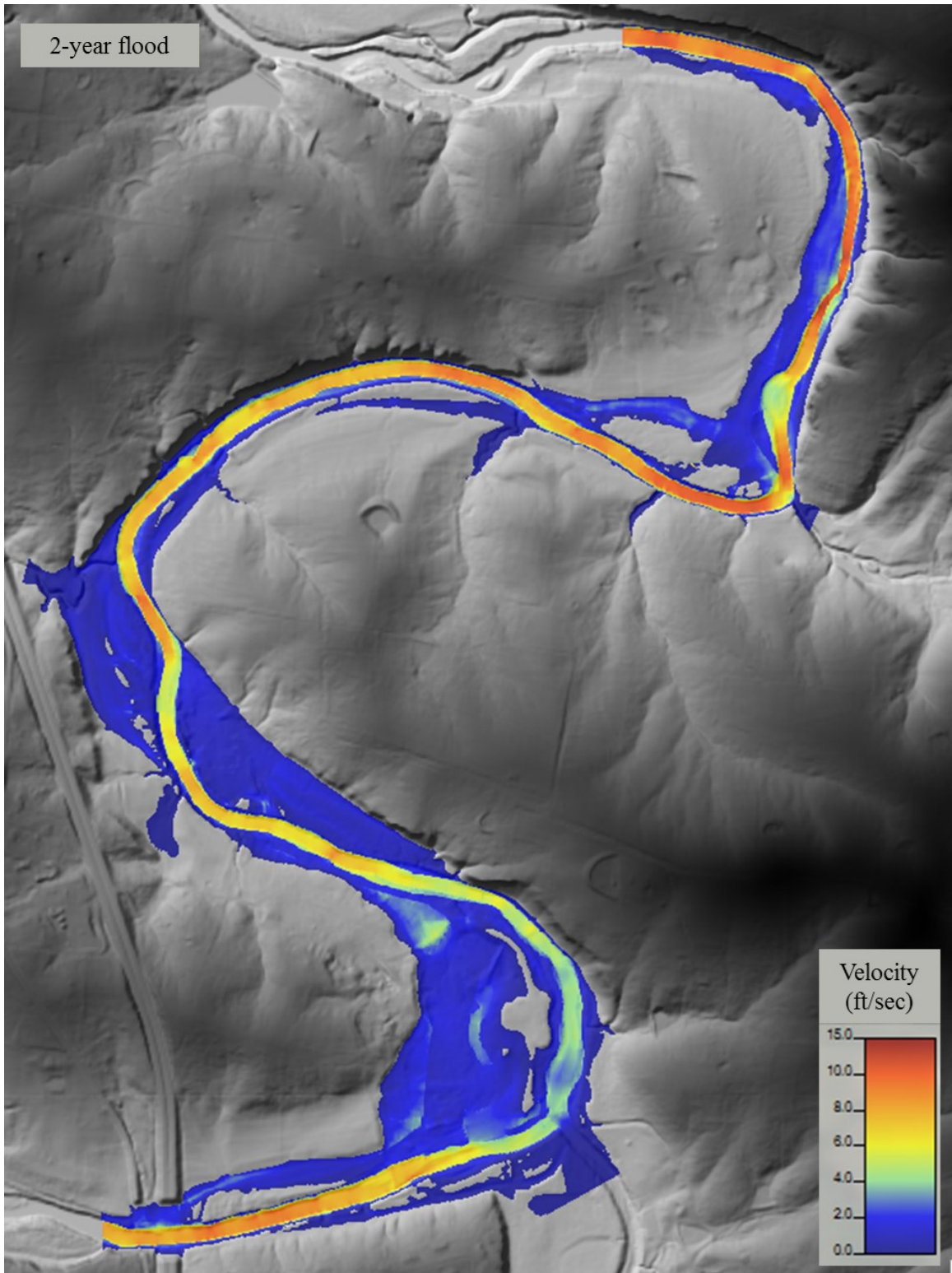


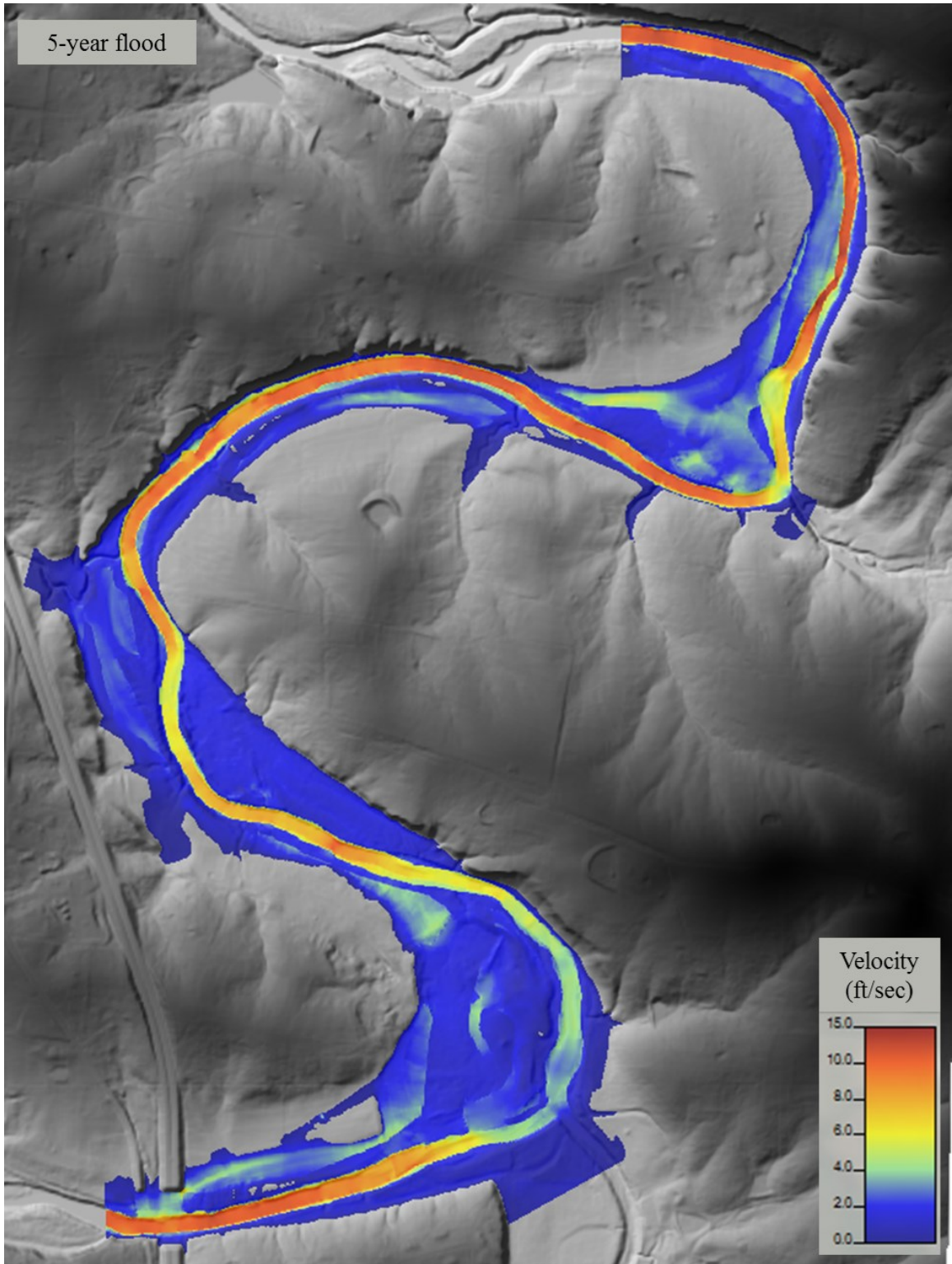


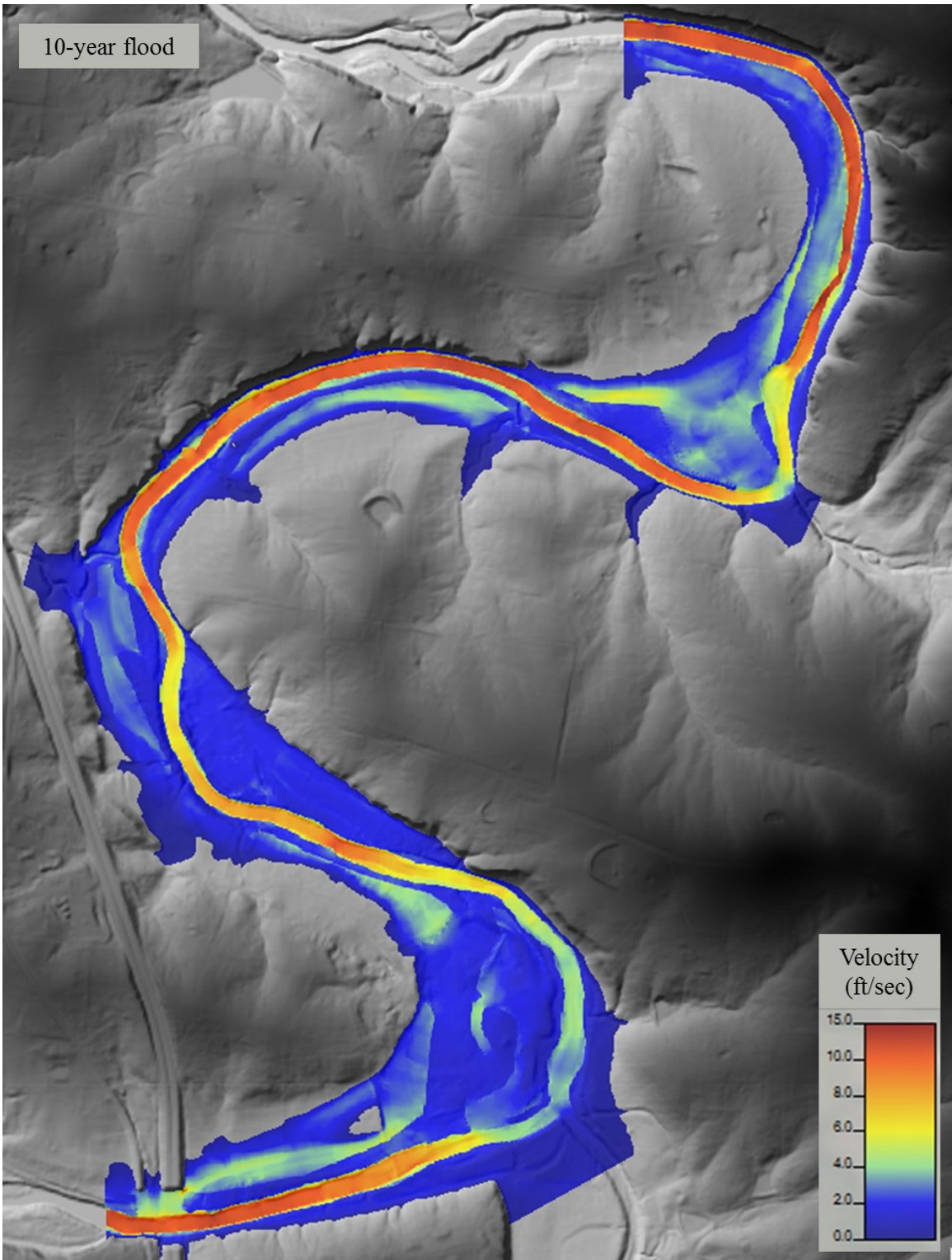


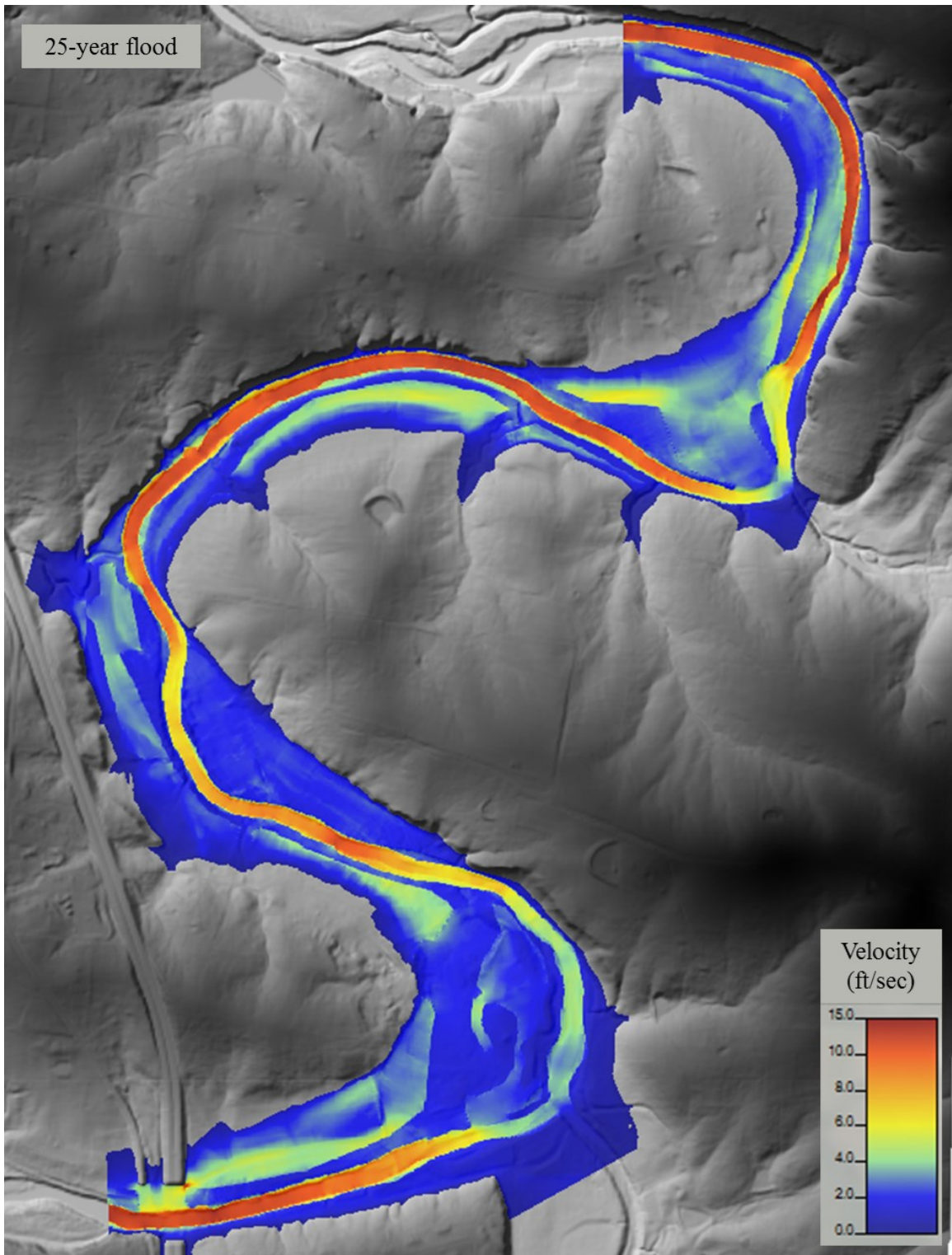
Appendix D – Post-construction velocity models.

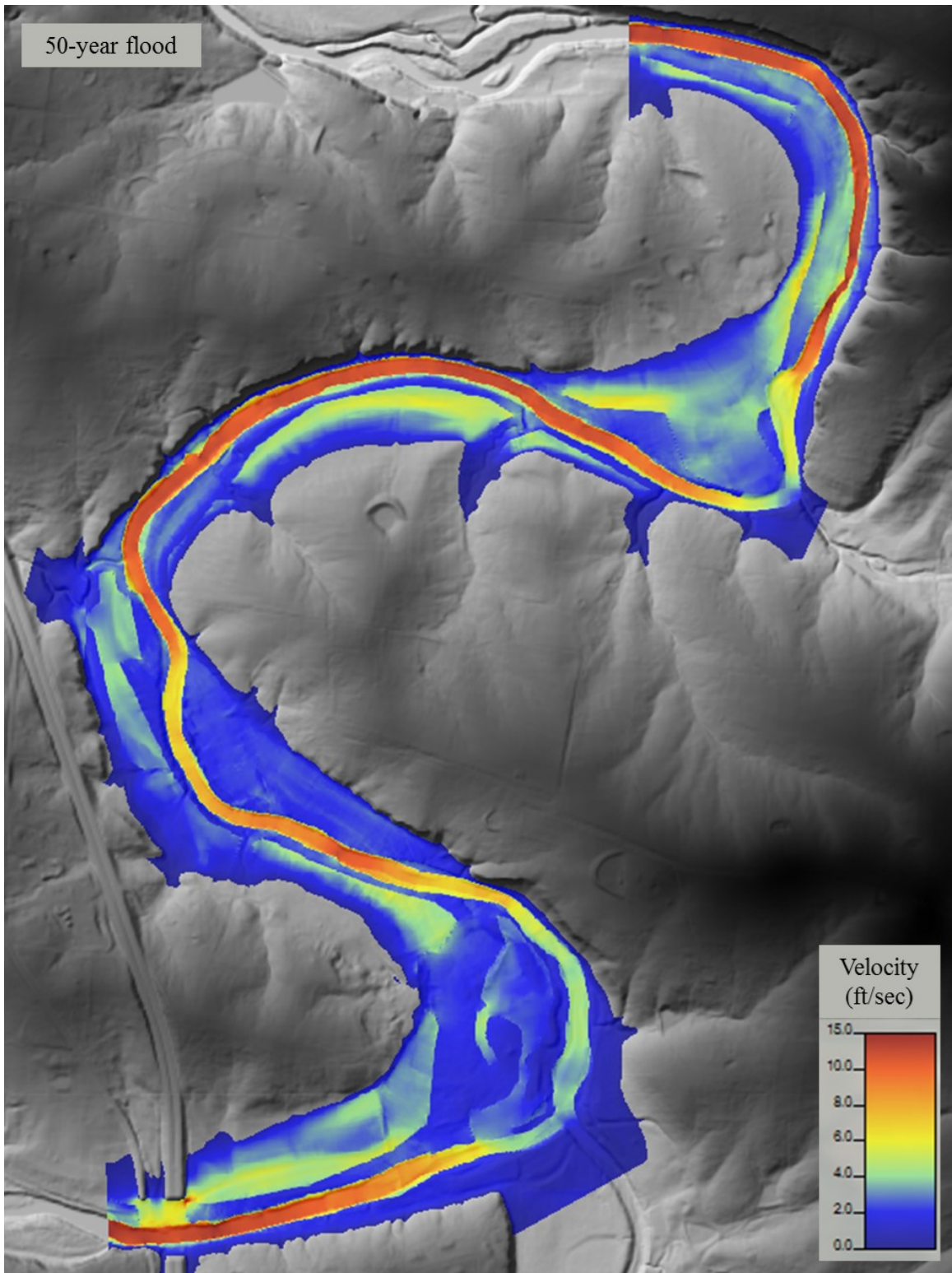


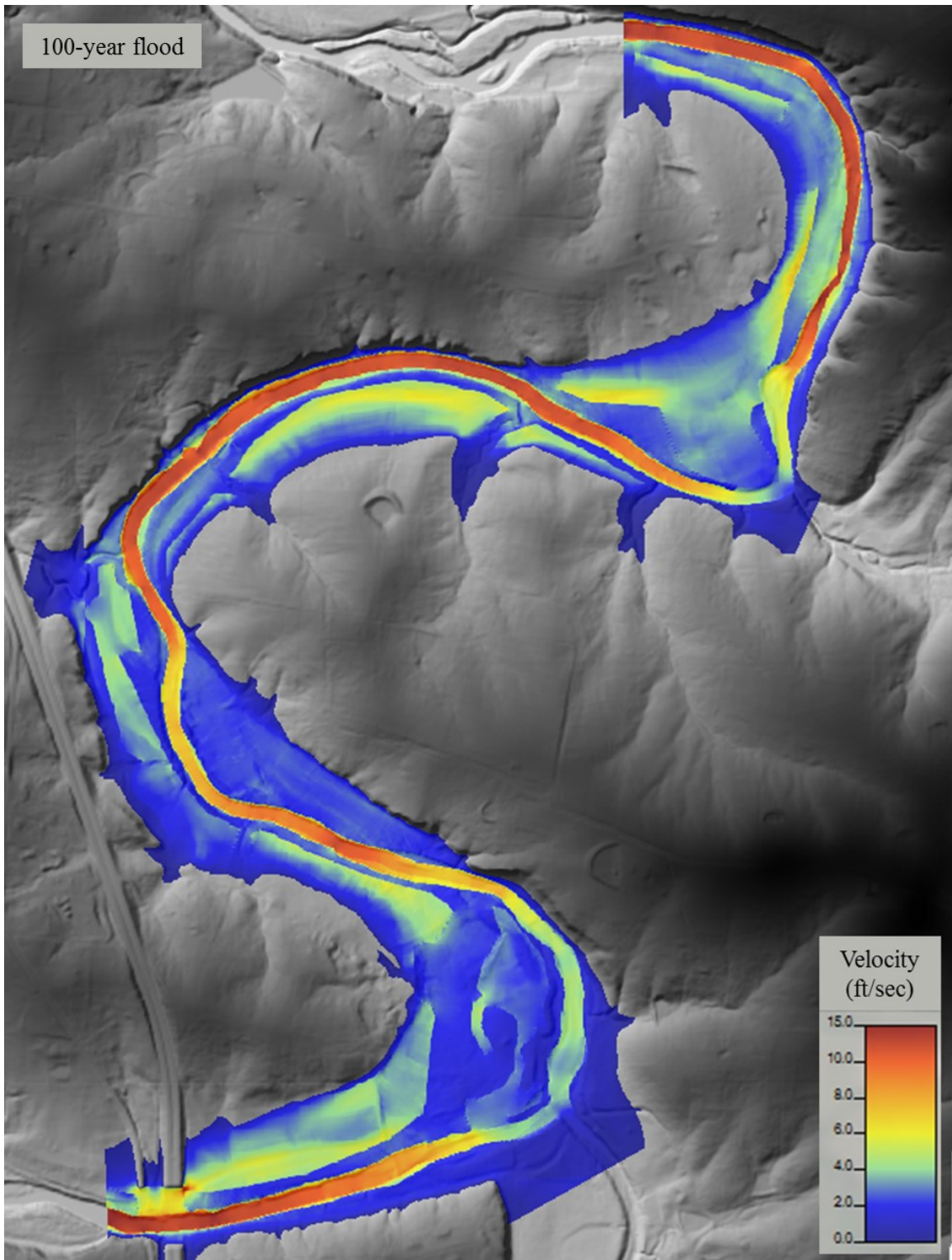




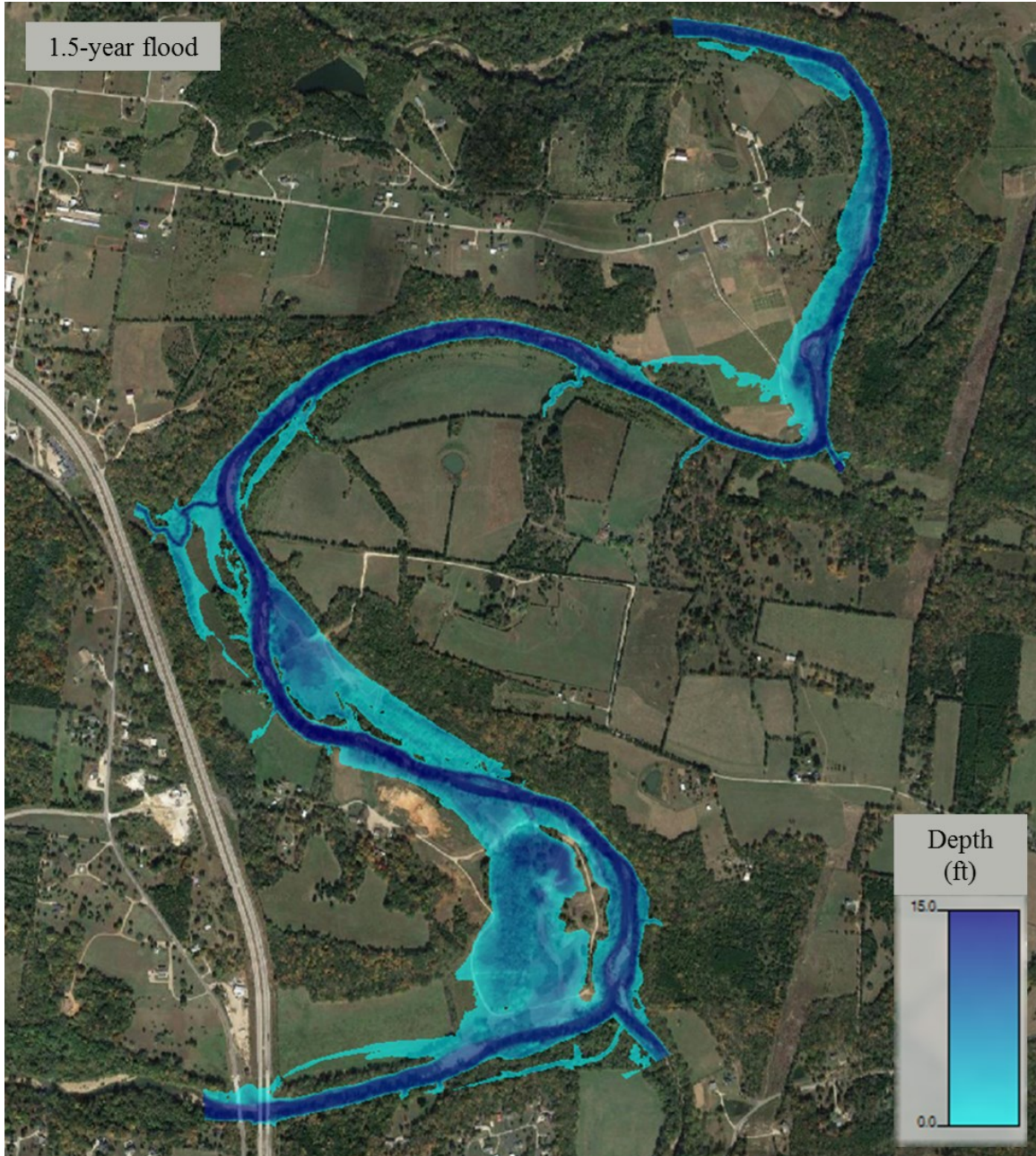


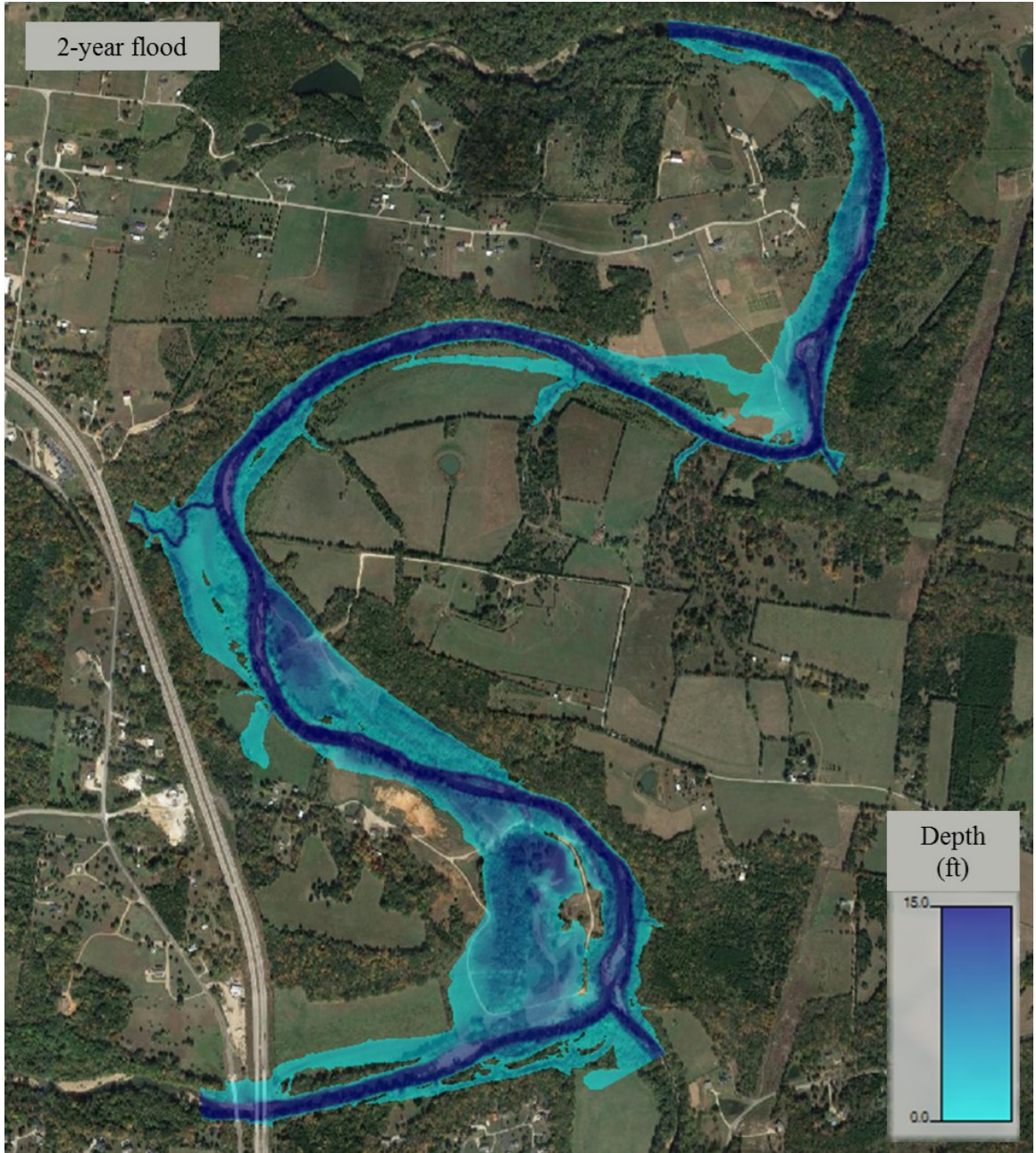


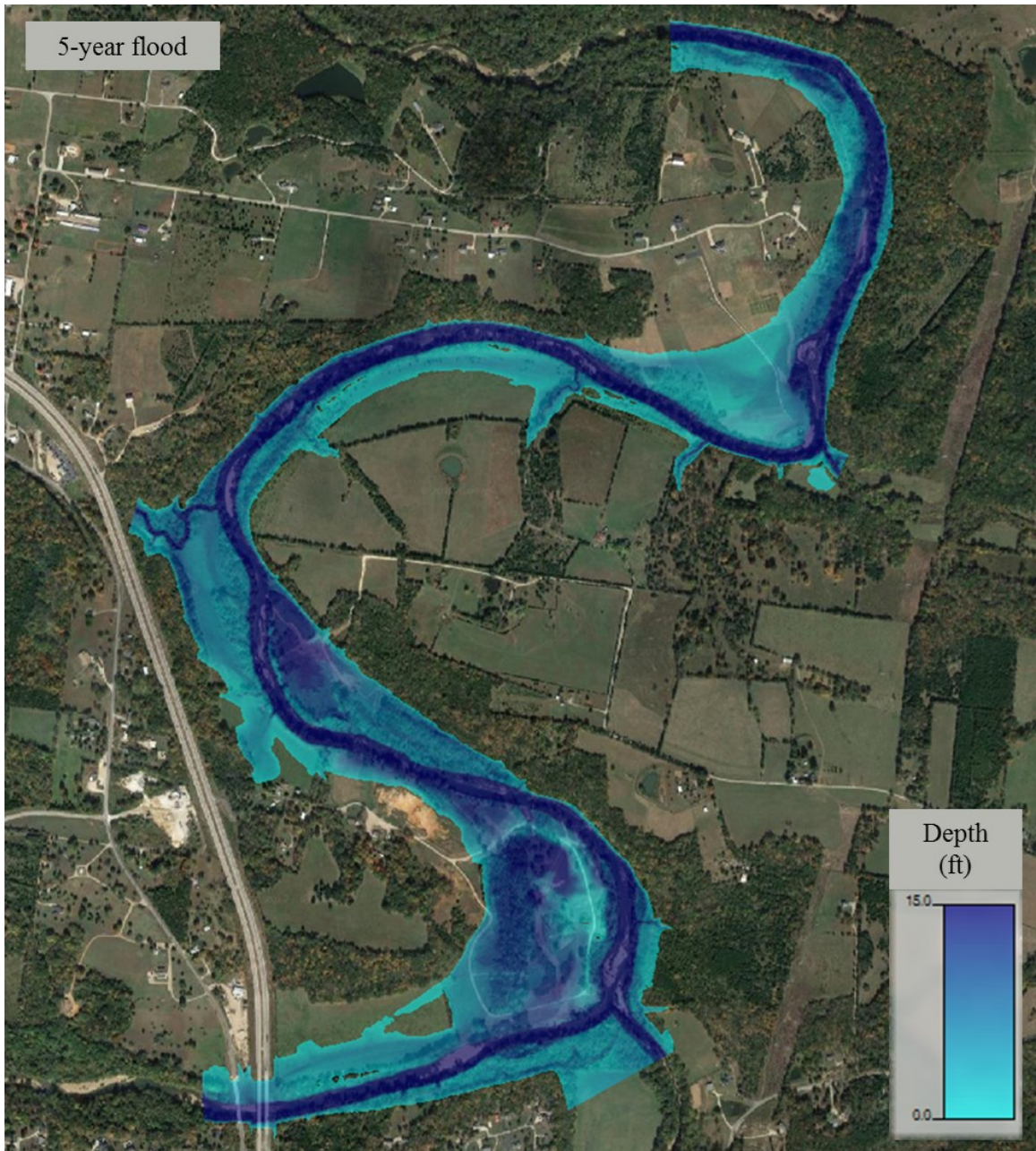


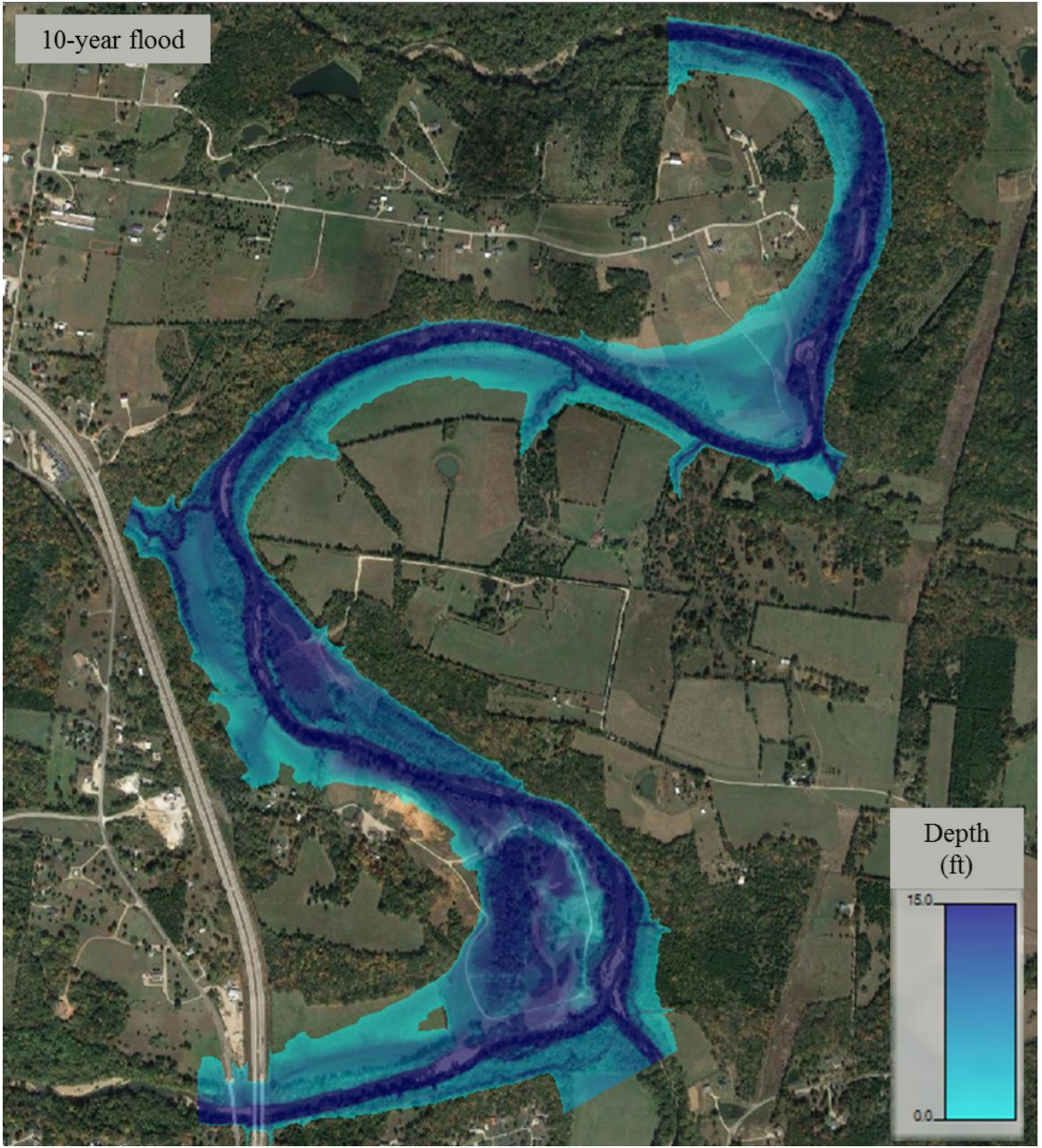


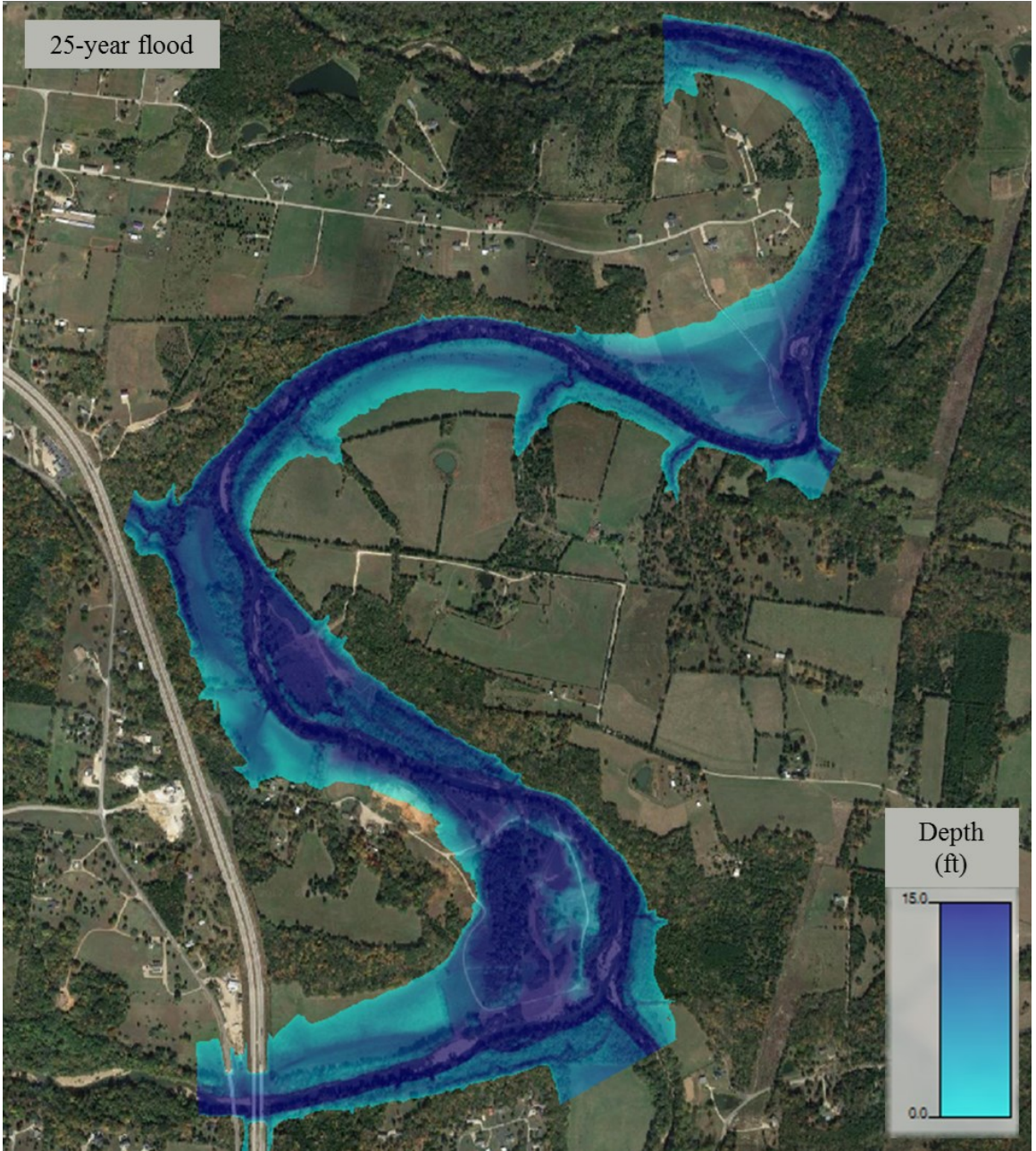
Appendix E – Pre-construction water depth model simulations.

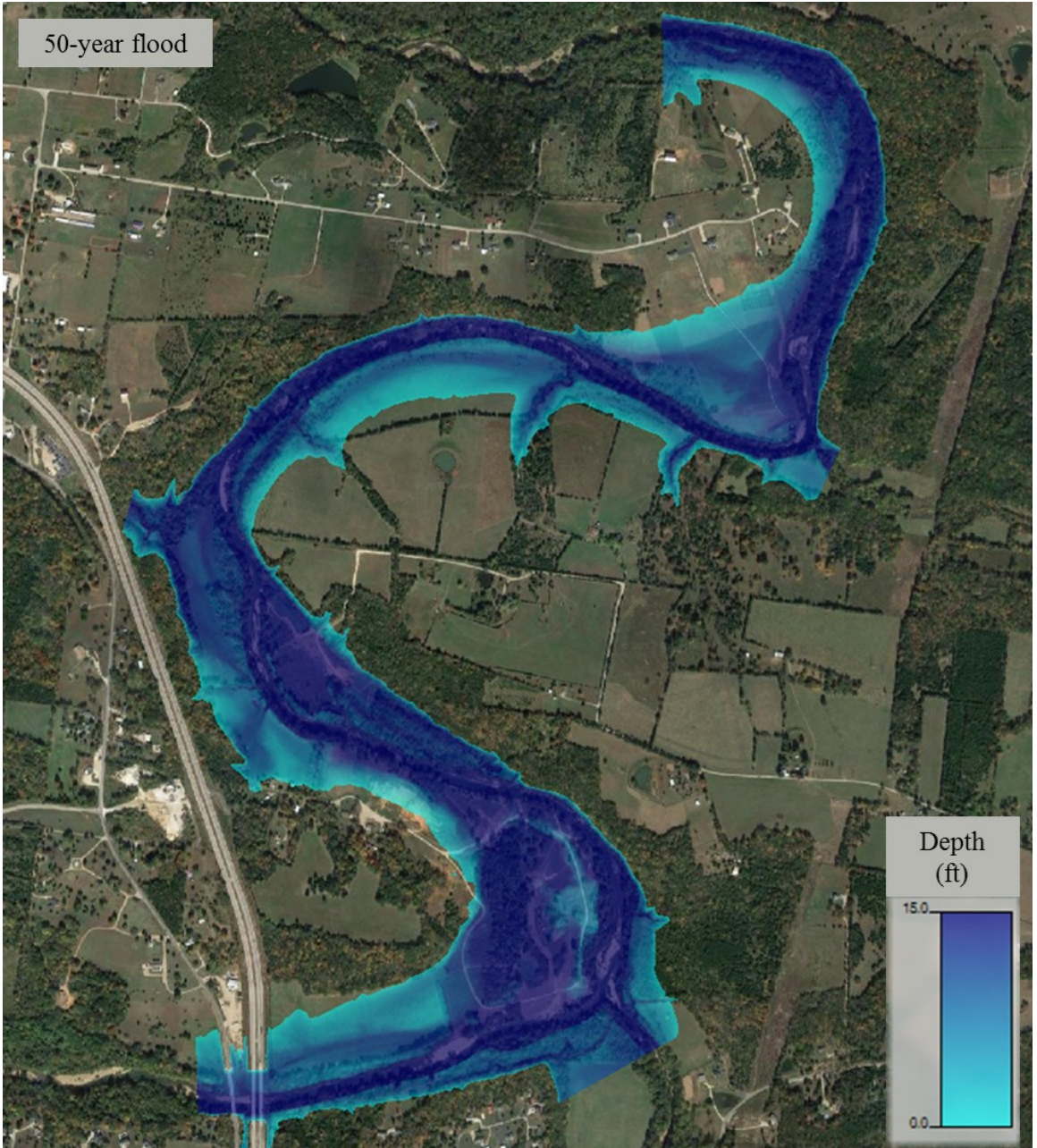


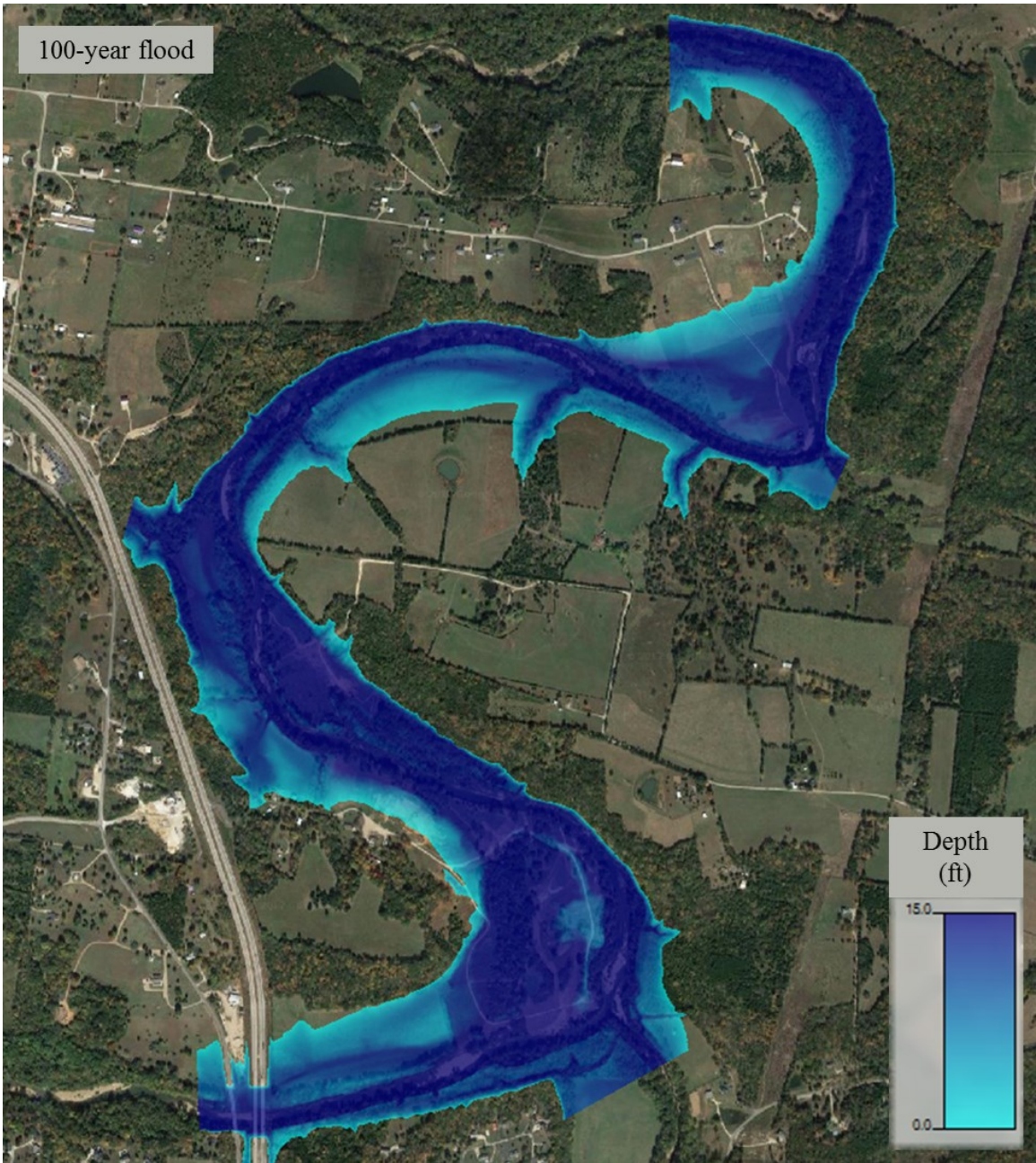












Appendix F – Post-construction water depth model simulations.

